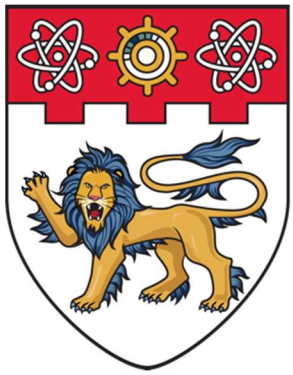

NANYANG TECHNOLOGICAL UNIVERSITY
SINGAPORE

PROLONGED IN VIVO GENE SILENCING USING MULTILAYERED NANOPARTICLES AS A SIRNA DELIVERY SYSTEM

TAN YANG FEI

SCHOOL OF MATERIALS SCIENCE AND ENGINEERING

2017

PROLONGED IN VIVO GENE SILENCING USING MULTILAYERED NANOPARTICLES AS A SIRNA DELIVERY SYSTEM

TAN YANG FEI

SCHOOL OF MATERIALS SCIENCE AND ENGINEERING

A thesis submitted to the Nanyang Technological University
in partial fulfilment of the requirement for the degree of
Doctor of Philosophy

2017

Statement of Originality

I hereby certify that the work embodied in this thesis is the result of original research and has not been submitted for a higher degree to any other University or Institution.

. . . . . .
Date

. . . . . .
TAN YANG FEI

Supervisor Declaration Statement

I have reviewed the content and presentation style of this thesis and declare it is free of plagiarism and of sufficient grammatical clarity to be examined. To the best of my knowledge, the research and writing are those of the candidate except as acknowledged in the Author Attribution Statement. I confirm that the investigations were conducted in accord with the ethics policies and integrity standards of Nanyang Technological University and that the research data are presented honestly and without prejudice.

. . . . . .
Date

. . . . . .
Input Supervisor Name Here

Authorship Attribution Statement

This thesis contains material from 2 papers in communication in 2 following peer-reviewed journals where I was the first author.

Chapter 4 and 5 will be published as Li-Fong Seet, Yang Fei Tan, Subbu Venkatraman, Tina T. Wong entitled SPARC Silencing Reduces Collagen Deposition in the Mouse Model of Conjunctival Scarring.

The contributions of the co-authors are as follows:

- Prof Wong and Prof Subbu provided the initial project direction and edited the manuscript drafts.
- I prepared the manuscript drafts. The manuscript was revised by Dr Seet, Dr Wong and Prof Subbu.
- I co-designed the study with Dr Seet and performed all the laboratory work at the School of Materials Science and Engineering (MSE) and the Singapore Eye Research Institute [1]. I also analyzed the data.
- All experiments, sample processing and analysis were done by me at MSE and SERI.
- Dr Seet conducted most of the animal surgeries, assisted by me. She also gave guidance in analysis and result representations.

Chapter 6 will be published as Yang Fei Tan, Ying Shi Lee, Li-Fong Seet, Kee Woei Ng, Subbu Venkatraman, Tina T. Wong entitled Release Mechanism Study of Layer-by-Layer Nanoparticles in Cells.

The contributions of the co-authors are as follows:

- Prof Wong and Prof Subbu provided the initial project direction and edited the manuscript drafts.
- I prepared the manuscript drafts. The manuscript was revised by Prof Ng, Dr Wong and Prof Subbu.

- I designed the study with Ying Shi Lee at the School of Materials Science and Engineering (MSE) and the Singapore Eye Research Institute [1]. I also analyzed the data.
- All experiments, sample processing and analysis were done by me and Ying Shi Lee at MSE and SERI.
- Dr Wong, Prof Ng and Prof Subbu gave guidance in analysis and result representations.

. . . . . .
Date

. . . . . .
Yang Fei Tan

Abstract

Currently, there are various diseases without effective mode of cure. Many interventions are hampered by undesirable proteins produced over time. One example is the accumulation of excessive collagen protein at surgical site in post glaucoma surgery patients, rendering surgery failure. Excessive collagen accumulation results in scarring. Current anti-proliferative agents used such as 5 Fluorouracil and Mitomycin C lack specificity, indiscriminately affecting tissues adversely when applied topically or subconjunctivally injected, causing complications. Thus, there is a need for an effective anti-scarring agent with localized, specific action that also gives a prolonged effect over time. siRNA has been explored to prevent fibrosis but its use was limited due to the lack of stable and sustained delivery systems. This work reports on the successful development of a new nanocarrier system for the management of fibrosis. The new carrier has a hydroxy apatite core, with alternating layers of siRNA and a cationic peptide. While the siRNA silences a fibroblast gene responsible for producing a key mediator of fibrosis called *SPARC*, the nanocarrier is formulated to protect the siRNA, improve cell uptake and ensure specific prolonged silencing of genes for 2 weeks. The Layer by Layer nanoparticle of HA|ARG|siRNA|ARG|siRNA|ARG configuration was 242 nm in hydrodynamic diameter with 49.3 mV surface charge. The nanoparticle has a positively charged outermost layer to protect the siRNA and to bind electrostatically to cellular membranes when added to cells, facilitating cell uptake. FESEM and TEM imaging showed that the NPs were spherical, with smooth surfaces, smaller than 200 nm in diameter and uniform in size. The designed nanoparticles (at various dosages) did not cause any toxic effects on MCF cells over 2 weeks and *in vitro* studies showed sustained *SPARC* knockdown without affecting cell growth and maintained siRNA presence in cells for 2 weeks with a single dose treatment. In addition, *in vivo* studies in the mouse model of conjunctival scarring showed that a single dose injection into the conjunctiva facilitated *SPARC* knockdown, leading to prolonged efficacy of fibrosis suppression. Moreover, the nanoparticle treatment did not cause tissue apoptosis or foreign body response. Mechanism studies were conducted to investigate the breakdown behaviour of the particles, focusing on the release patterns of siRNA. This is

the first demonstration of a stabilized siRNA delivery system showing sustained action against fibrosis over 2 weeks with a single injection.

Lay Summary

Currently, there are various diseases without effective mode of cure. Many diseases are caused by the production of undesirable proteins due to various reasons. One example is scarring observed in patients after glaucoma surgeries. Glaucoma surgeries are conducted to create alternative pathways to drain eye fluid to relieve pressure in the eye. However, scarring which is caused by the excessive production of collagen protein, will block these pathways and render the surgeries to fail. There are various drugs presently used to suppress scarring. Unfortunately, they can cause harmful side effects by destroying all tissues at the surgical site. Thus, there is a need for an effective protein suppressor with specific action that can also suppress the undesirable protein production for extended time. siRNA (molecules that interfere with protein production) can be used to suppress undesirable protein production but its use was limited due to its vulnerability and lack of suitable systems available currently to bring it safely to the site of action. This work reports on the successful development of a new siRNA carrier system for the management of scarring. The new carrier has a core, with alternating layers of siRNA and a positively charged polymer. While the siRNA prevents the production of *SPARC* protein, a key protein responsible for scarring, the carrier is formulated to protect the siRNA, improve cell entry and ensure that only *SPARC* protein was suppressed for 2 weeks. The multilayered nanoparticle has a positively charged outermost layer to protect the siRNA and to bind to cell surface when added to cells, facilitating cell entry. Studies conducted in mice showed that a single injection of the carrier into the mice eyes suppressed *SPARC* protein production, leading to long term scarring suppression. Moreover, the nanoparticle treatment did not cause harm to tissues in the eye or rejection from the body. Studies were also conducted to investigate the breakdown behaviour of the particles, focusing on how siRNA is released from the particles inside cells. This is the first time siRNA has been delivered to the injury site successfully with a carrier showing extended effect against scarring over 2 weeks with a single injection.

Acknowledgements

This dissertation would not have been possible without funding from a Clinician Scientist Award grant (NMRC/CSA-SI/0001/2015) awarded to Associate Professor Tina Wong and the Singapore National Research Foundation under its Translational and Clinical Research (TCR) Programme (NMRC/TCR/002-SERI/2008) administered by the Singapore Ministry of Health's National Medical Research Council. Animal studies were funded by a SingHealth Foundation Research Grant (SHF/FG583P/2014) to Lee Fong Seet and partially funded by the SERI core grant (NMRC/CG/015/2013).

Special thanks are conveyed to my research project supervisor Professor Subbu Venkatraman and co-supervisor Associate Professor Tina Wong for their continual guidance and support and to my mentor Dr. Seet Li Fong from Singapore Eye Research Institute for her incisive recommendations concerning the scope of the research.

I am very grateful for all the help rendered to me by my friends and peers at the Ocular Therapeutic Engineering Centre (OTEC) and SERI for making my journey so far memorable and smooth. I am especially grateful to my peer and personal friend Chaw Su Yin for all the brain storming sessions we had whenever I faced any problems related to my project. I also like to thank Toh Li Zhen and Stephanie Chu from SERI for all the help they rendered me whenever I was conducting experiments over at SERI. I also like to thank Alice Ng, Lee Ying Shi, Revathy, Chua Hwee Yee and Anastasia Darwitan from OTEC for their help when I was conducting some of my experiments at OTEC.

Also, I would like to show my appreciation to Cao Ye, Chan Jing Ni, Tan Wei Ni Dulcia, Seah Xin Ying, Joseph Rini Rachel and Ragavendra for their tremendous support and friendship.

Table of Contents

Table Captions

Figure Captions

compared with MCF cells treated with control NPs loaded with respective doses of scrambled siRNA. All samples were normalized with an appropriate housekeeping gene and repeated in triplicates. $p^* < 0.05$.

Figure 4.5 A) FESEM image of 5 layered LbL NPs, B) TEM image of 5 layered LbL NPS.

Figure 4.6 Cell viability study tracking 5000 MCF cell growth after treatment with 3 different 5 Layered LbL NPs at dosages 9, 18, 27 and 216 µg for a span of 2 weeks. The 3 LbL NPs were: a) NPs loaded with *SPARC* siRNA (si*SPARC*), b) NPs loaded with scrambled siRNA (siSCRAM) and c) NPs loaded with dextran sulphate in place of siRNA (Control).

Figure 5.1 Cellular uptake of LbL nanoparticles loaded with FITC-siRNA. (A) Confocal microscopic analysis of intracellular trafficking of the LbL nanoparticles from 30 minutes to 14 days incubation with conjunctival fibroblasts. Nuclei were visualized by staining with DAPI. All time points were compared with control cells with no particle treatments, showing no green FITC signals. (B) Flow cytometry analysis of uptake of LbL nanoparticles in conjunctival fibroblasts at the same time points as (A). Representative scatter plots with gate lines are shown. Pink scatter indicate cells positive for green fluorescence, gated using cells cultured for the corresponding length of time but in the absence of nanoparticles. Indicated values denote the %mean ± SD of fluorescence-positive cells (n=3). (D) Graphical representation of the flow cytometry data in (B). *p=9.38e-3 (post-hoc Bonferroni-adjusted) between 4 and 8 h, but p>0.5 between 8 h, 12 h, 24 h and 7 days.

Figure 5.2 Effects of siRNA-loaded LbL nanoparticles on endogenous gene silencing. qPCR analysis of *SPARC* (top; *p=6.00e-9, **p=3.82e-7) and Col1a1 (bottom; *p=2.30e-5, **p=1.62e-3) expression upon treatment with the nanoparticles for 7 or 14 days. Indicated p values were post-hoc Bonferroni-adjusted, n=3.

Figure 5.3 Tissue toxicity of LbL nanoparticles. (A) Representative scatter plots of annexin V-stained samples from experimental surgery alone (left), surgery cum treatment with LbL nanoparticles loaded with scrambled siRNA (middle), and surgery cum treatment with LbL nanoparticles loaded with *SPARC* siRNA. L, late apoptic or dead cells; E, early apoptotic cells; V, viable cells. Indicated values denote the %mean ± SD of cells in the associated quadrant (n=5). (B) % annexin V-positive cells in conjunctival tissues treated as indicated. (C) % viable cells in conjunctival tissues treated as indicated. Each symbol represents a pool of tissues from 3 eyes of independent animals. Cell samples included MCF cells. Samples harvested after 14 days post treatments.

Figure 5.4 Prolonged endogenous gene silencing delivered by LbL nanoparticles in the mouse model of conjunctival scarring. (A) Slit lamp photographs of LbL nanoparticles loaded with scrambled (left) or *SPARC* siRNAs in the conjunctiva immediately after injection post-surgery. (B) qPCR analysis of *SPARC* and Col1a1 (bottom) expression upon treatment with the nanoparticles for 7 days. The mean fold changes and the associated p values comparing the effects of *SPARC* siRNA-loaded particles against that of scrambled siRNA-loaded particles are indicated. Each symbol represents a pool of tissues from 3 eyes of independent animals. (C) Immunoblot analyses of *SPARC* and COL1A1 (bottom) expression upon treatment with the nanoparticles for 7 days. Densitometry values, expressed as ratios with GAPDH, are shown below. (D) qPCR analysis of *SPARC* and Col1a1 (bottom) expression upon treatment with the nanoparticles for 14 days. (D) Immunoblot analyses of *SPARC* and COL1A1 (bottom) expression upon treatment with the nanoparticles for 14 days.

Figure 5.5 Absence of fibrous encapsulation of LbL nanoparticles in the conjunctiva at 14 days. (A) Hematoxylin and eosin staining of conjunctival tissues subjected to experimental surgery and injected with nanoparticles loaded with scrambled (left) or *SPARC* siRNA. Areas containing high density of coalesced nanoparticles are indicated by the green dotted lines. (B) Picrosirus red staining of the conjunctival tissues. Areas containing high density of coalesced nanoparticles are indicated by the white dotted lines. Scale bar, 100 μm. (C) Immunostaining of the conjunctival tissues with type I collagen

antibody. Nuclei were visualized by DAPI staining (blue). Areas containing high density of coalesced nanoparticles are indicated by the dotted lines. Overlays of the immunofluorescence with bright field data are also shown. Scale bar, 50 μm.

Figure 5.6 Minimal inflammatory response in the conjunctiva injected with LbL nanoparticles at 14 days. Immunostaining of conjunctival tissues with (A) CD45 antibody (green) and (B) F4/80 antibody (green). Nuclei were visualized by DAPI staining (blue). Areas containing high density of coalesced nanoparticles are indicated by the dotted lines. Bright field (BF) and overlays of BF with immunofluorescence data are shown. Arrowheads indicate cells that stained positive for the markers. Insets are magnified versions of the area indicated by the red arrows. Scale bar, 50 μm.

Figure 6.1 Graph of cumulative siRNA release from 3 and 5 layered LbL NPs over 14 days. Three-layered LbL particles (HA-ARG-6FAM siRNA-ARG) and five-layered LbL particles (HA-ARG-6FAM siRNA-ARG-6FAM siRNA-ARG) fabricated from 1 mg HA respectively were dispersed in 600 μl of PBS and constantly shaken at 37˚C over 14 days. At the stipulated time points, the particle samples were centrifuged down and the supernatant collected and measured with the Tecan plate reader to affirm release amount compared against 6FAM siRNA standard curve. Fresh PBS was added for subsequent time point measurements. All samples and measurements were conducted in triplicates.

Figure 6.2 CLSM images from left, bright field, blue channel, green channel, red channel and overlay. Sample images (B), which were treated with TRITC HA core NP and CellLight (staining lysosomes green) were compared with control cells (A) not treated with particles but treated with CellLight (staining lysosomes green). Control cells showed no red signals but only green signals. Images were taken at 40X magnification, 2X zoom. CLSM images taken 3 days after treatment.

Figure 6.3 Graph of FRET degradation trend over 14 days. Outer siRNA was tagged with FITC and the adjacent inner Poly-L-Arginine layer was tagged with TRITC (HA-ARG-siRNA-TRITC ARG-FITC siRNA-ARG). 0.108 mg of particles were treated to

30000 MCF cells. At stipulated time points, the cells were trypsinized and suspended in 0.4% trypan blue, centrifuged and then suspended in 200 uL of PBS for testing with Guava flow cytometer. The cell samples were subjected to blue laser excitation (488nm) and only the FITC tagged onto siRNA would be excited. If the adjacent TRITC tagged Poly-L-Arginine was still in close proximity, the TRITC would be able to receive the emission from FITC and get excited to release red signals. The FRET effect was measured and compared with controls over a period of time. TRITC signals were compared with TRITC signals of control cell samples treated in the same way but with particles with only TRITC tagged Poly-L-Arginine. Similarly, FITC signals were compared with FITC signals of control cell samples treated in the same way but with particles with only FITC tagged siRNA. That was done so as to only consider signals involved in FRET for the analysis.

Figure 6.4 Graph of FRET degradation trend over 14 days. Inner siRNA was tagged with FITC and the adjacent inner Poly-L-Arginine layer was tagged with TRITC (HA-TRITC ARG- FITC siRNA- ARG- siRNA-ARG). 0.108 mg of particles were treated to 30000 MCF cells. At stipulated time points, the cells were trypsinized and suspended in 0.4% trypan blue, centrifuged and then suspended in 200 uL of PBS for testing with Guava flow cytometer. The cell samples were subjected to blue laser excitation (488nm) and only the FITC tagged onto siRNA would be excited. If the adjacent TRITC tagged Poly-L-Arginine was still in close proximity, the TRITC would be able to receive the emission from FITC and get excited to release red signals. The FRET effect was measured and compared with controls over a period of time. TRITC signals were compared with TRITC signals of control cell samples treated in the same way but with particles with only TRITC tagged Poly-L-Arginine. Similarly, FITC signals were compared with FITC signals of control cell samples treated in the same way but with particles with only FITC tagged siRNA. That was done so as to only consider signals involved in FRET for the analysis.

Figure 7.1 Graph of cumulative siRNA release from 5 (HA/ARG/6FAM siRNA/ARG/6FAM siRNA/ARG) and 7 layered (HA/ARG/6FAM siRNA/ARG/6FAM siRNA/ARG/6FAM siRNA/ARG) LbL NPs over 21 days. Each NP fabricated from 1 mg of HA were dispersed in 600 µl of PBS and constantly shaken at 37˚C over 21 days. At the

stipulated time points, the particle samples were centrifuged down and the supernatant collected and measured with the Tecan plate reader to affirm release amount compared against FAM siRNA standard curve. Fresh PBS was added for subsequent time point measurements. All samples and measurements were conducted in triplicates.

Figure 7.2 Graph of cumulative siRNA release percent from 7 layered (HA/ARG/6FAM siRNA/ARG/6FAM siRNA/ARG/6FAM siRNA/ARG) LbL NPs over 21 days. All samples and measurements were conducted in triplicates.

Figure 7.3 Confocal microscopy of human retroperitoneal fibroblast cells imaged one day after treatment of NP with FITC tagged HA core (FITC-HA/ARG/siRNA/ARG/siRNA/ARG/siRNA/ARG). Images were taken at 40X magnification and 4.3X zoom. Sample cells were compared with untreated control cells which showed no green FITC signals.

Abbreviations

5-FU	5-fluorouracil
6FAM	6-carboxyfluorescein
ApoB	apolipoprotein B
ARG	poly-l-arginine
ARVO	association for research in vision and ophthalmology
CLSM	confocal laser scanning microscope
CSII	continuous subcutaneous insulin infusion
DXS	dextran sulphate
ECM	extracellular matrix
FESEM	field emission scanning electron microscope
FITC	fluorescein isothiocyanate
FRET	fluorescence resonance energy transfer
GFS	glaucoma filtration surgery
HA	hydroxyapatite
HAART	highly active antiretroviral therapy
HIV	human immunodeficiency virus
IOP	intraocular pressure
LbL	layer by layer
MCF	mouse conjunctival fibroblast
MDI	multiple daily injections
MMC	mitomycin C
mRNA	messenger RNA
NP	Nanoparticle
PEI	polyethyleneimine
PLGA	poly(lactic-co-glycolic acid)
qPCR	polymerase chain reaction
RISC	RNA-induced silencing complex
RNA	ribonucleic acid

RNAi	RNA interference
RRM2	M2 subunit of ribonucleotide reductase
SCRAM	scrambled siRNA
siRNA	short interfering ribonucleic acid
SPARC	secreted protein acidic and Cysteine rich
T1D	type 1 diabetes
T2D	type 2 diabetes
TEM	transmission electron microscope
TRITC	tetramethylrhodamine

Chapter 1

Introduction

This chapter briefly introduces the significance of RNAi therapy as the next revolutionary approach to treat diseases. It briefly describes the advantages of using the Layer by Layer polymeric nanoparticle system to transport siRNA safely into cells to bring about a prolonged gene silencing effect. The chapter then take on the scarring problem faced by many patients post glaucoma filtration surgeries as a platform to show how the LbL system can effectively bring about prolonged anti-fibrotic relief. In summary, this chapter contains several sections to introduce the background, problem statement, hypothesis, objective and scope.

1.1 Background

RNA interference (RNAi), first discovered as a natural cellular process of gene silencing *via* double-stranded RNAs [1], showed great promise as a powerful tool to treat diseases using small interfering RNA (siRNA) molecules. However, the *in vivo* delivery of siRNAs is fraught with challenges, including the major problem of the susceptibility of the negatively-charged naked siRNA to degradation by nucleases, and non-renewability upon cell division [2, 3], as well as the inability of the naked siRNA to enter target cells. Indeed, although at least 22 RNAi-based drugs have entered clinical trials [4], the majority have not progressed beyond phase I. It is now recognized that administration of naked siRNA either systemically or locally is not efficacious, due to the issues mentioned above. Even with nanocarrier-encapsulated siRNA, the target tissue bioavailability of the siRNAs is low [5]. It is clear that the ability to stably deliver adequate therapeutic amounts of siRNA *in vivo*, and extending the time of exposure, will substantially boost the effectiveness and efficacy of siRNAs as therapeutic agents.

Attempts to stabilize the siRNA against both clearance by the reticulo-endothelial system, and against degradation by nucleases, have been partially successful; however tissue bioavailability is too low for successful clinical translation, except when the target tissue is the liver [6]. Both chemical modifications and conjugation to the siRNA have been used to escape nuclease degradation and liver tissue targeting [7]. While it is now recognized that a stabilizing delivery system is a must for siRNA action *in vivo*, success is not guaranteed, as seen by the recent announcement of the termination of Alnylam's Phase 3 study in patients with hereditary amyloidosis with cardiomyopathy [8]. Revusiran, the drug whose development has been halted, is an siRNA conjugated to a sugar (N-acetyl Galactosamine or GalNAc) to aid cellular internalization. Although it has not been proven that the siRNA delivery system of revusiran was the cause of the patient deaths, other methods to improve the bioavailability of siRNA may yield safer and more effective RNAi therapeutics. One approach is based on biological or polymeric constructs designed to protect the siRNA while facilitating its transport to the cytoplasm of targeted cells [9], and enhancing bioavailability via localized rather than systemic administration. In this respect,

non-viral polymeric delivery vehicles are particularly appealing due to simplicity of preparation, with the possibility of scalable production, and fewer health risks. The layer-by-layer (LbL) self-assembly technique, driven mainly by electrostatic interactions of oppositely charged polymers around a nano-sized core, create cationic nanoparticles that are stable [10]. I recently demonstrated that LbL particles comprised of of poly-L-arginine (ARG) and dextran sulphate (DXS) polyelectrolytes atop a hydroxyapatite (HA) core successfully delivered gene silencing *in vitro* through its siRNA load [11]. The main aim of the layer-by-layer approach is to sustain the release of encapsulated cargo over several days rather than hours. I hypothesize that these LbL nanoparticles can be further engineered to achieve extended endogenous gene silencing in a single application by successive multi-layering of siRNA layers around biocompatible HA. HA has chemical, biological and crystallographic properties that are similar with the mineral phase of human bone [12]. Although LbL technology based on gold nanoparticles as a platform for prolonged gene silencing has also been reported previously [13], long-term safety is a concern since gold nanoparticles have been associated with genetic, hepatic, renal and reproductive toxicity even at lower doses [14, 15]. Hence, for long-term clinical applications, HA is preferable to gold as core material in nano-carriers. Furthermore, in my application, I consider ocular fibrosis following surgery in the eye, where current methods of reducing a fibrosis-induced blockage of a surgically-opened channel are non-selective and inadequate: localized administration in the eye is facile and is expected to increase bioavailability.

Fibrosis is a prominent pathological feature of a wide range of diseases as well as the end result of aberrant wound healing. Many organs, including liver, bone marrow, lung, kidney, gastrointestinal tract, skin, eye, and endomyocardium, can fail due to uncontrolled fibrosis. It is likely that fibrotic disease may be reversible at the early and even advanced stages but there is a point when it becomes irreversible [16]. Although the negative impact of fibrosis on morbidity and mortality is well recognized, effective anti-fibrotic therapy remains elusive [17]. Conjunctival fibrosis is the condition I am considering here, and it occurs to varying degrees following surgery to treat ocular disease, and is a major cause of surgical failure [18]. Conjunctival fibrosis is progressive, with the late phase being marked by elevated collagen production, a sign of excessive accumulation of extracellular matrix

(ECM) components [19]. Fibrosis suppression, therefore, may require a prolonged therapeutic approach that extends from the early to late phase of wound healing. A target gene associated with conjunctival fibrosis is secreted protein acidic and rich in cysteine (SPARC), a 32 kDa calcium-binding matricellular protein established to be involved in collagen fibrillogenesis and assembly [20]. SPARC is a prime target for anti-fibrotic therapy given its conspicuous induction at sites of wound healing and tissue remodelling, including the wounded conjunctiva [19]. Conversely, when SPARC is deficient, as in the *SPARC* knockout mouse, altered collagen fibrillogenesis and delayed conjunctival fibrosis was observed [21]. Importantly, SPARC expression was amenable to silencing by RNAi and its suppression was associated with reduced type I collagen expression [22].

Here, I report the development of multi-layered LbL nanoparticles for sustained delivery of *SPARC* siRNA to the conjunctiva after experimental surgery. In the mouse model of conjunctival scarring [21], a single-dose conjunctival injection of the modified nanoparticles achieved *SPARC* silencing for at least 14 days. Furthermore, type I collagen transcript expression was down-regulated with no tissue toxicity or foreign body response to the nanoparticles. Thus, by multi-layering siRNA on an HA-LbL system, these nanoparticles have the capacity to deliver safe, effective and prolonged endogenous gene silencing via a single application for the treatment of tissue fibrosis.

1.2 Significance and problem statement

Currently, there are various diseases without effective mode of cure. The effectiveness of many interventions are hampered as a result of the patient's body producing certain undesirable proteins due to various reasons. One example is the scarring problem in post glaucoma surgery patients.

Glaucoma is an eye disorder that causes progressive and irreversible loss of sight, affecting the quality of life of patients in various ways. Studies have shown that neurodegeneration in glaucoma causes impairments of visual functions such as form, motion and color perception, and pupil response to light [23]. Glaucoma is the leading cause of irreversible

blindness worldwide. The number of cases reported in 2010 totaled to more than 60 million. This figure is predicted to rise to 80 million by 2020 [24]. The disease is more rampant in the older population. It is estimated that 1 out of every 40 adults over 40 years of age has glaucoma with a loss of visual function [25].

The most common surgical intervention for severe glaucoma condition is a trabeculectomy. Unfortunately, post-operative success is hindered by excessive scar tissue formation around the surgical site [26-28]. Moreover, the current anti-proliferative agents used lack specificity and have been associated with complications [29-32]. Thus, there is a need for an effective anti-scarring agent with localized, specific action that also gives a prolonged effect over a desired period of time.

Scar tissue formation is actually caused by the body's natural defense system to heal wounds. It is mainly the result of over production of collagen at the wound site. The problem can be easily remedied if the spike in collagen RNA caused by the body's reaction to the wound is controlled with the use of siRNA. However, siRNA is fragile and susceptible to attack by the body's natural immune system. Furthermore, it is negatively charged and thus not easily up-taken into cells. A delivery system which can protect and deliver siRNA into cells to reduce collagen RNA levels over a span of 2 weeks can largely ease the scarring problem, increasing glaucoma surgery success rates dramatically.

In this work, RNAi therapy is investigated for its therapeutic potential to reduce post-operative scarring via the silencing of collagen expression. Due to its highly specific targeting via base-pair interactions, an almost unrestricted choice of targets, low production costs compared with protein therapies, and minimal side effects [33], RNAi has gained traction as an important alternative therapeutic solution. However, due to limitations such as siRNA being degraded by nucleases in the body, cleared by the reticulo-endothelial system and its inability to penetrate cells, an appropriate delivery system is required for RNAi therapy to be feasible. Some of the limitations can be overcome by localized deliveries or encapsulation within nanoparticles.

The recent advances in nanotechnology have made the use of polymeric nanoparticles popular for gene delivery. By incorporating natural polymers such as chitosan, poly(lactic-co-glycolic acid) (PLGA) and polyethyleneimine [34] [34], researchers have created carriers with low toxicity, high biodegradability and biocompatibility [35]. In particular, cationic polymers such as poly-L-arginine and PEI increase cell transfection due to their charge, protect the siRNA against degradation and induce intracellular release from endosomes based on the "proton-sponge effect" [36, 37]. The use of poly-L-arginine is explored in this project to protect siRNA and also to improve its ability to be up-taken into cells.

The layer-by-layer (LbL) self-assembly technique is a unique method to synthesize multilayered films composed of polycationic and polyanionic polymers. The assembly process is driven mainly by electrostatic interactions. In this project, it is used to create cationic nanoparticles (NPs), incorporating siRNA layers for higher gene loading and prolonged release while still maintaining cell penetration and RNA protection. With regards to RNAi therapy, LbL particles present an added potential advantage because the multiple layers can possibly ensure the repetitive administration of the siRNA as the layers degrade. Prolonged gene silencing is one of the main challenges siRNA delivery systems face as the siRNA is diluted upon cell division, quickly degraded and not renewed [3]. Thus, the silencing effect is often transient. LbL particles with multiple layers can potentially offer long-lasting controlled release and thus a prolonged gene silencing effect.

Hydroxyapatite (HA), a complex material found in tooth enamel and bone, is becoming an important biomaterial candidate. Due to its excellent biocompatibility and bioactivity, HA crystals are currently being used as bone implants or as coatings on prostheses [38, 39]. HA is chosen as a core material for the LbL particles as its slow dissolution made it suitable for a prolonged-release vector, while its biocompatibility and low cytotoxicity as substantiated by multiple studies [40-42] made it an attractive biomaterial for gene therapy. The significance of the research is to propose a LbL NP designed to incorporate siRNA to combat scar tissue formation. The NP is formulated to protect the siRNA, improve the up-take of siRNA into cells, ensure specific silencing of the particular gene in question

(*SPARC*) and to ensure prolonged knockdown effect of the RNA in question (*SPARC* RNA) for a period of 2 weeks both *in vitro* and *in vivo*. If proven successful, this designed system can potentially be used to transport other siRNAs to target other diseases requiring prolonged therapeutic effects.

1.3 Problem statement

Although siRNA therapy is selective and effective against fibrosis, its efficacy depends on encapsulation in sufficient amounts in a cationic nano-carrier. Such carriers are not easy to design as they must be able to not only encapsulate enough siRNA for prolonged gene silencing effects but also protect the siRNA from degradation and ensure effective cellular entry. Our hypothesis is that a layer-by-layer system based on a hydroxyapatite core offers the best system

1.4 Hypotheses

Hypothesis 1:

Localized delivery of siRNA can greatly enhance its efficacy against fibrosis.

Hypothesis 2:

Using a layer-by-layer design enables encapsulation and protection of siRNA in localized delivery, and enables cellular penetration and sustained action in fibroblasts.

1.5 Objectives and Scope

The objective of the project is to design a layer by layer nanoparticle incorporating *SPARC* siRNA that can significantly knockdown both *SPARC* and collagen RNA both *in vitro* and *in vivo* for a period of 14 days. The designed particle will be focused on inhibiting scar tissue formations caused by collagen RNA spike in patients after glaucoma surgeries in this project. By silencing collagen gene through experiments conducted, the designed

particle will exhibit its potential in delivering siRNA into cells and achieving prolonged effect for 14 days. If the designed particle manage to achieve gene silencing over 2 weeks, the release mechanism of siRNA from the particles will be investigated to gain insight on how the particles achieve prolonged gene silencing.

HA will be used as the core of the layer by layer nanoparticle designed. Poly-L-arginine will be the positively charged polymer used in the fabrication of the particles. *SPARC* siRNA will be the siRNA loaded in the particles. Primary mouse conjunctival fibroblast cells will be used for *in vitro* tests while wild type C57 mice will be used for *in vivo* tests. The knockdown of the RNA will only be followed for a period of 14 days. This project will focus on knocking down collagen RNA in cells, inhibiting scar tissue formation post glaucoma surgeries to illustrate the effectiveness of the designed particle as a siRNA delivery vehicle for prolonged effect over 14 days.

1.6 Dissertation Overview

The dissertation is organized into the following 7 chapters.

Chapter 1 briefly introduces the significance of RNAi therapy as the next revolutionary approach to treat diseases. It briefly describes the advantages of using the Layer by Layer polymeric nanoparticle system to transport siRNA safely into cells to bring about a prolonged gene silencing effect. The chapter then takes on the scarring problem faced by many patients post glaucoma filtration surgeries as a platform to show how the LbL system can effectively bring about prolonged anti-fibrotic relief. The hypothesis, objective and scope of this thesis are presented.

Chapter 2 summarizes the background and current research progress related to the work investigated in the thesis. It provides a review on the current research and challenges of fibrosis in post glaucoma surgery patients. It introduces the use of RNAi therapy as an alternative way to curb fibrosis and gives detailed background to why the Layer by Layer

polymeric nanoparticle system is the ideal delivery system for siRNA. The chapter also describes the advantages of the various reagents used in the design and formulation of the delivery system designed in this work.

Chapter 3 presents the materials and methods used in this thesis.

Chapter 4 describes the optimisation of Layer by Layer nanoparticles and also the characterization of the optimized particles. As the objective of this project is aimed at achieving a particle configuration enabling the trafficking of enough siRNA into cells for gene silencing over 2 weeks, the amount of siRNA loading and number of siRNA layers were tweaked and investigated upon to find the optimal configuration. The optimized particle was then fabricated and characterized. This chapter will give insight to the amount of siRNA needed to achieve prolonged gene silencing over extended periods and also how siRNA loaded in multiple layers affect gene silencing.

Chapter 5 describes the uptake of the optimized LbL NP into MCF *in vitro*. Upon affirmation of the entry of the particles into MCF cells, *SPARC* and Collagen I mRNA within cells treated with the particles were quantified on day 7 and 14 to observe any gene silencing induced by the particles. With observable signs of *SPARC* and Collagen I gene silencing over 14 days *in vitro*, cells from conjunctival tissues harvested from mice treated with the particles were tested for toxicity. After verification that particle treatment used was not toxic in mice, particles were then injected sub-conjunctivally into mice post simulated glaucoma surgeries. The conjunctival were then harvested on day 7 and 14 for *SPARC* and Collagen I mRNA and protein quantification to ascertain the effectivity of the particles in prolonged gene silencing. Immuno-staining of cryo sections of the treated mice eye was also done to observe any toxicity and activity effects.

Chapter 6 describes the investigation in the release behaviour of *SPARC* siRNA from the LbL NPs designed. The significance of this study is to observe how the NPs release siRNA to explain why the NPs were able to achieve prolonged gene silencing within cells. NPs were shaken in PBS at 37˚C and the supernatant was collected periodically to quantify the

siRNA amount released. That provided insight in the release profile of the designed particle as compared to other particles of similar configurations which were, however, not able to deliver prolonged gene silencing effects. Next, adjacent siRNA and Poly-L-Arginine layers within the particles were tagged with FRET (fluorescence resonance energy transfer)-pairs and the NPs were added to cells to track the periods in which the layers would detach from each other within cells. This approach was intended to show the release behaviour of siRNA *in vitro* and explain why prolonged gene silencing was achieved with the NP configuration designed.

Chapter 7 presents discussion and conclusions from all the above findings and proposes possible future work. The chapter will focus on a possible application to utilize the system for type I diabetes mellitus management which can potentially be better than the current treatment especially in patient compliances.

1.7 Findings and Outcomes

This research led to several novel outcomes:

1. Designed and fabricated of an effective LbL NP system capable of delivering siRNA into MCF cells and elicit effective and prolonged *SPARC* and collagen gene knockdown over 14 days both *in vitro* and *in vivo* with a single application.
2. Performed the appropriate release experiments to observe the behaviour patterns of LbL NPs releasing loaded siRNA upon entry into cells to gain insight on prolonged gene silencing properties.
3. Demonstrated the flexibility in modification of the devised LbL NP system to cater to different application requirements.

References

[1] A. Fire, S. Xu, M. K. Montgomery, S. A. Kostas, S. E. Driver, C. C. Mello. *nature*. **1998**, 391, 806-811.

[2] S. H. Ku, S. D. Jo, Y. K. Lee, K. Kim, S. H. Kim. *Advanced Drug Delivery Reviews*. **2016**, 104, 16-28.

[3] Y. Takabatake, Y. Isaka, M. Mizui, H. Kawachi, S. Takahara, E. Imai. *Biochemical and biophysical research communications*. **2007**, 363, 432-437.

[4] C.-f. Xu, J. Wang. *Asian Journal of Pharmaceutical Sciences*. **2015**, 10, 1-12.

[5] P. Angart, D. Vocelle, C. Chan, S. Walton. *Pharmaceuticals*. **2013**, 6, 440.

[6] A. Wittrup, J. Lieberman. *Nat Rev Genet*. **2015**, 16, 543-552.

[7] R. Kanasty, J. R. Dorkin, A. Vegas, D. Anderson. *Nat Mater*. **2013**, 12, 967-977.

[8] K. Garber, Nature Research, 2016.

[9] T. C. Roberts, K. Ezzat, S. EL Andaloussi, M. S. Weinberg. *SiRNA Delivery Methods: Methods and Protocols*. **2016**, 291-310.

[10] S. Correa, E. C. Dreaden, L. Gu, P. T. Hammond. *Journal of Controlled Release*. **2016**, 240, 364-386.

[11] Y. F. Tan, R. C. Mundargi, M. H. A. Chen, J. Lessig, B. Neu, S. S. Venkatraman, T. T. Wong. *Small*. **2014**, 10, 1790-1798.

[12] S. V. Dorozhkin. *Biomaterials*. **2010**, 31, 1465-1485.

[13] S. K. Lee, C. H. Tung. *Advanced functional materials*. **2013**, 23, 3488-3493.

[14] I. M. M. Paino, V. S. Marangoni, R. d. C. S. de Oliveira, L. M. G. Antunes, V. Zucolotto. *Toxicology letters*. **2012**, 215, 119-125.

[15] U. Taylor, A. Barchanski, W. Garrels, S. Klein, W. Kues, S. Barcikowski, D. Rath, in *Nano-biotechnology for biomedical and diagnostic Research*, Springer, 2012, 125-133.

[16] R. Bataller, D. A. Brenner. *Journal of clinical investigation*. **2005**, 115, 209.

[17] V. J. Thannickal, Y. Zhou, A. Gaggar, S. R. Duncan. *The Journal of clinical investigation*. **2014**, 124, 4673.

[18] W. H. Morgan, D. Y. Yu. *Clinical & experimental ophthalmology*. **2012**, 40, 388-399.

[19] L.-F. Seet, S. Finger, S. Chu, L. Toh, T. Wong. *Current molecular medicine*. **2013**, 13, 911-928.

[20] J. Trombetta-eSilva, A. D. Bradshaw. *The open rheumatology journal*. **2012**, 6, 146.

[21] L.-F. Seet, R. Su, V. Barathi, W. S. Lee, R. Poh, Y. M. Heng, E. Manser, E. N. Vithana, T. Aung, M. Weaver. *PloS one*. **2010**, 5, e9415.

[22] L. F. Seet, R. Su, L. Z. Toh, T. T. Wong. *Journal of cellular and molecular medicine*. **2012**, 16, 1245-1259.

[23] M. Cesareo, E. Ciuffoletti, F. Ricci, F. Missiroli, M. A. Giuliano, R. Mancino, C. Nucci, in *Progress in Brain Research*, Vol. Volume 221 (Eds: B. Giacinto, N. Carlo), Elsevier, 2015, 359-374.

[24] H. A. Quigley, A. T. Broman. *British Journal of Ophthalmology*. **2006**, 90, 262-267.

[25] H. A. Quigley. *The Lancet*. 377, 1367-1377.

[26] E. M. Addicks, H. A. Quigley, W. Green, A. L. Robin. *Archives of Ophthalmology*. **1983**, 101, 795-798.

[27] S.-P. A. Atreides, G. L. Skuta, A. C. Reynolds. *International Ophthalmology Clinics*. **2004**, 44, 61-106.

[28] D. A. Morris, M. O. Peracha, D. H. Shin, C. Kim, S. C. Cha, Y. Y. Kim. *Archives of Ophthalmology*. **1999**, 117, 1149-1154.

[29] D. S. Greenfield, I. J. Suñer, M. P. Miller, T. A. Kangas, P. F. Palmberg, H. W. Flynn, Jr. *Archives of Ophthalmology*. **1996**, 114, 943-949.

[30] E. D. MUCKLEY, R. A. LEHRER. *Optometry and Vision Science*. **2004**, 81, 499-504.

[31] L. J. Katz, L. B. Cantor, G. L. Spaeth. *Ophthalmology*. **1985**, 92, 959-963.

[32] E. J. Higginbotham, R. K. Stevens, D. C. Musch, K. O. Karp, P. R. Lichter, T. J. Bergstrom, G. L. Skuta. *Ophthalmology*. **1996**, 103, 650-656.

[33] R. K. M. Leung, P. A. Whittaker. *Pharmacology & Therapeutics*. **2005**, 107, 222-239.

[34] K. Xu, D. A. Cantu, Y. Fu, J. Kim, X. Zheng, P. Hematti, W. J. Kao. *Acta biomaterialia*. **2013**, 9, 8802-8814.

[35] Y. Gao, X.-L. Liu, X.-R. Li. *Int J Nanomedicine*. **2011**, 6, 1017-1025.

[36] O. Boussif, F. Lezoualc'h, M. A. Zanta, M. D. Mergny, D. Scherman, B. Demeneix, J.-P. Behr. *Proceedings of the National Academy of Sciences*. **1995**, 92, 7297-7301.

[37] J.-P. Behr. *CHIMIA International Journal for Chemistry*. **1997**, 51, 34-36.

[38] D. Wahl, J. Czernuszka. *Eur Cell Mater*. **2006**, 11, 43-56.

[39] A. Moroni, F. Pegreffi, M. Cadossi, A. Hoang-Kim, V. Lio, S. Giannini. *Expert review of medical devices*. **2005**, 2, 465-471.

[40] V. Uskoković, D. P. Uskoković. *Journal of biomedical materials research Part B: Applied biomaterials*. **2011**, 96, 152-191.

[41] A. Y. P. Mateus, C. C. Barrias, C. Ribeiro, M. P. Ferraz, F. J. Monteiro. *Journal of Biomedical Materials Research Part A*. **2008**, 86, 483-493.

[42] M. Ferraz, A. Mateus, J. Sousa, F. Monteiro. *Journal of Biomedical Materials Research Part A*. **2007**, 81, 994-1004.

Chapter 2

Literature Review

This chapter summarizes the background and current research progress related to the work investigated in the thesis. It provides a review on the current research and challenges of fibrosis in post glaucoma surgery patients. It introduces the use of RNAi therapy as an alternative way to curb fibrosis and gives detailed background to why the Layer by Layer polymeric nanoparticle system is the ideal delivery system for siRNA. The chapter also describes the advantages of the various reagents used in the design and formulation of the delivery system designed in this work.

2.1 Anti-scarring agent for glaucoma filtration surgeries

2.1.1 Prevalence of glaucoma

Glaucoma is an eye disorder related to the dysfunction of the optic nerves. It causes progressive and irreversible loss of sight, affecting the quality of life of patients in various ways. Studies have shown that neurodegeneration in glaucoma involves retinal ganglion cells, the optic nerve and also extends to the central regions of the visual system, causing impairments of visual functions such as form, motion and color perception, and pupil response to light [1]. Glaucoma is the leading cause of irreversible blindness worldwide. The number of cases reported in 2010 totaled to more than 60 million. This figure is predicted to rise to 80 million by 2020 [2]. As the disease disproportionately affects the older population, an estimated 1 out of every 40 adults over 40 years of age has glaucoma with a loss of visual function [3]. Elevated intraocular pressure [4] is the most common characteristic across glaucoma patients, as it is the rise in IOP that triggers the eventual death of the retinal ganglion cells. Thus, treatment is often targeted towards reducing the IOP via ophthalmic drops or when medical therapy is ineffective, surgical intervention [5].

2.1.2 Limitations of current treatment

The most common surgical intervention in cases of severe glaucoma is a trabeculectomy. It involves the opening of a filtration channel, diverting aqueous humor from the anterior chamber to the subconjunctival space, thus forming a “bleb”, the new site of aqueous filtration. Yet, post-operative success is immensely hindered by excessive extracellular matrix deposition, resulting in scar tissue formation, around the bleb [6-8]. Moreover, although the current use of anti-proliferative agents, such as mitomycin C (MMC) and 5-fluorouracil (5-FU), effectively inhibits the surge in fibroblast replication, their lack of specificity has been associated with complications such as bleb leakage, corneal erosion [9], endophthalmitis [10-13] and hypotony [14]. Currently to combat the drawbacks of MMC and 5-FU, there are many researchers exploring different dosages and different modes of application of the drugs in attempt to minimize the side effects. For instance, Nagarwal et al. [15] developed 5-fluorouracil (5-FU) loaded chitosan/TPP nanoparticles

by ionic gelation for potential ocular application. The 5-FU loaded chitosan/TPP nanoparticles ranged from approximately 114 to 192 nm in size, and had a positive zeta potential (30±4 mV). The encapsulation efficiency, loading capacity, and recovery of nanoparticles were 8.12-34.32%, 3.14-15.24%, and 24.22-67%, respectively. *In vivo* bioavailability studies showed that the bioavailability of 5-FU was significantly improved by encapsulating 5-FU into chitosan/TPP nanoparticles as compared with 5-FU solution after a single instillation. There were also other deliveries of the two drugs with the use of hydrogels. However, the indiscriminating destructive effects of the drugs remains.

Thus, there is a need for an effective anti-scarring agent with localized, specific action that also has a prolonged effect over the desired period of time. Much research has been done to develop an alternative means of anti-scarring therapy with varying degrees of success [16-22]. Of late, with the decoding of the human genome, gene therapy has been popularly researched on and utilized as a potential mode of anti-fibrosis alternative.

2.2 Gene therapy and RNA interference (RNAi)

2.2.1 Mechanism of RNAi technology

In this work, gene therapy is investigated for its therapeutic potential to reduce post-operative scarring via the silencing of collagen expression. RNA interference (RNAi) was first discovered by Fire, Mello et al. as a natural cellular process of gene silencing via double-stranded RNAs [23] and has since evolved into a powerful tool to not only probe gene function, but also treat disorders. In RNAi, double stranded RNA duplexes of 21-23 nucleotides, otherwise known as small interfering RNA (siRNA) molecules, are introduced into the cytoplasm of a cell. These siRNAs bind to the Argonaute protein, an essential catalytic component of the RNA-induced silencing complex (RISC). This RNA-protein complex is then guided to the homologous target mRNA. One strand of the siRNA binds to its complementary sequence which undergoes endonucleolytic cleavage, thus preventing the translation of the target mRNA into protein [24]. The guide strand bound to RISC can serve as a template in multiple degradation cycles.

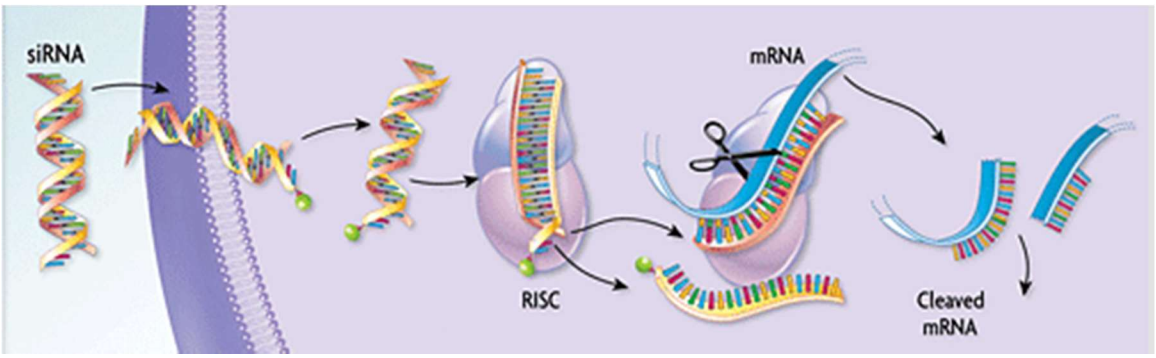

Figure 2.1 Schematic of RNAi mechanism. siRNA enters cytoplasm of cell and binds to RISC, which binds to complementary mRNA and cleaves it. (Source: Biogene Blog, https://www.creative-biogene.com/blog/in)

2.2.2 Advantages of RNAi

Due to its highly specific targeting via base-pair interactions, an almost unrestricted choice of targets, low production costs compared with protein therapies, and minimal side effects [25], RNAi has gained traction as an important alternative therapy. Recent clinical trials have included studies in retinal degeneration, dominantly inherited brain and skin diseases, viral infections, respiratory disorders, cancer and metabolic diseases [26].

2.2.3 RNAi for cancer treatment

In its first human clinical trial, delivered siRNA via a targeted nanoparticle delivery system showed localization at melanoma tumors and a reduction in the target mRNA (M2 subunit of ribonucleotide reductase (RRM2)) and its associated protein when compared to pre-dosing tissue [27]. This demonstrated for the first time, the ability of siRNA to silence genes in humans. The potential of RNAi in inhibiting oncogenesis has also been proven in a host of in vitro studies [28]. For example, the RAS oncogenes that are implicated in pancreatic and colon carcinomas often only contain a point mutation that differentiates them from their normal counterparts. A study by Brummelkamp et al. used siRNA to target the oncogenic K-RAS allele and found that siRNA could not only specifically and stably inhibit expression of the oncogenic allele, but also lead to a loss of anchorage-independent

growth and tumorigenicity [29].

2.2.4 RNAi for HIV treatment

Apart from cancer, infectious diseases has been labeled as another promising target of this new technology. The current treatment, highly active antiretroviral therapy (HAART), suffers from issues such as drug resistance and toxicity [30]. To overcome the problem of drug resistance, siRNA has been introduced directly during HIV-encoded viral transcripts [31, 32], directing RNAi to multiple regions of the viral genome. Alternatively, one could use RNAi to interfere with the function of the co-factors necessary for HIV survival. For example, Martinez et al. showed that siRNA could block the expression of two HIV entry co-receptors, CXCR4 and CCR5, and therefore inhibit infection of cells by the X4 or R5 HIV strains [33]. Thus, RNAi presents a promising alternative therapy to HIV treatment.

2.2.5 Limitations of RNAi

RNAi technology presents encouraging revolutionary potentials in tackling otherwise difficult diseases today. Yet, despite the excitement over its novel clinical applications, the technology still faces a few drawbacks. The first is its off-target effect. The siRNA guide strand may interact with other non-targets with similarity in sequences, thus silencing extraneous genes. Careful design of the siRNA sequences and rigorous testing is therefore needed to ensure specificity and to minimize off-targeting effect [34]. Secondly, many siRNAs are immunostimulatory as they are recognized by toll-like receptors and induce excessive cytokine release and other undesired inflammatory effects. This immunostimulatory effect can be mediated by the chemical modification of the siRNA, such as the introduction of 2'-O-methyl-modified nucleotides [35]. The most difficult challenge RNAi technology faces, however, is its need for a delivery mechanism. Without a delivery mechanism, naked RNA is rapidly degraded *in vivo* and is unable to penetrate cells due to its negative charge (~40 negative phosphate charges) and large size (~13kDa) [36].

2.2.6 Types of RNAi Delivery Systems

2.2.6.1 Modified naked siRNA

Naked siRNA faces difficulties in reaching the cytoplasm of the cells to express any therapeutic effect. Currently, three types of gene delivery systems are available to address this problem, namely modified naked siRNA, viral and non-viral vectors. Naked siRNAs can be modified to increase nuclease stability, cell uptake and gene silencing efficiency, while reducing immune responses and off-target effects. For example, modifications at the 2' position of the ribose ring protect siRNA from endonuclease degradation [37]. Cholesterol-conjugated siRNAs are widely used to improve uptake in liver cells via low-density lipoprotein uptake system [26].

2.2.6.2 Viral vectors

Viral vectors include adenovirus, lentivirus and herpes simplex virus. For example, DNA-based siRNA constructs targeting vascular endothelial growth factor were incorporated into lentivirus and adenovirus vectors and shown to downregulate gene expression as well as induce anti-neovascularization effects in animal models [38].

However, although viral vectors have a high gene silencing efficiency, the safety risks that accompany them, namely their potential for mutagenicity and their inflammatory and immunogenic effects, severely limit their clinical applicability and thus make non-viral vectors a more attractive option as a siRNA delivery vehicle.

2.2.6.3 Non-viral vectors

There are many different types of non-viral siRNA vectors. For instance, Jensen et al. designed a spherical gold nanoparticles conjugated with siRNA duplexes to combat Glioblastoma [39]. There are various different categories of non-viral vectors.

2.2.6.3.1 Lipid carriers

The two major categories of non-viral vectors are lipid and polymeric carriers. Among the lipid systems, cationic liposomes are the most common siRNA carriers as their positive charges help to stabilize the negatively charged nucleic acid [40], thus improving the low transfection efficiency as compared to neutral liposomes. As such, some cationic liposomes, such as Lipofectamine 2000 and Oligofectamine are now commercially available and have been demonstrated to provide protection from enzymatic degradation as well as efficient gene silencing [41, 42].

2.2.6.3.2 Polymeric nanoparticles

The recent advances in nanotechnology have also made the use of polymeric nanoparticles popular for gene delivery. By incorporating natural polymers such as chitosan, poly(lactic-co-glycolic acid) (PLGA) and polyethyleneimine [43] [43], researchers have created carriers with low toxicity, high biodegradability and biocompatibility [44]. In particular, cationic polymers such as PEI, increase cell transfection due to their charge, protect the siRNA against degradation and induce intracellular release from endosomes based on the "proton-sponge effect" [45, 46].

In a study by Höbel et al., PEI complexed with siRNA showed efficient vascular endothelial growth factor knockdown upon gene delivery, leading to reduced tumor cell proliferation and angiogenesis with no hepatotoxicity or other side effects [47]. A further advantage of NPs is that they can be functionalized to target specific cells. For example, Dickerson et al. decorated the surface of siRNA-loaded nanogels with the ephrin mimetic peptide (YSA peptide) which binds to the ephrin type A receptor 2 (EphA2 receptor) on ovarian cancer cells, thus offering targeted delivery of the epidermal growth factor receptor (EGFR)-inhibiting siRNA to the specific site [48].

2.3 Layer by Layer (LbL) nanoparticles

2.3.1 Mechanism of LbL self-assembly

The layer-by-layer (LbL) self-assembly technique is a unique method to create cationic nanoparticles with multiple layers of siRNA for higher RNAi loading and prolonged release while still maintaining cell penetration and RNA protection. The technique was first introduced in the 1990s by Gero Decher [49] to synthesize multilayered films composed of polycationic and polyanionic polymers. The assembly process is driven mainly by electrostatic interactions, but other driving forces, such as hydrogen bonding [50-53], hydrophobic interactions [51, 54], van der Waals forces [55], covalent bonding [56, 57], metal coordination [58, 59] and bio-specific recognition [60, 61] have also been explored. To prepare these LbL particles, a charged substrate is first immersed in a solution of an oppositely charged polyelectrolyte. After enough time is given for the first monolayer to be adsorbed, the substrate is removed and washed to remove excess uncoated polyelectrolyte. The substrate is then dipped into the second polyelectrolyte, whose charge is opposite to the previous polyelectrolyte, thus reversing the charge of the particle. This process can then be repeated as many times as one desires, enabling one to choose the number of layers for the particle as well as the composition of each layer [62] (see Figure 2.2 below).

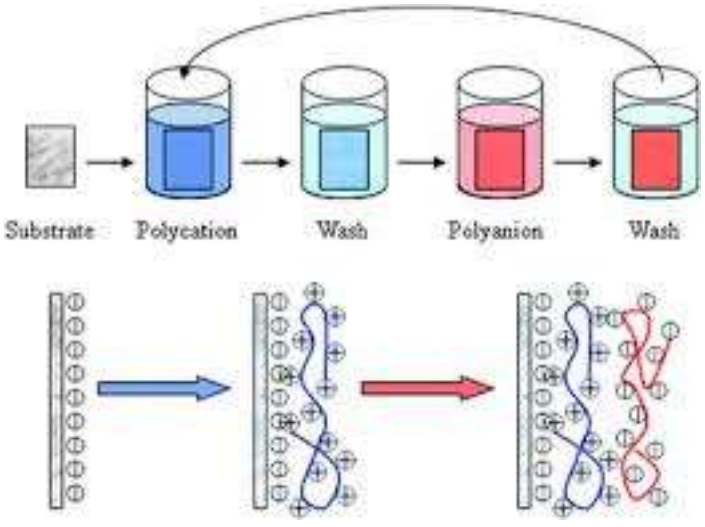

Figure 2.2 Schematic of LbL self-assembly process [63].

2.3.2 Advantages of LbL self-assembly technique

The LbL self-assembly process offers numerous advantages. First of all, the design flexibility in the number of layers allows the researcher to tune the amount of drug loaded, whereas traditional nanovectors have a fixed loading capacity. In addition, by changing the pH at which the assembly process is carried out, studies have shown that further tuning can be done to the amount of drug loaded [64]. Secondly, it allows for multiple therapeutics to be encapsulated in one particle, thus increasing potency and minimizing the problem of drug resistance.

For example, Deng et al. constructed a LbL nanoparticle with both the anticancer drug doxorubicin and siRNA, resulting in an enhanced effect of reduction in target gene expression in breast cancer tumors by 80% [65]. Furthermore, more research is being conducted on tuning the release profiles of the therapeutic from each layer such that the release of appropriate drug could be controlled by the surrounding temperature or pH, making this technology highly attractive in the field of targeted nanomedicine [66-68].
Finally, the assembly process is usually performed in aqueous medium with little mechanical force where the drug or nucleic acid involved is not degraded [69]. With all the mentioned advantages, this facile, rapid and versatile technique has thus opened avenues for the consistent and manipulated control of therapeutic delivery vehicle design, making it an extremely attractive option for clinical application.

2.3.3 Application of LbL nanoparticles: gene silencing for liver diseases

LbL nanoparticles has various applications in gene therapy. One example is the cysteamine modified gold nanoparticle (AuCM)/siRNA/PEI/hyaluronic acid (HA) as synthesized by Lee et al. via the LbL method [70]. The HA allows active targeting of the LbL nanoparticles to the liver cells, which are abundant in HA receptors. The goal is to deliver ApoB-specific siRNA and silence ApoB, a protein responsible for carrying cholesterol to tissues which is also related to liver cirrhosis. LbL nanoparticles were assembled as shown in Figure 2.3 and tested for their cellular uptake and *in vitro* target-specific gene silencing effect of ApoB.

The mean hydrodynamic size of the final particle was 37.3 ± 8.8 nm with a final zeta potential of -12.1 ± 1.5mV.

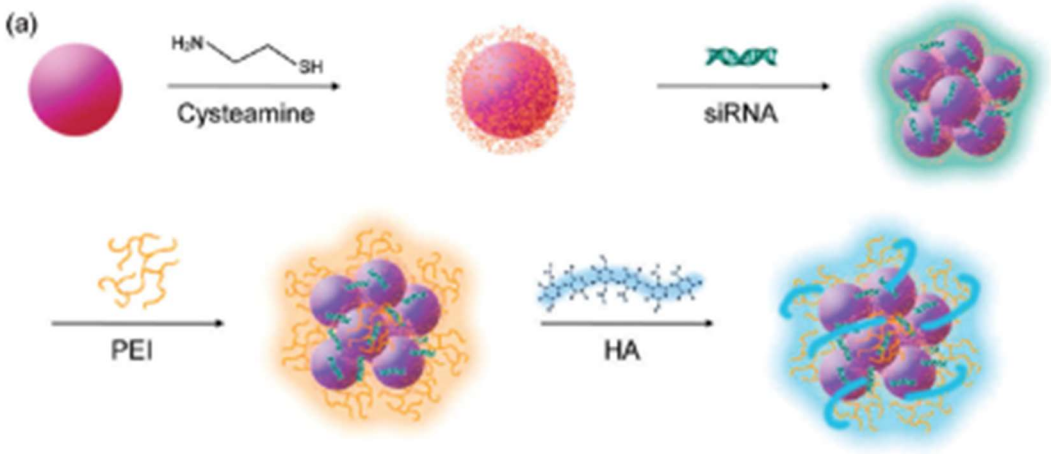

Figure 2.3 Schematic representation for the preparation of the layer-by-layer assembled AuCM/siRNA/PEI/HA complex [70].

Transmission electron microscopy (TEM) analysis showed cellular uptake of the particles after a 24h incubation period. *In vitro* gene silencing in B16F1 cells with the LbL particles reduced mRNA levels by 70%, which was significantly higher than the c.a. 20% observed by the Lipofectamine gold standard. There was also a dose-dependent *in vivo* gene-silencing effect with the reduction of ApoB mRNA by 20% with the highest dosage of 1.8nmol of siRNA/mouse. Thus, this complex was concluded to have potential for the target-specific treatment of various liver diseases.

2.3.4 LbL nanoparticles for gene therapy

With regards to RNAi therapy, LbL particles present an added potential advantage because the multiple layers can possibly ensure the repetitive administration of the siRNA as the layers degrade. Prolonged gene silencing is one of the main challenges siRNA delivery systems face as the siRNA is diluted upon cell division, quickly degraded and not renewed [71]. Thus, the silencing effect is often transient. LbL particles with multiple layers offer long-lasting controlled release, resulting in a prolonged gene silencing effect. In fact, a

three-week long effect was demonstrated both *in vitro* and *in vivo* with a multi-layered siRNA and polypeptide LbL particle [72].

Furthermore, siRNA LbL nanoparticles were reported to have an extended serum half-life of up to 28 h, which is much higher than the reported half-life of siRNA-loaded nanoparticles [65, 73]. Thus, in this study, LbL particles were the chosen gene therapy delivery vehicle due to their ability to protect siRNA from degradation, as well as their prolonged gene silencing effect.

2.3.5 Design of LbL nanoparticles

2.3.5.1 Choice of core material

Previous studies with LbL particles have used melamine formaldehyde [74], polystyrene latex, gold nanoparticles and silica as the cores, as well as biocompatible materials such as calcium carbonate, and poly(D.L-lactide-co-glycolide) (PLGA) [75]. For example, Wan et al. fabricated LbL particles with silica as the core and alternate layers of cationic poly (allyl amine hydrochloride) and anionic polyelectrolyte P (DMA-co-TPAMA). The model drug molecules of Rhodamine B and cisplatin were incorporated into the layers and their co-release was found to be triggered by a pH of 5-6 [76]. This pH-dependent release is desired when targeting the acidic tumor environment. A study by Lee et al. [70] used gold nanoparticles as the core material with assembled layers of cationic PEI and siRNA for the silencing of apolipoprotein B (ApoB) in liver cells. This LbL complex caused a drastic dose-dependent reduction of ApoB mRNA to ~20%.

Hydroxyapatite (HA) is a complex material found in tooth enamel and bone that is becoming an important candidate biomaterial. Due to its excellent biocompatibility and bioactivity, HA crystals are currently being used as bone implants or as coatings on prostheses [77, 78]. HA nanoparticles have also been investigated for their role as non-viral gene carriers [79, 80], and anti-cancer drug delivery vehicles [81]. The one drawback of HA as a biomaterial, however, is that the ultimate fate of HA nanoparticles within the body is currently unknown and studies have reported that a multiplicity of factors including

particle shape, cell type and dosage per cell influence cytotoxicity of the particles *in vitro* [82]. In order to address the issue of cell cytotoxicity, preliminary studies have tracked the movement of these particles within the cell and revealed that the majority of the nanoparticles are dissolved within the lysosomes within 24 h of uptake [83].

HA was chosen as a core material for the LbL particles as its slow dissolution made it suitable for a prolonged-release vector, while its biocompatibility and low cytotoxicity as substantiated by multiple studies [84-86] made it an attractive biomaterial for gene therapy. However, further clearance studies on fibroblast cells in particular would have to be conducted to confirm that HA as a core material has minimal cytotoxic effect.

2.3.5.2 Choice of cationic polyelectrolyte

The positively charged layers of the LbL particle are typically comprised of cationic polypeptides such as poly-L-lysine, or native and synthetic polymers such as chitosan and polyethyleneimine [43]. Poly-l-arginine (ARG) was selected for this design due to its high cationic property, transfection efficiency and low cytotoxicity [65]. ARG is the only polypeptide with side groups that are charged at almost every pH (the pKa of the side groups is 12.5), and is therefore a strong polycation, ideal for LbL NP fabrication [87].

Furthermore, when ARG is coated onto cores such as liposomes, the resultant particles show the highest transfection efficiency when compared to other polypeptide coatings such as poly-l-lysine [88]. This high transfection efficiency is further associated with low cytotoxicity as measured by the MTT assay when ARG nanoparticles are administered to cells [89]. This combination would facilitate entry of the designed LbL particle into the cell, while maintaining cell viability.

2.3.5.3 Choice of target gene for silencing

The layers of ARG are alternated with negatively-charged siRNA designed to silence *SPARC* (secreted protein, acidic and rich in cysteine). Also known as osteonectin and BM-

40, SPARC is a 32 kDa calcium-binding matricellular protein responsible for the modulation of cell-extracellular matrix (ECM) interactions and collagen assembly [90]. *SPARC* expression has been associated with various fibrotic diseases [91-94], as well as atherosclerotic lesions [95], with higher levels of SPARC transiently found at sites of wound healing [96, 97] and tissue remodeling [98].

On the contrary, in the absence of SPARC, animals were unable to generate a robust fibrotic response to an injury [99] and had lower levels of collagen when compared to wild-type animals [100]. As a result, there is strong evidence for the effect of SPARC on fibrosis, and specifically, in the production of collagen. The specific binding mechanism between SPARC and collagen is described by Hohenster et al. [90].

As a certain level of collagen is still necessary to maintain structural integrity in the fibroblast cells, a direct knockdown of collagen is unadvisable. As SPARC only modulates collagen production associated with the fibrotic response, targeting SPARC is an indirect method of reducing collagen levels without interfering with normal functionality. As such, *SPARC* siRNA has been explored as an anti-fibrotic tool in both *in vitro* and *in vivo* studies [101, 102]. In a study by Seet et al. [103], *SPARC*-null mice not only had less collagen than their wild-type counterparts after a glaucoma filtration surgery, but after 14 days, 87% of the mice with the SPARC deficiency retained their blebs for aqueous filtration, resulting in an increase in both surgical survival and filtration efficiency. These findings led themselves to the hypothesis that SPARC can be a highly effective anti-fibrotic tool to prevent post-operative subconjunctival scarring after a glaucoma filtration surgery.

For the first time, *SPARC*-silencing siRNA will be incorporated in an LbL system based on HA and ARG and investigated as a biocompatible, effective anti-scarring agent with prolonged effect. The agent will aim at having a prolonged silencing effect (14 days) on collagen RNA (brought about by silencing *SPARC* RNA) to inhibit scar tissue formation. The LbL system serves to protect the *SPARC* siRNA layers from phagocytosis, enabling more efficient and effective cellular uptake and subsequent release of *SPARC* siRNA to silence *SPARC* RNA, achieving prolonged knock down effect in *SPARC* gene.

References

[1] M. Cesareo, E. Ciuffoletti, F. Ricci, F. Missiroli, M. A. Giuliano, R. Mancino, C. Nucci, in *Progress in Brain Research*, Vol. Volume 221 (Eds: B. Giacinto, N. Carlo), Elsevier, 2015, 359-374.

[2] H. A. Quigley, A. T. Broman. *British Journal of Ophthalmology*. **2006**, 90, 262-267.

[3] H. A. Quigley. *The Lancet*. 377, 1367-1377.

[4] P. Karagianni, C. Sampanis, C. Katsoulis, G. Miserlis, S. Polyzos, I. Zografou, S. Stergiopoulos, I. Douloumbakas, C. Zamboulis. *Hippokratia*. **2009**, 13, 93-96.

[5] L. V. K. Dina Erickson, Garrett R. Scott. *Primary Care Optometry News*. **2014**.

[6] E. M. Addicks, H. A. Quigley, W. Green, A. L. Robin. *Archives of Ophthalmology*. **1983**, 101, 795-798.

[7] S.-P. A. Atreides, G. L. Skuta, A. C. Reynolds. *International Ophthalmology Clinics*. **2004**, 44, 61-106.

[8] D. A. Morris, M. O. Peracha, D. H. Shin, C. Kim, S. C. Cha, Y. Y. Kim. *Archives of Ophthalmology*. **1999**, 117, 1149-1154.

[9] J.-g. Yang, N.-x. Sun, L.-j. Cui, X.-h. Wang, Z.-h. Feng. *Acta pharmacologica Sinica*. **2009**, 30, 413-423.

[10] D. S. Greenfield, I. J. Suñer, M. P. Miller, T. A. Kangas, P. F. Palmberg, H. W. Flynn, Jr. *Archives of Ophthalmology*. **1996**, 114, 943-949.

[11] E. D. MUCKLEY, R. A. LEHRER. *Optometry and Vision Science*. **2004**, 81, 499-504.

[12] L. J. Katz, L. B. Cantor, G. L. Spaeth. *Ophthalmology*. **1985**, 92, 959-963.

[13] E. J. Higginbotham, R. K. Stevens, D. C. Musch, K. O. Karp, P. R. Lichter, T. J. Bergstrom, G. L. Skuta. *Ophthalmology*. **1996**, 103, 650-656.

[14] P. T. Zacharia, S. R. Deppermann, J. S. Schuman. *American journal of ophthalmology*. **1993**, 116, 314-326.

[15] R. C. Nagarwal, P. N. Singh, S. Kant, P. Maiti, J. K. Pandit. *Chemical and Pharmaceutical Bulletin*. **2011**, 59, 272-278.

[16] T. Shao, X. Li, J. Ge. *Diagnostic pathology*. **2011**, 6, 64.

[17] N. C. Deva, J. Zhang, C. R. Green, H. V. Danesh-Meyer. *Inflammation*. **2012**, 35, 1276-1286.

[18] T. T. Wong, A. L. Mead, P. T. Khaw. *Investigative ophthalmology & visual science*. **2003**, 44, 1097-1103.

[19] S. Arslan, O. Aydemir, M. Güler, A. F. Dağlı. *Current eye research*. **2012**, 37, 228-233.

[20] A. L. Mead, T. T. Wong, M. F. Cordeiro, I. K. Anderson, P. T. Khaw. *Investigative Ophthalmology & Visual Science*. **2003**, 44, 3394-3401.

[21] S. Grisanti, P. Szurman, M. Warga, R. Kaczmarek, F. Ziemssen, O. Tatar, K. U. Bartz-Schmidt. *Investigative ophthalmology & visual science*. **2005**, 46, 191-196.

[22] M. R. Butler, C. M. P. Ponce, Y. E. Weinstock, S. Orengo-Nania, P. Chevez-Barrios, B. J. Frankfort. *Investigative ophthalmology & visual science*. **2013**, 54, 4982-4990.

[23] A. Fire, S. Xu, M. K. Montgomery, S. A. Kostas, S. E. Driver, C. C. Mello. *nature*. **1998**, 391, 806-811.

[24] M. Stevenson. *New England Journal of Medicine*. **2004**, 351, 1772-1777.

[25] R. K. M. Leung, P. A. Whittaker. *Pharmacology & Therapeutics*. **2005**, 107, 222-239.

[26] B. L. Davidson, P. B. McCray. *Nature Reviews Genetics*. **2011**, 12, 329-340.

[27] M. E. Davis, J. E. Zuckerman, C. H. J. Choi, D. Seligson, A. Tolcher, C. A. Alabi, Y. Yen, J. D. Heidel, A. Ribas. *Nature*. **2010**, 464, 1067-1070.

[28] Z. Wang, D. D. Rao, N. Senzer, J. Nemunaitis. *Pharmaceutical research*. **2011**, 28, 2983-2995.

[29] T. R. Brummelkamp, R. Bernards, R. Agami. *Cancer cell*. **2002**, 2, 243-247.

[30] K. Barton, B. Burch, N. Soriano‐Sarabia, D. M. Margolis. *Clinical Pharmacology & Therapeutics*. **2013**, 93, 46-56.

[31] C. D. Novina, M. F. Murray, D. M. Dykxhoorn, P. J. Beresford, J. Riess, S.-K. Lee, R. G. Collman, J. Lieberman, P. Shankar, P. A. Sharp. *Nature medicine*. **2002**, 8, 681-686.

[32] N. S. Lee, T. Dohjima, G. Bauer, H. Li, L. Ming-Jie, A. Ehsani, P. Salvaterra, J. Rossi. *Nature biotechnology*. **2002**, 20, 500.

[33] M. A. Martínez, A. Gutiérrez, M. Armand-Ugón, J. Blanco, M. Parera, J. Gómez, B. Clotet, J. A. Esté. *Aids*. **2002**, 16, 2385-2390.

[34] A. L. Jackson, S. R. Bartz, J. Schelter, S. V. Kobayashi, J. Burchard, M. Mao, B. Li, G. Cavet, P. S. Linsley. *Nature biotechnology*. **2003**, 21, 635-637.

[35] A. D. Judge, G. Bola, A. C. Lee, I. MacLachlan. *Molecular Therapy*. **2006**, 13, 494-505.

[36] Y. Zhang, A. Satterlee, L. Huang. *Molecular Therapy*. **2012**, 20, 1298-1304.

[37] Y.-L. Chiu, T. M. Rana. *Rna*. **2003**, 9, 1034-1048.

[38] B. Guo, Y. Zhang, G. Luo, L. Li, J. Zhang. *The Anatomical Record*. **2009**, 292, 633-639.

[39] S. A. Jensen, E. S. Day, C. H. Ko, L. A. Hurley, J. P. Luciano, F. M. Kouri, T. J. Merkel, A. J. Luthi, P. C. Patel, J. I. Cutler. *Science translational medicine*. **2013**, 5, 209ra152-209ra152.

[40] K. Glebova, A. Marakhonov, A. Baranova, M. Y. Skoblov. *Molecular Biology*. **2012**, 46, 349-361.

[41] W. J. Kim, C.-W. Chang, M. Lee, S. W. Kim. *Journal of controlled release*. **2007**, 118, 357-363.

[42] C. Yuan, E. J. Zins, A. F. Clark, A. J. Huang. **2007**, 13, 2083-2095.

[43] K. Xu, D. A. Cantu, Y. Fu, J. Kim, X. Zheng, P. Hematti, W. J. Kao. *Acta biomaterialia*. **2013**, 9, 8802-8814.

[44] Y. Gao, X.-L. Liu, X.-R. Li. *Int J Nanomedicine*. **2011**, 6, 1017-1025.

[45] O. Boussif, F. Lezoualc'h, M. A. Zanta, M. D. Mergny, D. Scherman, B. Demeneix, J.-P. Behr. *Proceedings of the National Academy of Sciences*. **1995**, 92, 7297-7301.

[46] J.-P. Behr. *CHIMIA International Journal for Chemistry*. **1997**, 51, 34-36.

[47] S. Höbel, I. Koburger, M. John, F. Czubayko, P. Hadwiger, H. P. Vornlocher, A. Aigner. *The journal of gene medicine*. **2010**, 12, 287-300.

[48] E. B. Dickerson, W. H. Blackburn, M. H. Smith, L. B. Kapa, L. A. Lyon, J. F. McDonald. *Bmc Cancer*. **2010**, 10, 10.

[49] G. Decher. *science*. **1997**, 277, 1232-1237.

[50] S. Bai, Z. Wang, J. Gao, X. Zhang. *European polymer journal*. **2006**, 42, 900-907.

[51] T. Serizawa, S. Kamimura, N. Kawanishi, M. Akashi. *Langmuir*. **2002**, 18, 8381-8385.

[52] E. Hao, T. Lian. *Langmuir*. **2000**, 16, 7879-7881.

[53] E. Kharlampieva, S. A. Sukhishvili. *Journal of Macromolecular Science, Part C: Polymer Reviews*. **2006**, 46, 377-395.

[54] N. Kotov. *Nanostructured Materials*. **1999**, 12, 789-796.

[55] M. Sato, M. Sano. *Langmuir*. **2005**, 21, 11490-11494.

[56] J. Chen, L. Huang, L. Ying, G. Luo, X. Zhao, W. Cao. *Langmuir*. **1999**, 15, 7208-7212.

[57] G. K. Such, J. F. Quinn, A. Quinn, E. Tjipto, F. Caruso. *Journal of the American Chemical Society*. **2006**, 128, 9318-9319.

[58] H. Lee, L. J. Kepley, H. G. Hong, T. E. Mallouk. *Journal of the American Chemical Society*. **1988**, 110, 618-620.

[59] M. Wanunu, A. Vaskevich, S. R. Cohen, H. Cohen, R. Arad-Yellin, A. Shanzer, I. Rubinstein. *Journal of the American Chemical Society*. **2005**, 127, 17877-17887.

[60] Y. Lvov, K. Ariga, I. Ichinose, T. Kunitake. *Journal of the Chemical Society, Chemical Communications*. **1995**, 2313-2314.

[61] T. Hoshi, S. Akase, J.-i. Anzai. *Langmuir*. **2002**, 18, 7024-7028.

[62] P. Li, N. Zhang. *Current gene therapy*. **2011**, 11, 58-73.

[63] Y. Xiang, S. Lu, S. P. Jiang. *Chemical Society Reviews*. **2012**, 41, 7291-7321.

[64] B. Jiang, J. B. Barnett, B. Li. *Nanotechnol Sci Appl*. **2009**, 2, 21-27.

[65] Z. J. Deng, S. W. Morton, E. Ben-Akiva, E. C. Dreaden, K. E. Shopsowitz, P. T. Hammond. *ACS Nano*. **2013**, 7, 9571-9584.

[66] K. C. Wood, J. Q. Boedicker, D. M. Lynn, P. T. Hammond. *Langmuir*. **2005**, 21, 1603-1609.

[67] B. G. De Geest, N. N. Sanders, G. B. Sukhorukov, J. Demeester, S. C. De Smedt. *Chemical Society Reviews*. **2007**, 36, 636-649.

[68] A. G. Skirtach, A. M. Yashchenok, H. Möhwald. *Chemical Communications*. **2011**, 47, 12736-12746.

[69] K. Ariga, Y. M. Lvov, K. Kawakami, Q. Ji, J. P. Hill. *Advanced drug delivery reviews*. **2011**, 63, 762-771.

[70] M.-Y. Lee, S.-J. Park, K. Park, K. S. Kim, H. Lee, S. K. Hahn. *ACS nano*. **2011**, 5, 6138-6147.

[71] Y. Takabatake, Y. Isaka, M. Mizui, H. Kawachi, S. Takahara, E. Imai. *Biochemical and biophysical research communications*. **2007**, 363, 432-437.

[72] S. K. Lee, C. H. Tung. *Advanced functional materials*. **2013**, 23, 3488-3493.

[73] A. Akinc, M. Goldberg, J. Qin, J. R. Dorkin, C. Gamba-Vitalo, M. Maier, K. N. Jayaprakash, M. Jayaraman, K. G. Rajeev, M. Manoharan. *Molecular Therapy*. **2009**, 17, 872-879.

[74] U. Manna, S. Patil. *Langmuir*. **2009**, 25, 10515-10522.

[75] Y. F. Tan, R. C. Mundargi, M. H. A. Chen, J. Lessig, B. Neu, S. S. Venkatraman, T. T. Wong. *Small*. **2014**, 10, 1790-1798.

[76] X. Wan, G. Zhang, S. Liu. *Macromolecular rapid communications*. **2011**, 32, 1082-1089.

[77] D. Wahl, J. Czernuszka. *Eur Cell Mater*. **2006**, 11, 43-56.

[78] A. Moroni, F. Pegreffi, M. Cadossi, A. Hoang-Kim, V. Lio, S. Giannini. *Expert review of medical devices*. **2005**, 2, 465-471.

[79] S. Zhu, K. Zhou, B. Huang, S. Huang, F. Liu, Y. Li, Z. Xue, Z. Long. *Sheng wu yi xue gong cheng xue za zhi= Journal of biomedical engineering= Shengwu yixue gongchengxue zazhi*. **2005**, 22, 980-984.

[80] S. Bisht, G. Bhakta, S. Mitra, A. Maitra. *International journal of pharmaceutics*. **2005**, 288, 157-168.

[81] P. Venkatesan, N. Puvvada, R. Dash, B. P. Kumar, D. Sarkar, B. Azab, A. Pathak, S. C. Kundu, P. B. Fisher, M. Mandal. *Biomaterials*. **2011**, 32, 3794-3806.

[82] X. Zhao, S. Ng, B. C. Heng, J. Guo, L. Ma, T. T. Y. Tan, K. W. Ng, S. C. J. Loo. *Archives of toxicology*. **2013**, 87, 1037-1052.

[83] M. Motskin, D. Wright, K. Muller, N. Kyle, T. Gard, A. Porter, J. Skepper. *Biomaterials*. **2009**, 30, 3307-3317.

[84] V. Uskoković, D. P. Uskoković. *Journal of biomedical materials research Part B: Applied biomaterials*. **2011**, 96, 152-191.

[85] A. Y. P. Mateus, C. C. Barrias, C. Ribeiro, M. P. Ferraz, F. J. Monteiro. *Journal of Biomedical Materials Research Part A*. **2008**, 86, 483-493.

[86] M. Ferraz, A. Mateus, J. Sousa, F. Monteiro. *Journal of Biomedical Materials Research Part A*. **2007**, 81, 994-1004.

[87] A. Díez-Pascual, P. Shuttleworth. *Materials*. **2014**, 7, 7472.

[88] P. Opanasopit, J. Tragulpakseerojn, A. Apirakaramwong, T. Ngawhirunpat, T. Rojanarata, U. Ruktanonchai. *Int. J. Nanomedicine*. **2011**, 6, 2245-2252.

[89] M. Lozano, G. Lollo, M. Alonso-Nocelo, J. Brea, A. Vidal, D. Torres, M. Alonso. *Journal of nanoparticle research*. **2013**, 15, 1515.

[90] E. Hohenester, T. Sasaki, C. Giudici, R. W. Farndale, H. P. Bächinger. *Proceedings of the National Academy of Sciences*. **2008**, 105, 18273-18277.

[91] X. Zhou, F. K. Tan, J. D. Reveille, D. Wallis, D. M. Milewicz, C. Ahn, A. Wang, F. C. Arnett. *Arthritis & Rheumatism*. **2002**, 46, 2990-2999.

[92] A. Francki, A. D. Bradshaw, J. A. Bassuk, C. C. Howe, W. G. Couser, E. H. Sage. *Journal of Biological Chemistry*. **1999**, 274, 32145-32152.

[93] R. H. Pichler, C. Hugo, S. J. Shankland, M. J. Reed, J. A. Bassuk, T. F. Andoh, D. M. Lombardi, S. M. Schwartz, W. M. Bennett, C. E. Alpers. *Kidney international*. **1996**, 50, 1978-1989.

[94] C. Kuhn, R. J. Mason. *The American journal of pathology*. **1995**, 147, 1759.

[95] C. R. Dhore, J. P. Cleutjens, E. Lutgens, K. B. Cleutjens, P. P. Geusens, P. J. Kitslaar, J. H. Tordoir, H. M. Spronk, C. Vermeer, M. J. Daemen. *Arteriosclerosis, thrombosis, and vascular biology*. **2001**, 21, 1998-2003.

[96] A. D. Bradshaw, M. J. Reed, E. H. Sage. *Journal of Histochemistry & Cytochemistry*. **2002**, 50, 1-10.

[97] M. Reed, P. Puolakkainen, T. Lane, D. Dickerson, P. Bornstein, E. H. Sage. *Journal of Histochemistry & Cytochemistry*. **1993**, 41, 1467-1477.

[98] T. F. Lane, E. H. Sage. *The FASEB Journal*. **1994**, 8, 163-173.

[99] T. P. Strandjord, D. K. Madtes, D. J. Weiss, E. H. Sage. *American Journal of Physiology-Lung Cellular and Molecular Physiology*. **1999**, 277, L628-L635.

[100] B. S. Harris, Y. Zhang, L. Card, L. B. Rivera, R. A. Brekken, A. D. Bradshaw. *American Journal of Physiology-Heart and Circulatory Physiology*. **2011**, 301, H841-H847.

[101] X. Zhou, F. K. Tan, X. Guo, F. C. Arnett. *Arthritis & Rheumatism*. **2006**, 54, 2626-2631.

[102] A. M. Camino, C. Atorrasagasti, D. Maccio, F. Prada, E. Salvatierra, M. Rizzo, L. Alaniz, J. B. Aquino, O. L. Podhajcer, M. Silva, G. Mazzolini. *The Journal of Gene Medicine*. **2008**, 10, 993-1004.

[103] L.-F. Seet, R. Su, V. Barathi, W. S. Lee, R. Poh, Y. M. Heng, E. Manser, E. N. Vithana, T. Aung, M. Weaver. *PloS one*. **2010**, 5, e9415.

Chapter 3

Experimental Methodology

This chapter describes the materials, fabrication methodology and experimental methodology used in this work. The Layer by Layer nanoparticle fabrication method is described in this chapter. How the designed particle configuration came to be was also described. The characterization methods of the particles fabricated are detailed, together with the various in vitro and in vivo experiments conducted to prove the effectiveness of the designed particle in prolonged gene silencing in this chapter.

3.1 Materials

The siRNAs used in this study were: scrambled control siRNA 5'-GCUCACAGCUCAAUCCUAAUC-3', *SPARC* siRNA 5'-AACAAGACCUUCGACUCUUCC-3'. These siRNAs as well as fluorescein isothiocyanate (FITC)-tagged *SPARC* siRNA were custom-synthesized and purchased from Bioneer Corp. (South Korea). The hydroxy apatite nanopowder (<200 nm diameter) used in this study was purchased from Sigma-Aldrich (USA). The Poly-L-Arginine HCl (molecular weight > 70000 Da) used in this study was purchased from Sigma-Aldrich (USA).

3.2 Methods

3.2.1 Preparation of siRNA LbL Nanoparticles

The LbL nanoparticle fabrication was based on previously established method [1]. Hydroxyapatite (HA) nanoparticles at 10 mg/ml, were added to a 0.5 mg/ml ARG solution, in a volume ratio of 1:10, with maximum vortex mixing and light sonication for 10 minutes. The ARG-coated nanoparticles were suspended in 0.1 M NaCl and mixed with siRNA for 1 h. Subsequently, the ARG-siRNA coated nanoparticles were exposed to another coating with a 0.5 mg/mL ARG solution. The nanoparticles were then resuspended in sterile phosphate buffered saline (PBS) and stored at 4 ˚C before use. This method will generate a three-layer configuration, HA-ARG-siRNA-ARG. To study the effects of increasing loads of siRNA in this configuration, the ARG-coated particles were incubated with 0.4, 0.8 or 1.2 pmol of siRNA per μg HA. To study the effects of increasing siRNA layers, five-layer configuration (HA-ARG-siRNA-ARG-siRNA-ARG) was obtained where the above coating steps were repeated with 1.2 pmol of siRNA per μg HA and finally another layer of ARG with 0.5 mg/ml ARG solution.

3.2.2 Cell culture and Particle Optimization

Primary conjunctival fibroblasts were obtained from the eyes of C57BL6/J mice and cultured as previously described [2]. The fibroblasts were cultured in DMEM supplemented with 10% FBS and 1% penicillin/streptomycin. Cells at passages of 6 or less were used.

Gene silencing of siRNA LbL nanoparticles was assessed in primary conjunctival fibroblasts. Briefly, 30000 cells/well were seeded on 12-well plates overnight, and treated with LbL nanoparticles. To study the effects of increasing loads of siRNA in three-layer configuration (HA-ARG-siRNA-ARG), 108 μg of LbL particles (ARG-coated particles incubated with 0.4, 0.8 or 1.2 pmol of siRNA per μg HA) were added to the cells. To study the effects of increasing another layer of siRNA in the LbL particles, 108 μg of single siRNA layer LbL particles (HA-ARG-siRNA-ARG) and 108 μg of double siRNA layer LbL particles (HA-ARG-siRNA-ARG-siRNA-ARG) were treated to cells. The cells added with *SPARC* siRNA LbL nanoparticles were compared with cells added with scrambled control siRNA nanoparticles. After treatment for 7 or 14 days, the cells were trypsinised and mRNA expression was analysed by real-time quantitative polymerase chain reaction (qPCR). The optimised particle configuration was then decided upon based on qPCR data. Subsequent studies will only focus on the optimised particle configuration.

3.2.3 Quantitative real-time PCR Assay for Cells

Conjunctival fibroblasts were processed and analysed as described previously [2]. RNA was extracted with RNeasy Kit (Qiagen, Singapore) in accordance to the manufacturer's instructions. First strand cDNA was synthesized using random hexamer primer (Invitrogen Co. Singapore) with Superscript III reverse transcriptase (Invitrogen Co. Singapore) according to the manufacturer’s instructions. qPCR was performed in a total volume of 10 μL in 384-well microtiter plates. Amplification and analysis of cDNA fragments were conducted using the Roche LightCycler 480 System (Roche Diagnostics Corp, Indianapolis, USA). All qPCR reactions were performed in triplicate. All mRNA levels were measured

as CT threshold levels. The best housekeeping gene was determined using the NormFinder software [3]. Actb and Rpl13a were the best housekeeping genes for the 7- and 14-day cultures respectively. Values were calculated as fold change by the 2-ΔΔCT method. Data is presented as fold changes relative to corresponding treatment with control scrambled siRNA. The primers used were as follows: Actb-forward, 5'-CACCCGCGAGCACAGCTTCT-3', and Actb-reverse, 5'-CGTTGTCGACGACCAGCGCA-3'; Rpl13a-forward, 5'-GAGGTCGGGTGGAAGTACCA-3', and Rpl13a-reverse, 5'-TGCATCTTGGCCTTTTCCTT-3'; *SPARC*-forward, 5'-AAACATGGCAAGGTGTGTCA-3', and *SPARC*-reverse, 5'-AAGTGGCAGGAAGAGTCGAA-3'; Col1a1-forward, 5'-CCCACCCCAGCCGCAAAGAG-3', and Col1a1-reverse, 5'-GCCATGCGTCAGGAGGGCAG-3'.

3.2.4 Physicochemical characterization

The electrophoretic mobility of the nanoparticles after the coating of each layer was measured in 0.2 μm filtered 0.1 M NaCl at room temperature using a Malvern Zetasizer 2000 (Malvern Instruments, UK). The zeta potential (ζ-potential) was calculated from the electrophoretic mobility (μ) using the Smoluchowski function $\zeta = \mu\eta/\varepsilon$ where η and ε were the viscosity and permittivity of the solvent respectively. Since the nanoparticles synthesized were charged, the surrounding ions near the nanoparticles in the solution will be distributed into an electrical double layer. The zeta potential of the nanoparticles was the potential at the slipping plane. The zeta size of the nanoparticles was measured based on dynamic light scattering theory using the same equipment. The zeta size measured was the hydrodynamic size of the nanoparticles. A total of 3 readings were measured for each sample and the experiment was conducted at least 3 times.

Field emission scanning electron microscopy (FESEM) was performed using the JEOL JSM-7600F microscope. The synthesized nanoparticles were freeze dried, scattered on carbon tape pasted on metal stubs and sputtered with gold before imaging with FESEM.

Transmission electron microscopy (TEM) was performed using the Carl Zeiss AG- Libra 120 TEM microscope (Carl Zeiss AG, Germany).

3.2.5 Cell Proliferation Assay

Cell proliferation analysis was performed using the xCelligence real time cell analyser (Roche Diagnostics GmbH, Penzberg, Germany) according to manufacturer's instructions. Fibroblasts were seeded onto the E-Plate 96 wells (Roche Diagnostics GmbH, Germany) at 5000 cells/well in normal culture medium, in triplicates, and treated with increasing amounts (9, 18, 27 and 216 μg) of nanoparticles loaded with either scrambled or *SPARC* siRNA. Adherent cell growth/density was monitored continuously for at least 14 days.

3.2.6 Cellular Uptake Assays

Cellular uptake of nanoparticles was assessed by confocal microscopy and flow cytometry. The confocal microscopic images were taken using the LSM 510 Meta Laser Scanning Confocal Microscope (Zeiss, Jena, Germany). Briefly, cells were seeded in a 4-well cover slip base chamber (Nalgene Nunc International, Napperville, IL, USA) at 5000 cells per well, treated with 18 μg of five-layered LbL nanoparticles loaded with FITC tagged *SPARC* siRNA and incubated at 37°C. The cells were imaged at a few time points after treatment (30 min, 1 h, 2 h, 4 h, 8 h, 12 h, 1 day, 7 days and 14 days). Cell nuclei were imaged by UV excitation of NucBlue staining. All time interval images were compared with control cells without particle treatments with the same imaging settings to ensure the controls showed no green FITC signals. The quantity of uptake was measured by flow cytometry. Briefly, the cells were seeded in 12-well plates at 30000 cells per well, treated with 0.108 mg of five-layered fluorescently labelled nanoparticles and trypsinized after incubation for 30 min, 1 hour, 2 hours, 4 hours, 8 hours, 12 hours, 1 day, 7 days and 14 days at 37°C. The cells were then resuspended in 200 μl of PBS containing 0.4% trypan blue to quench cell surface-bound fluorescence. The cell-associated fluorescence was measured by the Guava easyCyte System and the data analysed using the GuavaExpress Pro software (EMD Millipore, USA). All time interval cytometry samples were compared with control cells

without particle treatments. Only FITC signals of samples higher than the controls were considered positive FITC signals.

To ascertain that the particles end up in lysosomes after uptake, cells were seeded in a 4-well cover slip base chamber (Nalgene Nunc International, Napperville, IL, USA) at 5 × 10^3 cells per well, treated with 18 μg of five-layered LbL nanoparticles with TRITC tagged HA and incubated at 37°C. Two days after treatment, CellLight (lysosome GFP stain, Thermo Fisher Scientific) was added to the cells and incubated overnight to stain the MCF lysosomes green. The next day, the cell samples were washed, fixed and prepared for confocal scanning microscopy (CLSM) to observe for colocalisation of NPs and lysosomes.

3.2.7 Mouse Model of Conjunctival Fibrosis

The mouse model of conjunctival fibrosis was performed as described previously [4]. Wild type C57BL6/J mice used for this study were bred and maintained at the Department of Experimental Surgery (Singapore General Hospital, Singapore). All experiments with animals were approved by the Institutional Animal Care and Use Committee (IACUC) and treated in accordance with the Association for Research in Vision and Ophthalmology (ARVO) Statement on the Use of Animals in Ophthalmic and Vision Research. Experimental surgery was conducted on the left eye of each mouse to induce scarring. 108 μg LbL nanoparticles in 5 μl PBS, loaded with either scrambled or *SPARC* siRNA, were administered by direct injection into the conjunctiva at the surgical site immediately after surgery. Slit lamp microscopy was performed using the Righton NS2D digital slit lamp (Right Mfg. Co. Ltd., Tokyo, Japan). The mice were sacrificed and the conjunctival tissues harvested for evaluation after 7 or 14 days.

3.2.8 Tissue Apoptosis Assay

Annexin V in the conjunctival tissues was measured by flow cytometry. Apoptosis in the harvested tissues was measured using the Guava Nexin Reagent (EMD Millipore, USA) according to manufacturer's instructions. Five thousand cells were analysed for each

sample in a total of 5 samples for each condition (n=5). Cell populations were quantified using the Guava Nexin software (EMD Millipore, USA).

3.2.9 Quantitative real-time PCR Assay for Tissues

Tissues injected with nanoparticles from 5 mice were pooled as one group in a total of 5 groups for each condition (n=5). Tissues from the contralateral untreated eyes in each group of mice were similarly pooled and used as baseline for calculation of fold change in mRNA expression in each group. Conjunctival tissues were processed for qPCR as described previously [2]. RNA preparation, qPCR reactions and primer sequences were the same as that described for *in vitro* experimentation mentioned above. The best housekeeping gene was determined using the NormFinder software [3] to be Actb for both 7- and 14-day tissues. Data is presented as fold changes relative to contralateral untreated, unoperated eyes.

3.2.10 Immunoblotting Assay

Tissue samples from 5 mice were pooled as one group in a total of 3 groups for each condition (n=3). Conjunctival tissues from mice treated with nanoparticles were harvested after 7 or 14 days and processed as described previously [2]. Briefly, total tissue lysates were prepared by homogenization and lysis in a solution containing 20 mM Tris-buffer, pH 7.4, 150 mM NaCl, 1 mM EDTA, 0.5% Triton X-100, 2 mM MgCl2, 1 mM dithiothreitol, and 1x Complete Protease Inhibitors (Roche Diagnostics GmbH, Mannheim, Germany) followed by SDS-polyacrylamide gel electrophoresis and immunoblotting. Antibodies against SPARC and GAPDH were purchased from Cell Signalling Technology (Massachusetts, USA) and Santa Cruz Biotechnology, Inc. (Santa Cruz, CA, USA) respectively. The antibody against type I collagen was from MD Bioproducts (St Paul, MN, USA). Horseradish peroxidase (HRP)–conjugated secondary antibodies were from Jackson ImmunoResearch Laboratories, Inc. (West Grove, PA, USA). Densitometric quantitation was performed using advanced imaging technology Image Lab (Bio-Rad Laboratories, Inc., Hercules, California). Normalization to correct for variations in loading was performed

using GAPDH as the housekeeping protein.

3.2.11 Histochemical and Immunofluorescence Assays

Histological, picrosirius red polarization microscopy and immunofluorescence evaluation of cryosections of 14 day-old treated eyes were performed as described previously [2]. Antibodies against type I collagen, CD45 and F4/80 were obtained from Novus Biologicals (USA), BD Pharmingen (New Jersey, USA), and Abcam (Cambridge, UK) respectively. Labelling by the type I collagen antibody was detected using secondary antibodies conjugated to Alexa Fluor-594 (Invitrogen, Eugene, OR, USA) while labelling by the CD45 and F4/80 antibodies were detected using secondary antibodies conjugated to Alexa Fluor-488 (Invitrogen, Eugene, OR, USA). Nuclei were visualized by mounting the cells in DAPI-containing Vectashield mounting medium (Vector Laboratories, CA, USA). Labelled cells were visualized using the Olympus FluoView FV1000 confocal microscope (Olympus Corporation, Tokyo, Japan) while polarization microscopy was performed using the Nikon Eclipse Ti microscope (Nikon Instruments Inc., NY, USA).

3.2.12 Release Study

The release behaviour of FITC tagged siRNA from the three and five-layered particles were observed in PBS over a span of 14 days. Three-layered LbL particles and five-layered LbL particles fabricated with 1 mg HA respectively were dispersed in 600 µl of PBS and incubated at 37˚C with constant shaking over 14 days. The doses of particles were disassembled by overnight treatment of trypsin to find the total siRNA contents after measurements with the Tecan plate reader. At the stipulated time points, the particle samples were centrifuged down and the supernatant collected and measured with the Tecan plate reader to affirm release amount compared against a series of FITC siRNA standard curve (Tecan readings taken of FITC siRNA of known concentrations). Fresh PBS was added for subsequent time point measurements. All samples and measurements were conducted in triplicates.

3.2.13 FRET Pair Study

To investigate the disassembling behaviour of the designed LbL NPs within cells, fluorescence resonance energy transfer (FRET) mechanism was utilised. FRET describes the energy transfer between two chromophores [5]. A donor chromophore (excited by a laser usually) can transfer energy to an acceptor chromophore through non-radiative dipole-dipole coupling [6]. The energy transfer efficiency is inversely proportional to the sixth power of the distance between donor and acceptor. Thus, FRET effect is very sensitive to the distance between donor and acceptor. This sensitivity enables measurements of FRET efficiency to be used to determine if two fluorophores are within close proximity of each other [7].

In this work, the designed LbL NP has two siRNA layers, the inner and outer siRNA layers. The two layers were investigated separately. To observe how long it will take for the two layers of siRNA to detach from the NPs once the particles were uptaken into cells, FRET pair fluorophores (FITC and TRITC) were tagged (chemically bonded) to the siRNA and adjacent Ploy-L-Arginine layers respectively. Particles (0.108 mg) were treated to 30000 MCF cells. At stipulated time points (8 h, 12 h, 1 day, 4 days, 7 days, 10 days and 14 days after treatment), the cells were trypsinized and suspended in 0.4% trypan blue, centrifuged and then suspended in 200 μL of PBS for testing with Guava flow cytometer. The cell samples were subjected to blue laser excitation (488 nm) and only the FITC tagged onto siRNA would be excited. If the adjacent TRITC tagged Poly-L-Arginine was still in close proximity, the TRITC would be able to receive the emission from FITC and get excited to release red signals. The FRET effect was measured and compared with controls (Cell samples treated with either FITC or TRITC tagged layers) over a period of time. TRITC signals were compared with TRITC signals of control cell samples treated in the same way but with particles with only TRITC tagged Poly-L-Arginine. Similarly, FITC signals were compared with FITC signals of control cell samples treated in the same way but with particles with only FITC tagged siRNA. That was done so as to only consider signals involved in FRET for the analysis.

3.2.14 Statistical Analyses

Data are expressed as mean ± standard deviation (SD). Where only two treatment conditions were compared, the significance of differences between the two conditions was determined by the two-tailed Student's t-test using the Microsoft Excel 5.0 software, with significance at $p<0.05$. Where more than two treatment conditions were compared, the significance of differences between the conditions was determined by one-way ANOVA with Bonferroni post-hoc adjustment using SPSS statistics.

References

[1] S. V. Dorozhkin. *Biomaterials*. **2010**, 31, 1465-1485.

[2] L.-F. Seet, S. Finger, S. Chu, L. Toh, T. Wong. *Current molecular medicine*. **2013**, 13, 911-928.

[3] C. L. Andersen, J. L. Jensen, T. F. Ørntoft. *Cancer research*. **2004**, 64, 5245-5250.

[4] L.-F. Seet, R. Su, V. Barathi, W. S. Lee, R. Poh, Y. M. Heng, E. Manser, E. N. Vithana, T. Aung, M. Weaver. *PloS one*. **2010**, 5, e9415.

[5] P.-C. Cheng, in *Handbook of Biological Confocal Microscopy*, Springer, 2006, 162-206.

[6] V. Helms. *Principles of computational cell biology*, *John Wiley & Sons*, **2008**.

[7] J. Zheng. *Ion channels: methods and protocols*. **2006**, 65-77.

Chapter 4

Optimisation and Characterisation of LbL NPs

This chapter describes the optimisation of Layer by Layer nanoparticles and the characterization of the optimized particles. As the objective of this project is aimed at achieving a particle configuration which enables the trafficking of enough siRNA into cells for gene silencing over 2 weeks, the amount of siRNA loading and number of siRNA layers were tweaked and investigated upon to find the optimal configuration. The optimized particle was then fabricated and characterized. This chapter will give insight to the amount of siRNA needed to achieve prolonged gene silencing over extended periods and how siRNA loaded in multiple layers affect gene silencing.

To be published as Li-Fong Seet, Yang Fei Tan, Subbu Venkatraman, Tina T. Wong entitled SPARC Silencing Reduces Collagen Deposition in the Mouse Model of Conjunctival Scarring.

4.1 Effect of siRNA loading on *SPARC* silencing

The objective of the project was to develop a delivery system for bioactive siRNA which provides prolonged *SPARC* and collagen gene silencing effect in MCF cells for a period of 2 weeks. The LbL NP system was chosen as the encapsulating carrier to provide protection for the siRNA and for efficient uptake into cells.

In order to decide on the configuration of the NP, the relationship of the *SPARC* siRNA dose loaded in a layer within LbL NPs, to *SPARC* silencing and prolonged silencing effect must be established. To do this, 3 different prototypes of 3-layered LbL NPs were synthesized with the configuration HA|ARG|siRNA|ARG. The 3 prototypes had different amounts of siRNA loaded within their siRNA layer: 0.4, 0.8 and 1.2 nmol of *SPARC* siRNA were loaded within the 3 different prototypes. About 0.1 mg of each NP type and their respective controls (NPs with the same amounts of scrambled siRNA loaded), were added to 30000 MCF cells. The treated cells were harvested on day 7 and day 14 for qPCR assay to quantify *SPARC* RNA. After normalising all data with an appropriate housekeeping gene, the RNA levels of cells treated with *SPARC* siRNA NPs were compared with their respective controls to observe for any knockdown in RNA. The results were as below:

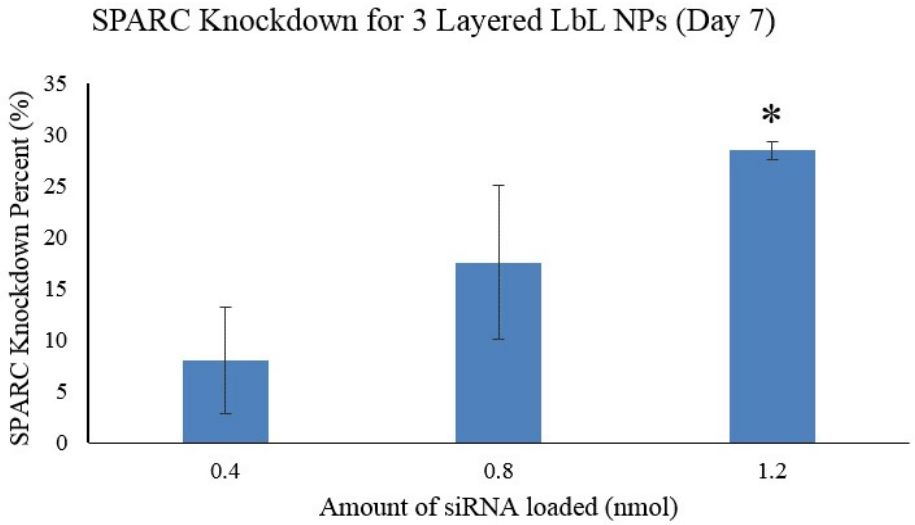

Figure 4.1 Graph showing day 7 *SPARC* RNA knockdown percent for MCF cells treated with 3 layered NPs loaded with 0.4, 0.8 and 1.2 nmol of *SPARC* siRNA compared with MCF cells treated

with control NPs loaded with respective doses of scrambled siRNA. All samples were normalized with an appropriate housekeeping gene and repeated in triplicates. $p^* < 0.05$.

The qPCR results showed that on day 7, 3 layered LbL NPs loaded with 0.4 and 0.8 nmol of *SPARC* siRNA caused *SPARC* RNA silencing of 8.01 ± 5.22 % ($p^* = 0.12$) and 17.54 ± 7.47 % ($p^* = 0.06$) respectively. However, the results were not significant when compared to their respective controls with $p^* > 0.05$ according to the student's t-test. The results showed that siRNA of 0.4 and 0.8 nmol loadings in LbL NPs were unable to achieve significant *SPARC* RNA knockdown in MCF cells after day 7 of treatment. On the other hand, the LbL NPs loaded with 1.2 nmol *SPARC* siRNA managed to silence *SPARC* RNA by 28.46 ± 0.88 % ($p^* = 0.00$) in MCF cells after day 7 of treatment when compared with controls. Furthermore, student's t-test showed that the knockdown was significant with $p^* < 0.05$. The results showed that *SPARC* RNA silencing effect in MCF cells increased with increasing *SPARC* siRNA loadings in 3 layered LbL NPs used for treatment. Generally, *SPARC* siRNA of 1.2 nmol loading within 3 layered LbL NPs were effective and sufficient in displaying significant *SPARC* RNA silencing in MCF cells after day 7 of treatment. The *SPARC* RNA silencing effect was observed after day 14 of treatment and the results were as below:

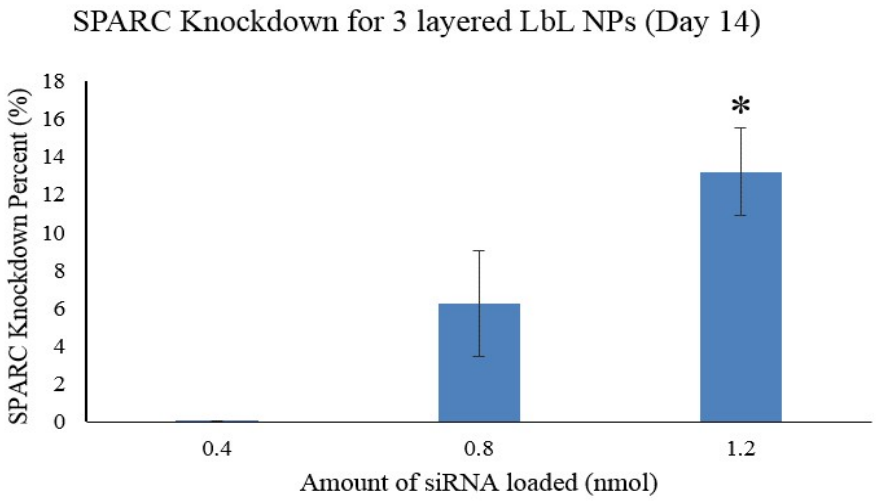

Figure 4.2 Graph showing day 14 *SPARC* RNA knockdown percent for MCF cells treated with 3 layered NPs loaded with 0.4, 0.8 and 1.2 nmol of *SPARC* siRNA compared with MCF cells treated with control NPs loaded with respective doses of scrambled siRNA. All samples were normalized with an appropriate housekeeping gene and repeated in triplicates. $p^* < 0.05$

The qPCR results showed that on day 14, 3 layered LbL NPs loaded with 0.4 and 0.8 nmol of *SPARC* siRNA caused *SPARC* RNA silencing of 0.01 ± 0.01 % (p* = 0.20) and 6.24 ± 2.82 % (p* = 0.06) respectively. The results were not significant when compared to their respective controls with p* > 0.05 according to the student's t-test. Thus it is clear that siRNA of 0.4 and 0.8 nmol loadings in LbL NPs were not able to achieve significant *SPARC* RNA knockdown in MCF cells after day 14 of treatment. In fact, as compared to day 7, both NPs showed reduced RNA silencing effect. On the other hand, the LbL NPs loaded with 1.2 nmol *SPARC* siRNA managed to silence *SPARC* RNA by 13.19 ± 2.32% (p* = 0.01) in MCF cells after day 14 of treatment when compared with controls. Furthermore, student's t-test showed that the knockdown was significant with p* < 0.05. The results showed that although the silencing effect of *SPARC* RNA in MCF cells was not as pronounced at day 14 as compared to day 7 for the 1.2 nmol *SPARC* siRNA loaded 3 layered LbL NPs treatment, there was still significant effective knockdown in *SPARC* RNA within the MCF cells at day 14, suggesting prolonged effect of *SPARC* RNA silencing for 14 days in MCF cells. It was also observed that for all 3 prototypes, the *SPARC* RNA silencing effect reduced quite significantly at day 14 as compared to day 7. That could be the result of the single siRNA layered LbL NPs fully releasing all the siRNA within the siRNA layer into the cytoplasm of the MCF cells, causing a reduction in the silencing effect as the days passed due to reduced availability of siRNA to bind to RNA within the cells.

4.2 Effect of number of siRNA layers on prolonged *SPARC* silencing effect

In order to maintain the *SPARC* RNA silencing effect level up to day 14 after treatment, an additional layer of 1.2 nmol of siRNA was added to the LbL NP configuration, resulting in the 5 layered LbL NP configuration HA|ARG|siRNA|ARG|siRNA|ARG. 0.108 mg of single (HA|ARG|siRNA|ARG) and double (HA|ARG|siRNA|ARG|siRNA|ARG) 1.2 nmol siRNA layered LbL NPs, as well as their respective scrambled siRNA loaded LbL NPs controls, were added to 30000 MCF cells in triplicates. Similar to the previous study, at day 7 and day 14 after NPs treatment, the cell samples were harvested and qPCR assays were conducted. The day 7 results were as below:

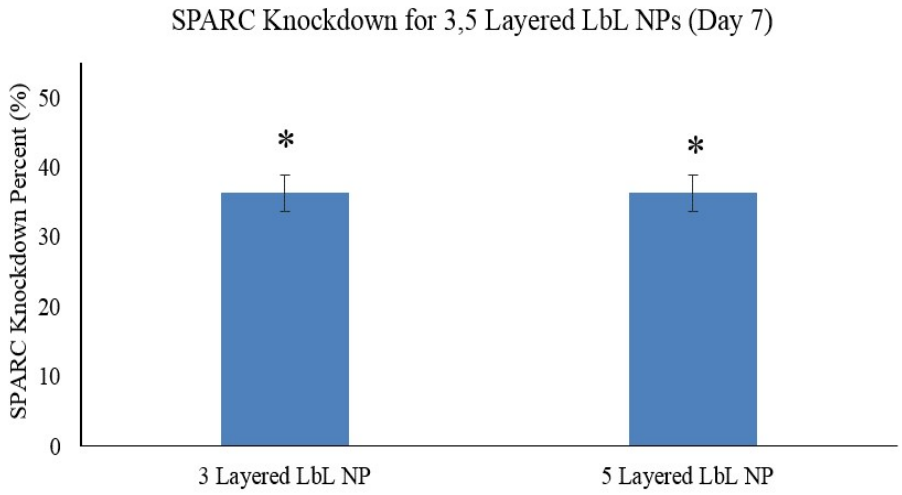

Figure 4.3 Graph showing day 7 *SPARC* RNA knockdown percent for MCF cells treated with 3/5 layered NPs loaded with 1.2 nmol of *SPARC* siRNA/siRNA layer compared with MCF cells treated with control NPs loaded with respective doses of scrambled siRNA. All samples were normalized with an appropriate housekeeping gene and repeated in triplicates. $p^* < 0.05$.

The qPCR results showed that on day 7, 3 layered LbL NPs loaded with single 1.2 nmol *SPARC* siRNA caused *SPARC* RNA silencing of 36.29 ± 2.62 % ($p^* = 0.002$) while the 5 layered LbL NPs loaded with double 1.2 nmol *SPARC* siRNA caused *SPARC* RNA silencing of 36.29 ± 2.64 % ($p^* = 0.002$). The results were both significant when compared to their respective controls with $p^* < 0.05$ according to the student's t-test. The results showed that at day 7, both prototypes delivered similar degree of siRNA silencing effect. Although the double layered siRNA NPs had twice the amount of siRNA as compared to the single layered siRNA NPs, there seemed to be no difference in silencing effect at day 7. It could be due to only one layer of the two siRNA layers releasing siRNA at day 7, thus attributing to similar silencing effect as compared to the single siRNA layered NPs. To observe if the additional siRNA layer was able to induce prolonged and more effective silencing, the cells were treated with the particles for 14 days. The results were as below:

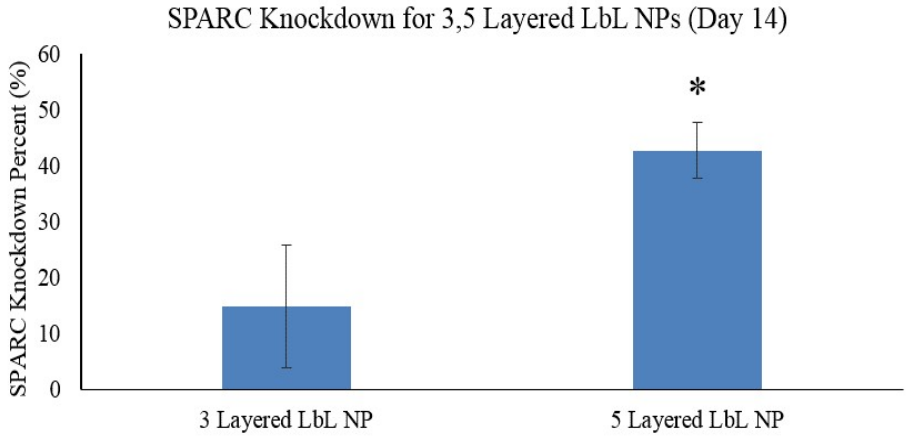

Figure 4.4 Graph showing day 14 *SPARC* RNA knockdown percent for MCF cells treated with 3/5 layered NPs loaded with 1.2 nmol of *SPARC* siRNA/siRNA layer compared with MCF cells treated with control NPs loaded with respective doses of scrambled siRNA. All samples were normalized with an appropriate housekeeping gene and repeated in triplicates. $p^* < 0.05$.

The qPCR results showed that on day 14, 3 layered LbL NPs loaded with single 1.2 nmol *SPARC* siRNA caused *SPARC* RNA silencing of 14.80 ± 10.88 % ($p^* = 0.985$) while the 5 layered LbL NPs loaded with double 1.2 nmol *SPARC* siRNA caused *SPARC* RNA silencing of 42.67 ± 4.98% ($p^* = 0.005$). Only the result of the 5 layered NPs was significant when compared to its control with $p^* < 0.05$ according to the student's t-test. The results showed that at day 14, similar to the observation mentioned earlier, the 3 layered NPs showed a reduced knockdown effect as compared to day 7. On the other hand, the 5 layered NPs with an additional siRNA layer showed a higher silencing effect at day 14 as compared to day 7. The results proved that the additional siRNA layer induced a more effective prolonged silencing effect with the *SPARC* RNA silenced increasing from 36.29% to 42.67%. The 5 layered LbL NP with double 1.2 nmol siRNA layers configuration (HA|ARG|siRNA|ARG|siRNA|ARG) was selected as the best prototype to achieve prolonged *SPARC* RNA silencing over a period of 2 weeks. This NP configuration was selected for further experimentation.

4.3 Particle Characterisation

4.3.1 Zeta size and zeta potential

After deciding on the ideal NP configuration for usage, detailed characterization was conducted on the NP. Throughout the synthesis of the 5 layered LbL NP, samples were taken after each layer was coated for analysis of their zeta size (hydrodynamic size) and zeta charge. The zeta size measured the hydrodynamic size of the particles and provided information on changes in NP size with different layers coated on the HA core. In addition, the size of the final completed NP provided information on whether the NPs were within acceptable cell uptake size. The zeta potential measurements of the various layers provided information on the charge of the particle surface, thereby revealing whether each layer was coated successfully. The measurement results were as below:

Table 4.1 Table showing zeta size and zeta potential of every layer of 5 layered LbL NP. Samples were taken after every layer of coating.

Layer by Layer Nanoparticles	Zeta size (nm)	PDI	Zeta potential (mV)
HA/ARG/	360 ± 11	0.39 ± 0.03	42 ± 1
HA/ARG/SPARC	570 ± 9	0.55 ± 0.06	-32.6 ± 0.4
HA/ARG/SPARC/ARG	275 ± 2	0.26 ± 0.02	47 ± 5
HA/ARG/SPARC/ARG/SPARC/	424 ± 4	0.46 ± 0.08	-23 ± 1
HA/ARG/SPARC/ARG/SPARC/ARG	242 ± 2	0.19 ± 0.02	49.3 ± 0.8

From the table, it was observed that the ARG layers were highly positive charged at about 42 to 49.3 mV. The *SPARC* siRNA layers were relatively highly negatively charged at about -32.6 to -23 mV. Since ARG used for coating was positive in charge while siRNA was negative in charge, it was evident that the fabrication was conducted correctly and effectively. It was also observed that the siRNA layers were generally not very compact during coating, and these were evidential from the increases in zeta size. This was remedied by the subsequent ARG coating after every siRNA coating which electrostatically held the NPs together forming more compact structures. Ana et al. [1] observed a non-linear increase in particle size with additional coating too. According to them, during LbL

assembly, particle size suffered oscillation due to the poly electrolyte nature of the outermost layer. In their work, particle size was significantly higher than 200 nm when poly styrene sulfonate (PSS) was used as the outermost coating layer of the LbL shell. They claimed that it was due to the slight aggregation process when using PSS. The behavior was reversible by the addition of the next poly allylamine hydrochloride (PAH) layer. Observed NPs restabilization was caused by the phenomenon of NPs collapse in the presence of oppositely charged polyelectrolytes able of decreasing their interparticle bridging activity. Also, this occurred due to the increased particle surface charge, which led to higher electrostatic repulsion and decrease of the area occupied by single polymer molecules. Similarly the siRNA layer in our work can be compared to the PSS layer while the poly l arginine layer in our work can be compared to their PAH layer.

The final LbL NP was about 242 nm in hydrodynamic diameter with a surface charge of 49.3 mV. The size of the NP was within cell uptake size range as it was similar in size as compared to a similar particle from a previous work [2] which could be taken up by fibroblast cells. Furthermore, studies have demonstrated that the particle size of nanoparticles ranging from 1 to 500 nm are suitable for ophthalmic formulations [3] and our particles are within the range. In addition, the NPs was designed with a positively charged ARG outermost layer. This not only protected the siRNA upon entering the cells, but also facilitated more effective and efficient cell uptake by binding electrostatically to the negatively charged cellular membranes following cell addition to MCF.

4.3.2 FESEM and TEM imaging

To observe size, shape and surface morphology of the fabricated NPs, FESEM imaging was employed. TEM imaging was also conducted to confirm the size and shape of the fabricated NPs. Images obtained were shown as below:

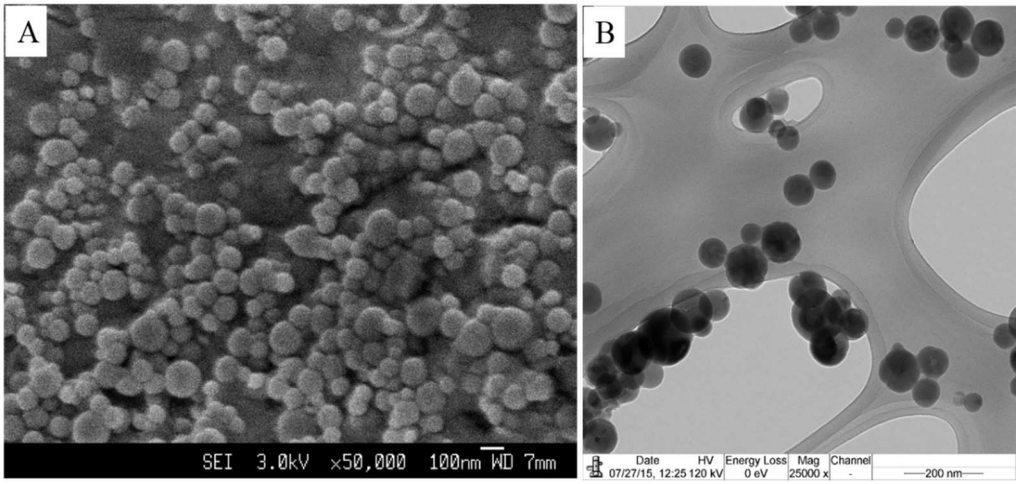

Figure 4.5 A) FESEM image of 5 layered LbL NPs, B) TEM image of 5 layered LbL NPS.

The FESEM image in Figure 4.5(A) showed that the 5 layered LbL NPs were spherical in shape and had relatively smooth surface morphologies. The NPs were observed to be smaller than 200 nm in diameter and were rather uniform in size. The TEM image in Figure 4.5(B) confirmed that the NPs was smaller than 200 nm in diameter, spherical and uniform in size.

Hence, from the surface charge, shape and size characterization data, it was affirmed that the 5 layered LbL NPs were of similar size with particles fabricated (using similar reagents) previously [2] and were expected to be taken up readily into MCF cells.

4.4 *In Vitro* Toxicity study

After completing the characterization studies on the 5 layered LbL NPs, it was ready for *in vitro* testing. To embark on any cell related tests, a toxicity study must first be conducted with the NPs on the MCF cells. Three different kinds of 5 layered LbL NPs that would be used for all *in vitro* tests were fabricated. The three 5 layered LbL NPs were, 1) NPs loaded with *SPARC* siRNA (si*SPARC*), 2) NPs loaded with scrambled siRNA (siSCRAM) and 3) NPs loaded with dextran sulphate in place of siRNA (Control). The 3 different types of NPs were added to 5000 MCF cells at varying doses of 9, 18, 27 and 216 µg. xCELLigence

was employed to track the growth of the MCF cells treated with the different NPs at different dosages in real time over a span of 14 days. The data was then represented graphically as below:

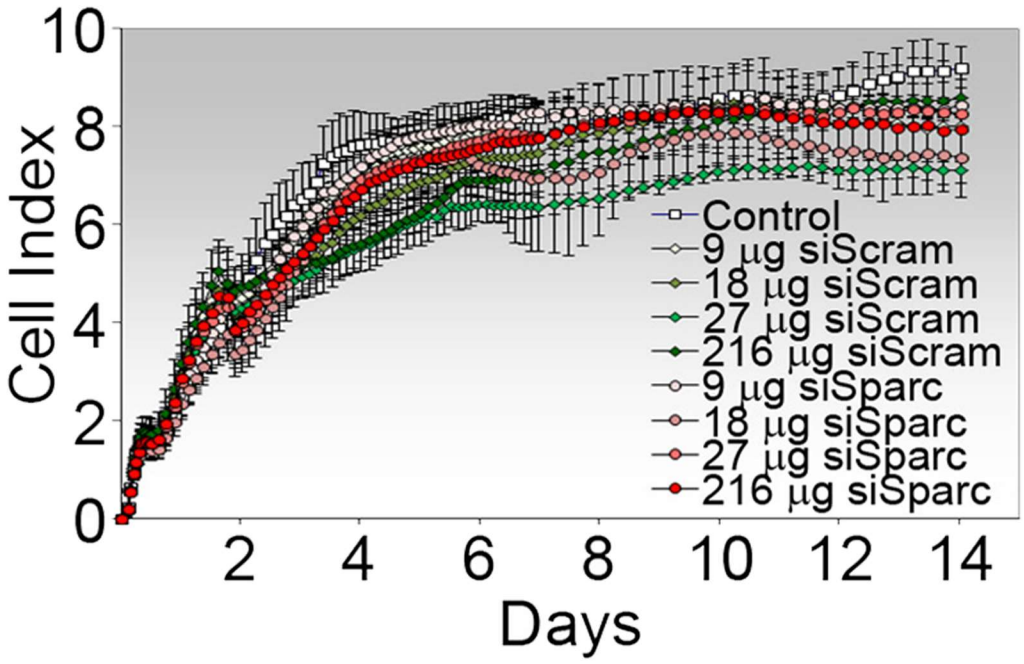

Figure 4.6 Cell viability study tracking 5000 MCF cell growth after treatment with 3 different 5 Layered LbL NPs at dosages 9, 18, 27 and 216 µg for a span of 2 weeks. The 3 LbL NPs were: a) NPs loaded with *SPARC* siRNA (si*SPARC*), b) NPs loaded with scrambled siRNA (siSCRAM) and c) NPs loaded with dextran sulphate in place of siRNA (Control).

From the cell viability graph in Figure 4.6, it was observed that all 3 types of LbL NPs at all the various dosages did not cause any toxicity effect on MCF cells over the 14 day time span. Hence, the 3 types of NPs could be used for *in vitro* tests over 14 days. Taking into consideration that *in vivo* testing of the NPs will be conducted in the mouse model after *in vitro* testing is completed, the ability to deliver the particles through a 30 gauge syringe needle was an important concern. To prevent leakage of particles from simulated glaucoma surgery site, only 5 µL of liquid volume can be injected into the subconjunctival space of the eye of a mouse. Therefore, 108 µg (for every 30000 cells meaning 18 µg for every 5000 cells) dosage was the selected dose as it was the maximum amount (after dispersing in 5

μL PBS) that could be injected at ease with the needle dedicated for subconjunctival injection in mice.

4.5 Summary

It was found that 2 layers of 1.2 nmol of *SPARC* siRNA coated onto 1 mg of HA with alternating Poly-L-arginine layers, fabricated into nanoparticles, was able to effectively reduce the amount of *SPARC* mRNA within MCF cells *in vitro* over two weeks. The optimized particle was found to have a zeta size of about 240 nm in diameter, with a zeta potential of about 50 mV. FESEM and TEM images of the particles showed that they were uniformly distributed, spherical in shape and below 200 nm in diameter. Up to 216 μg of particles added to MCF cells showed no effects in cell proliferation or toxicity. Due to the limitation in injectable volume of particles into the mice sub-conjunctival space, 108 μg of particles dispersed in 5μL PBS was selected as the dosage for the *in vivo* experiments.

References

[1] A. C. Santos, P. Pattekari, S. Jesus, F. Veiga, Y. Lvov, A. n. J. Ribeiro. *ACS applied materials & interfaces*. **2015**, 7, 11972-11983.

[2] Y. F. Tan, R. C. Mundargi, M. H. A. Chen, J. Lessig, B. Neu, S. S. Venkatraman, T. T. Wong. *Small*. **2014**, 10, 1790-1798.

[3] M. G. Qaddoumi, H. Ueda, J. Yang, J. Davda, V. Labhasetwar, V. H. Lee. *Pharmaceutical research*. **2004**, 21, 641-648.

Chapter 5

Cell Uptake and Prolonged Gene Silencing Activity

This chapter describes the uptake of the optimized LbL NP into MCF in vitro. Upon confirmation of the entry of the particles into MCF cells, SPARC and Collagen I mRNA within cells treated with the particles were quantified on day 7 and 14 to observe any gene silencing induced by the particles. With observable signs of SPARC and Collagen I gene silencing over 14 days in vitro, cells from conjunctival tissues harvested from mice treated with the particles were tested for toxicity. After verification that particle treatment used was not toxic in mice, particles were then injected into mice sub-conjunctival space post simulated glaucoma surgeries. The conjunctival tissues were then harvested on day 7 and 14 for SPARC and Collagen I mRNA and protein quantification to ascertain the effectiveness of the particles in prolonged gene silencing. Immuno-staining of cryo sections of the treated mice eye was also done to observe any toxicity and activity effects.

To be published as Li-Fong Seet, Yang Fei Tan, Subbu Venkatraman, Tina T. Wong entitled SPARC Silencing Reduces Collagen Deposition in the Mouse Model of Conjunctival Scarring.

5.1 Uptake of NPs

5.1.1 Observing Uptake Using CLSM

After finding the right dosage of NPs treatment for the MCF cells to ensure no toxicity, it was of paramount importance to investigate if the NPs were actually able to be internalised by the cells into the cytoplasm. To observe that, CLSM imaging was employed. 18 μg of 5 layered LbL NPs loaded with 2 layers of 1.2 nmol/layer FITC tagged siRNA were added to 5000 MCF cells in 4 welled cover slip base chambers. The samples were imaged at 30 min, 1 hour, 2 hours, 4 hours, 8 hours, 12 hours, 1 day, 7 days and 14 days to observe NP internalisation in MCF cells. This experiment provides information on the uptake behaviour of the NPs in MCF cells.

5.1.2 Observing Uptake Using Guava Flow Cytometry

Concurrent with CLSM imaging to observe internalisation, Guava flow cytometry was conducted to quantify the NPs internalisation into the MCF cells. A weighed amount (0.108 mg) of 5 layered LbL NPs loaded with 2 layers of 1.2 nmol/layer FITC tagged siRNA was added to 30000 MCF cells which were trypsinized at 30 min, 1 hour, 2 hours, 4 hours, 8 hours, 12 hours, 1 day, 7 days and 14 days. Next, the cells were centrifuged, re-dispersed in 150 μL of PBS and 50 μL of trypan blue (0.4%) was added to make up a total volume of 200 μL. The samples were then analyzed with flow cytometry within 30 min to quantify the FITC signals. The role of trypan blue was to quench the FITC within the NPs surface bound on the MCF cells. As trypan blue is unable to penetrate live cells, the FITC successfully entering the cells together with the NPs will not be quenched and thus can be quantified by the flow cytometry system to illustrate the amount of NPs entering the MCF cells at different time points.

5.1.3 Uptake Results

The CLSM images and Guava flow cytometry data for the *in vitro* uptake experiments were jointly presented as below:

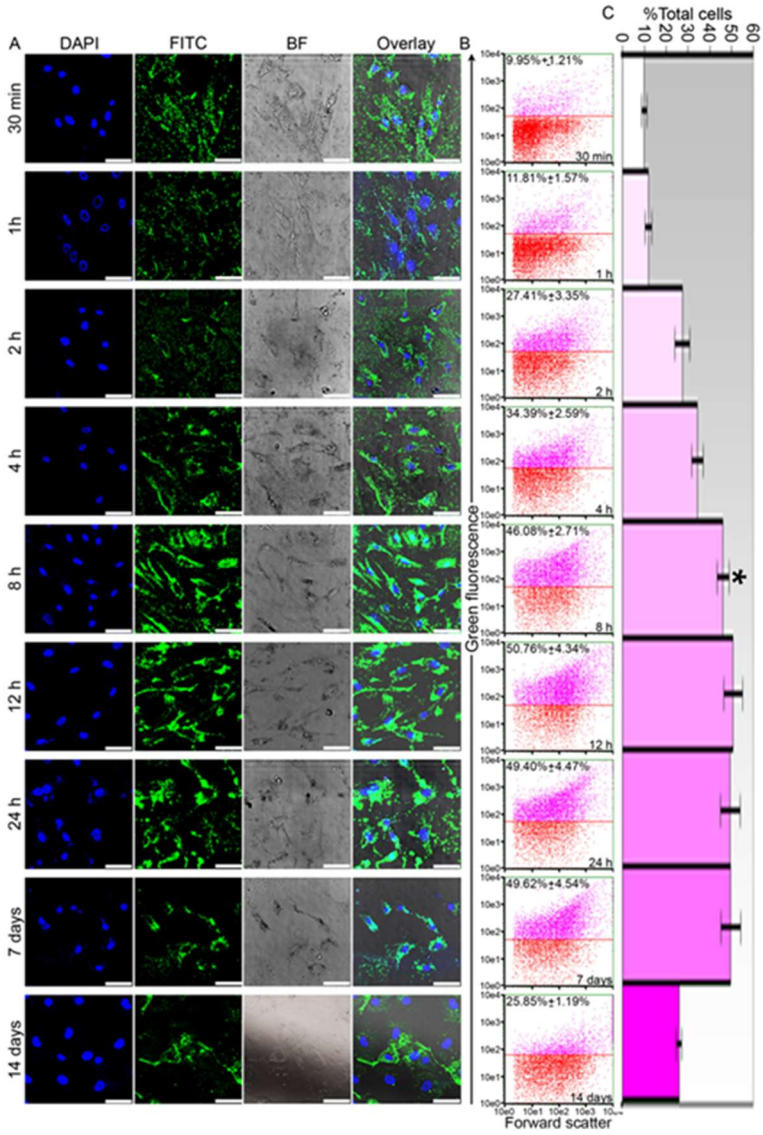

Figure 5.1 Cellular uptake of LbL nanoparticles loaded with FITC-siRNA. (A) Confocal microscopic analysis of intracellular trafficking of the LbL nanoparticles from 30 minutes to 14 days incubation with conjunctival fibroblasts. Nuclei were visualized by staining with DAPI. All time points were compared with control cells with no particle treatments, showing no green FITC signals. (B) Flow cytometry analysis of uptake of LbL nanoparticles in conjunctival fibroblasts at the same time points as (A). Representative scatter plots with gate lines are shown. Pink scatter indicate cells positive for green fluorescence, gated using cells cultured for the corresponding length of time but in the absence of nanoparticles. Indicated values denote the %mean ± SD of fluorescence-positive cells (n=3). (C) Graphical representation of the flow cytometry data in (B). *p=9.38e-3 (post-hoc Bonferroni-adjusted) between 4 and 8 h, but p>0.5 between 8 h, 12 h, 24 h and 7 days.

To verify cellular uptake of the nanoparticles, internalization of the five-layered LbL nanoparticles containing FITC-labelled *SPARC* siRNA was visualized by confocal microscopy. Internalization of the fluorescent siRNA was observed within 30 minutes of incubation and remained conspicuous even after 14 days (Figure 5.1 A). All time points were compared with control cells which were not treated with particles. All control cells showed no green FITC signals. The flow cytometry results confirmed that intracellular accumulation of the labelled siRNA increased progressively with time, with intracellular uptake detectable in 10% of the cells at 30 min, and reaching approximately 50% of total cells by 8 h (Figure 5.1 B, C). Importantly, 50% of the cells maintained the fluorescent signal for at least 7 days while at 14 days, the signal was retained in 26% of the cells (Figure 5.1 B, C). These data support the capacity of the five-layered siRNA-loaded nanoparticles to translocate rapidly into cells, and upon cell entry, maintain intracellular siRNA levels for at least 14 days.

5.2 qPCR RNA knockdown study

After affirming that the NPs in question can definitely enter the MCF cells, it was then important to investigate if the NPs which enter the cells were able to release *SPARC* siRNA into the cytoplasm to silence the *SPARC* and collagen genes, reducing the amount of *SPARC* and collagen RNA in the MCF cells. A weighed amount (0.108 mg) of 5 layered LbL NPs loaded with 2 layers of 1.2 nmol/layer *SPARC* siRNA were treated to 30000 MCF cells. On day 7 and day 14 after the treatment, the cells were trypsinized and qPCR was conducted to find out if *SPARC* and collagen RNA levels have reduced significantly as compared to control samples. As mentioned in the literature review, it was discovered that SPARC gene silencing is correlated with collagen suppression. Collagen is the silencing target gene to reduce scar tissue formation. However, as collagen is involved in various structural requirements in various cellular activities, silencing it directly can be risky. Since *SPARC* RNA spikes in amounts at injury sites, making use of this correlation to reduce collagen at injury sites is a better approach. The qPCR results are presented as follows:

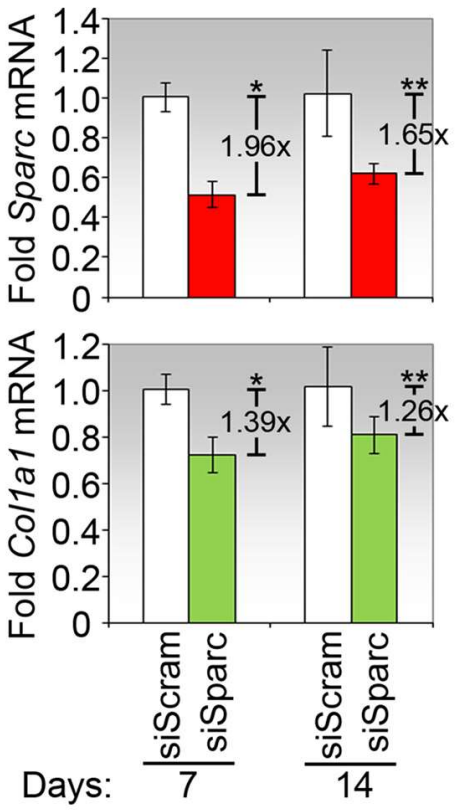

Figure 5.2 Effect of siRNA-loaded LbL nanoparticles on endogenous gene silencing. qPCR analysis of *SPARC* (top; *p=6.00e-9, **p=3.82e-7) and Col1a1 (bottom; *p=2.30e-5, **p=1.62e-3) expression upon treatment with the nanoparticles for 7 or 14 days. Indicated p values were post-hoc Bonferroni-adjusted, n=3.

Incubation of MCF cells with the five-layered LbL nanoparticles loaded with *SPARC* siRNA resulted in reduced *SPARC* mRNA expression when measured at both 7 and 14 days (Figure 5.2, top). The level of suppression was not significantly different between 7 and 14 days, indicating that the *SPARC* siRNA-loaded nanoparticles were able to sustain repression of *SPARC* expression for at least 14 days with no loss of activity *in vitro*. In addition, the five-layered *SPARC* siRNA-loaded nanoparticles were able to deliver the downstream effect of type I collagen suppression. *Col1a1* mRNA expression was reduced in both the 7- and 14-day cultures treated with the five-layered *SPARC* siRNA-loaded LbL nanoparticles (Figure 5.2, bottom). Hence, the five-layered nanoparticles have the capacity to not only deliver siRNAs that regulated gene expression, but also achieve this in a sustained manner that affect pertinent downstream pathways.

5.3 *In Vivo* Tissue Toxicity

To evaluate potential tissue toxicity of the five-layered siRNA-loaded LbL nanoparticles for *in vivo* application, experimental surgery was performed in the mouse conjunctiva using the mouse model of conjunctival scarring. GFS was conducted in mice eyes to simulate wound and scar tissue formation.

For the GFS, a slit was made at the conjunctiva of the mouse eye. A needle was then inserted through the slit to puncture the anterior chamber of the eye. Subsequently, the slit was stitched and the surgery was completed. LbL nanoparticles, loaded with either scrambled or *SPARC* siRNA, were then injected directly into the sub-conjunctival space at a concentration of 108 μg/5 μL per eye. Compared with experimental surgery alone, the injection of nanoparticles loaded with either scrambled or *SPARC* siRNAs did not increase the number of annexin V-positive cells (Figure 5.3 A, B) or cause loss of overall cell viability (Figure 5.3 A, C) after 14 days. The cell samples tested included MCF cells. Hence, the five-layered siRNA-loaded LbL nanoparticles were safe for *in vivo* applications.

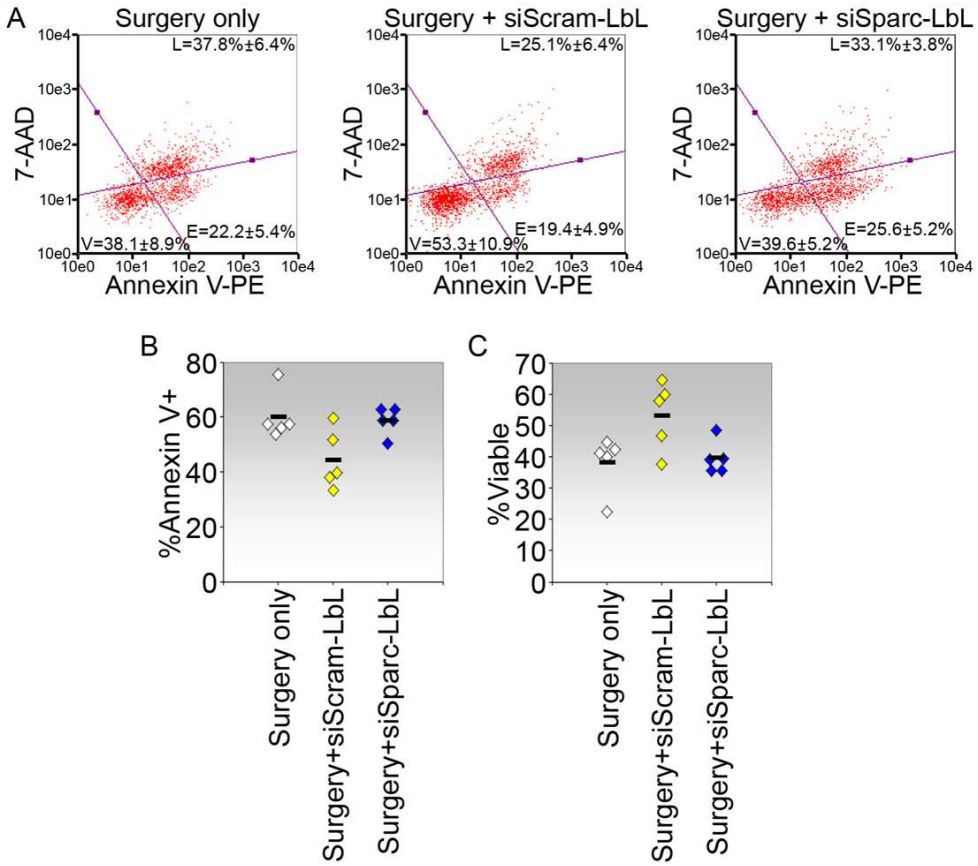

Figure 5.3 Tissue toxicity of LbL nanoparticles. (A) Representative scatter plots of annexin V-stained samples from experimental surgery alone (left), surgery cum treatment with LbL nanoparticles loaded with scrambled siRNA (middle), and surgery cum treatment with LbL nanoparticles loaded with *SPARC* siRNA. L, late apoptotic or dead cells; E, early apoptotic cells; V, viable cells. Indicated values denote the %mean ± SD of cells in the associated quadrant (n=5). (B) % annexin V-positive cells in conjunctival tissues treated as indicated. (C) % viable cells in conjunctival tissues treated as indicated. Each symbol represents a pool of tissues from 3 eyes of independent animals. Cell samples included MCF cells. Samples harvested after 14 days post treatments.

5.4 *In Vivo* Endogenous Gene Silencing and Anti-Fibrotic Effect

The capacity of the five-layered LbL nanoparticles to deliver siRNA for the regulation of *SPARC* expression was quantitatively determined at both the transcript and protein levels.

The results are presented as below:

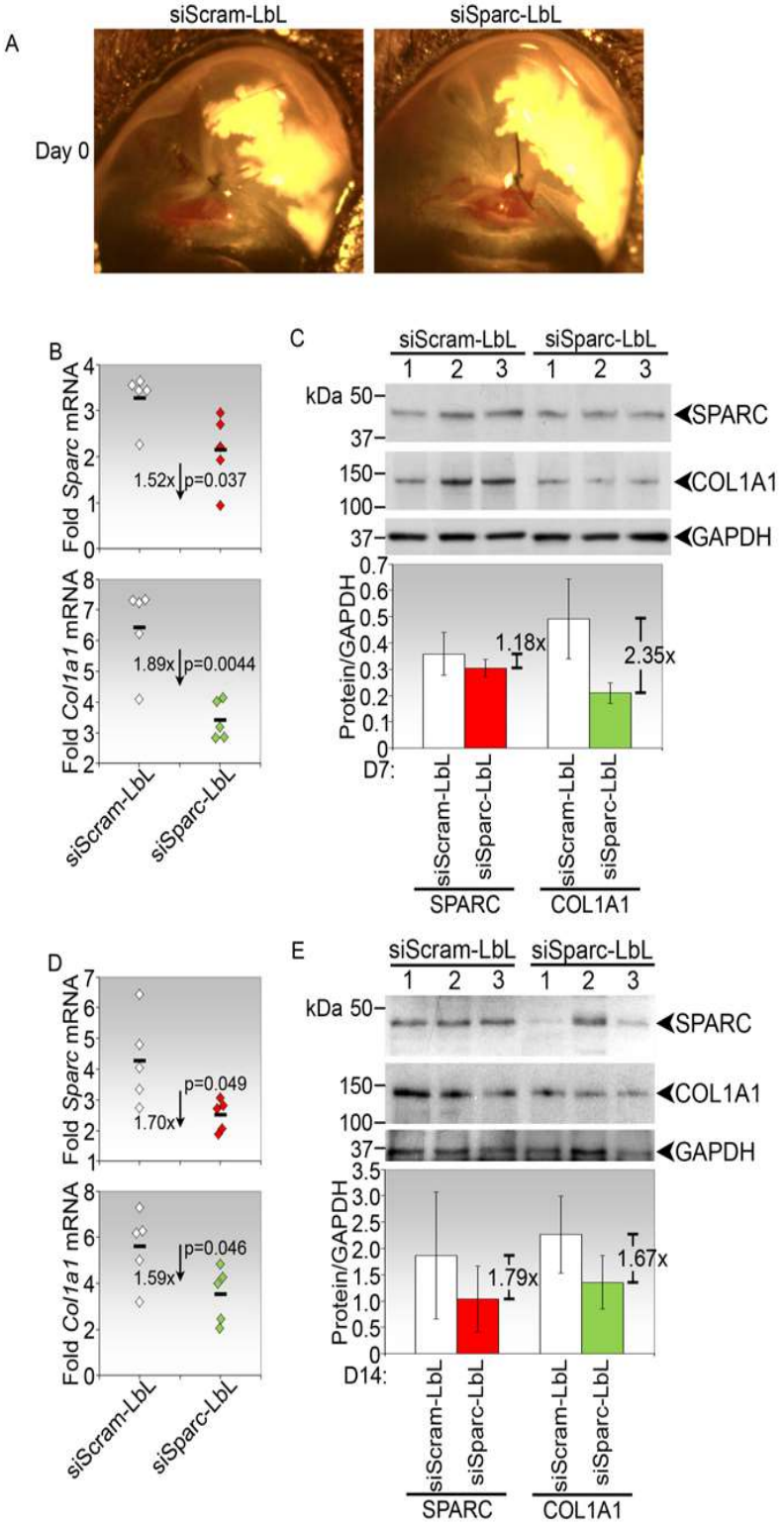

Figure 5.4 Prolonged endogenous gene silencing delivered by LbL nanoparticles in the mouse model of conjunctival scarring. (A) Slit lamp photographs of LbL nanoparticles loaded with

scrambled (left) or *SPARC* siRNAs in the conjunctiva immediately after injection post-surgery. (B) qPCR analysis of *SPARC* and Col1a1 (bottom) expression upon treatment with the nanoparticles for 7 days. The mean fold changes and the associated p values comparing the effects of *SPARC* siRNA-loaded particles against that of scrambled siRNA-loaded particles are indicated. Each symbol represents a pool of tissues from 3 eyes of independent animals. (C) Immunoblot analyses of SPARC and COL1A1 (bottom) expression upon treatment with the nanoparticles for 7 days. Densitometry values, expressed as ratios with GAPDH, are shown below. (D) qPCR analysis of *SPARC* and Col1a1 (bottom) expression upon treatment with the nanoparticles for 14 days. (D) Immunoblot analyses of SPARC and COL1A1 (bottom) expression upon treatment with the nanoparticles for 14 days.

The nanoparticles injected into the sub-conjunctival space of mouse eyes with experimental surgery can be immediately observed as coalesced white particles (Figure 5.4 A). A week after surgery, the *SPARC* siRNA-loaded LbL nanoparticles had caused a significant reduction in conjunctival *SPARC* mRNA levels by 1.52-fold compared with scrambled controls (Figure 5.4 B). Correspondingly, *Col1a1* mRNA levels were decreased by 1.89-fold relative to scramble controls (Figure 5.4 B). At the protein level, it can be observed that both SPARC and type I collagen were reduced in the tissues in mice injected with *SPARC* siRNA-loaded nanoparticles (Figure 5.4 C). Two weeks after surgery, *SPARC* expression levels remained significantly reduced in the tissues injected with *SPARC* siRNA-loaded nanoparticles by 1.70-fold with concurrent reduction of *Col1a1* mRNA expression by 1.59-fold when compared with scrambled controls (Figure 5.4 D). The levels of SPARC and type I collagen proteins were also lower in the tissues injected with the *SPARC* siRNA-loaded nanoparticles at 14 days (Figure 5.4 E). Hence, the five-layered LbL nanoparticles were effective in delivering gene silencing when loaded with siRNAs *in vivo* and possessed the capacity to prolong gene regulation along with established downstream effects.

5.5 Histopathology of Treated Eyes

The tendency of the nanoparticles to coalesce into a discrete mass may result in the adverse development of a foreign body reaction. However, histochemical examination of the operated eyes injected with either scrambled or *SPARC* siRNA-loaded LbL nanoparticles for 14 days did not reveal overt fibrous encapsulation of the coalesced nanoparticles (Figure 5.5 A). The coalesced nanoparticles were generally surrounded by collagen fibres which were neither thicker nor differ in maturation than those in the surrounding areas where nanoparticles were not present (Figure 5.5 B). Some nanoparticles appeared to settle on collagen fibres which may serve as scaffolds for stable deposition. Immunostaining with type I collagen antibody reaffirmed the lack of a collagenous capsule around the coalesced nanoparticles (Figure 5.5 C). These observations therefore suggest that the injected nanoparticles did not provoke a foreign body response since there was no apparent development of an end-stage fibrous capsule after two weeks.

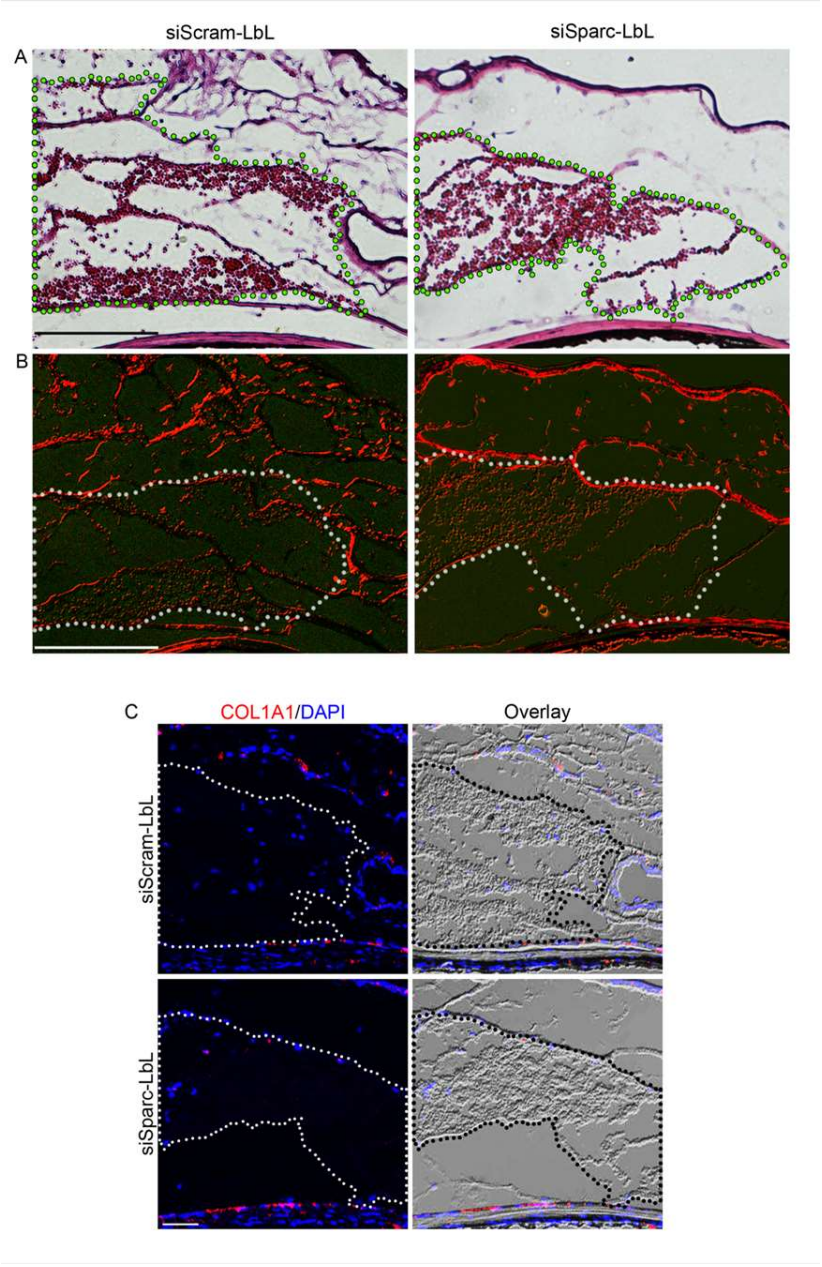

Figure 5.5 Absence of fibrous encapsulation of LbL nanoparticles in the conjunctiva at 14 days. (A) Hematoxylin and eosin staining of conjunctival tissues subjected to experimental surgery and injected with nanoparticles loaded with scrambled (left) or *SPARC* siRNA. Areas containing high density of coalesced nanoparticles are indicated by the green dotted lines. (B) Picrosirus red staining of the conjunctival tissues. Areas containing high density of coalesced nanoparticles are indicated by the white dotted lines. Scale bar, 100 μm. (C) Immunostaining of the conjunctival tissues with type I collagen antibody. Nuclei were visualized by DAPI staining (blue). Areas containing high density of coalesced nanoparticles are indicated by the dotted lines. Overlays of the immunofluorescence with bright field data are also shown. Scale bar, 50 μm.

To ascertain that there was no persistent inflammation in or near the injected nanoparticles, the 14 day-old eye sections were examined by immunostaining for proinflammatory cells. Immunolocalization with CD45, a marker for nonerythrocytic cells of hematopoietic origin, revealed the presence of a few of these cells within areas that are dense with nanoparticles (arrowheads, Figure 5.6 A). Immunostaining with F4/80, a general marker for murine macrophages, but not lymphocytes and polymorphonuclear cells, indicated that at least some of this proinflammatory mononucleated cells are derived from a macrophage lineage (arrowheads, Figure 5.6 B). Moreover, F4/80-positive cells were detected in the periphery of the area dense with nanoparticles, suggesting potential recruitment of these cells to this area. However, these cells appeared to be few in number and therefore not likely to mount a significant inflammatory response. Together, these data indicate that the five-layered LbL nanoparticles did not provoke a significant foreign body response in the treated conjunctiva, and hence their effectiveness as delivery vehicles is not expected to be diluted by host protective mechanisms.

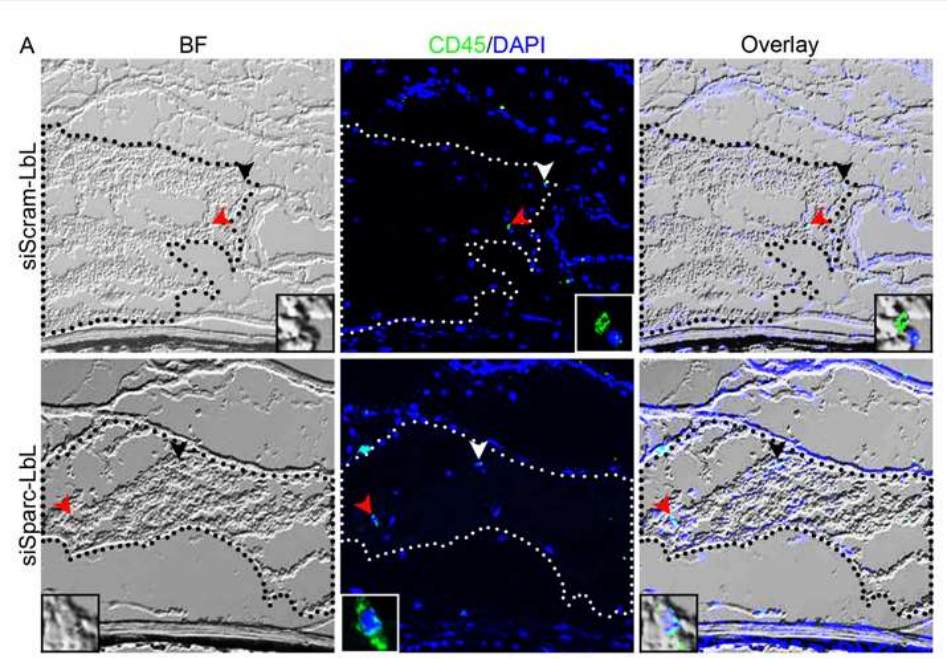

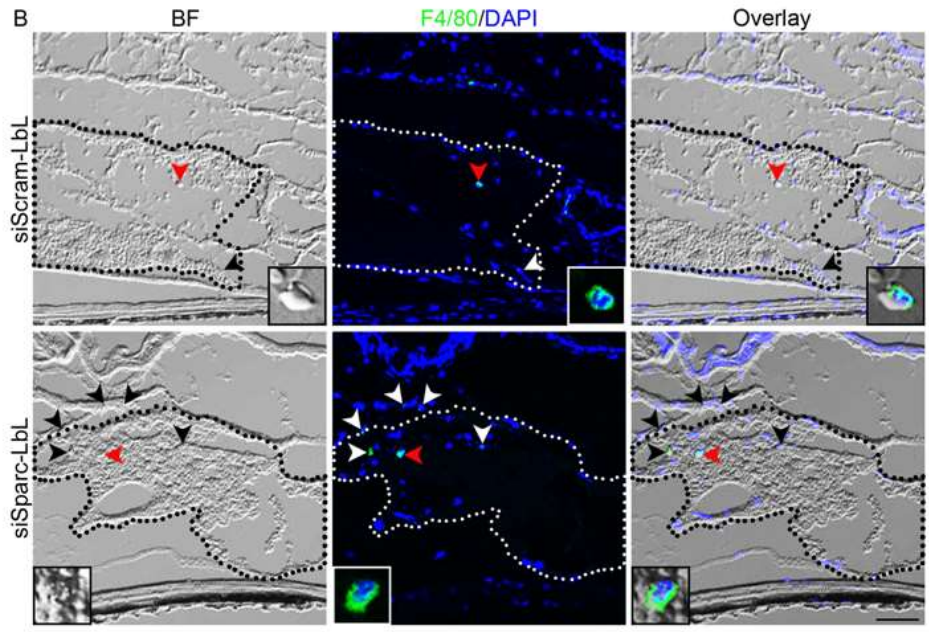

Figure 5.6 Minimal inflammatory response in the conjunctiva injected with LbL nanoparticles at 14 days. Immunostaining of conjunctival tissues with (A) CD45 antibody (green) and (B) F4/80 antibody (green). Nuclei were visualized by DAPI staining (blue). Areas containing high density of coalesced nanoparticles are indicated by the dotted lines. Bright field (BF) and overlays of BF with immunofluorescence data are shown. Arrowheads indicate cells that stained positive for the markers. Insets are magnified versions of the area indicated by the red arrows. Scale bar, 50 μm.

Chapter 6

LbL NP Release Mechanism Study

This chapter describes the investigation on the release behaviour of SPARC siRNA from the LbL NPs designed. The significance of this study is to observe how the NPs release siRNA and to explain why the NPs were able to achieve prolonged gene silencing within cells. NPs were shaken in PBS at 37˚C and the supernatant was collected periodically to quantify the siRNA amount released. That provided insight in the release profile of the designed particle as compared to other particles of similar configurations which were, however, not able to deliver prolonged gene silencing effects. Next, adjacent siRNA and Poly-L-Arginine layers within the particles were tagged with FRET (fluorescence resonance energy transfer)-pairs and the NPs were added to cells to track the periods in which the layers would detach from each other within cells. The FRET-pairs studies will show the release behaviour of siRNA in vitro and explain why prolonged gene silencing was achieved with the NP configuration designed.

To be published as Yang Fei Tan, Ying Shi Lee, Li-Fong Seet, Kee Woei Ng, Subbu Venkatraman, Tina T. Wong entitled Release Mechanism Study of Layer-by-Layer Nanoparticles in Cells.

6.1 Introduction

Ever since the discovery of nanotechnology, it has been widely applied in various fields. This includes the area of drug delivery, with various carriers being developed to traffic drugs within cells. To better introduce nanoparticles into cells, the interaction between nanoparticles and cells has been studied extensively [1]. Most research has focused on the effect of various nanoparticle characteristics (surface charge, size and shape) on the cellular uptake of nanoparticles [1].

For instance, Javier et al. designed a polyelectrolyte microcapsule-coated atomic force microscopy tip to investigate the cell uptake process of multilayer polyelectrolyte microcapsules. They found that microcapsules with positively charged outermost polyelectrolyte layers exhibit higher binding forces to cell membranes and higher cellular uptake efficiencies than microcapsules with negatively charged outermost polyelectrolyte layers [2]. Similarly, Vasir et al. investigated the interaction of PLGA nanoparticles with cell membranes. They also demonstrated that positively charged PLGA nanoparticles adhere more strongly to the cell membrane and have higher uptake efficiency than neutral or negatively charged PLGA nanoparticles [3].

The size and shape of LbL NPs for cellular uptake are also popular study topics between cell interaction and nanoparticles. Y.F.Tan et al. reported that their designed LbL NPs which were of about 200 nm in diameter (according to TEM and FESEM imaging), were able to be taken up by human fibroblasts [4]. Indeed, according to a review by S.D.Steichen et.al, it was reported that for passive targeting in cancer tumours, drug-carrying nanoparticles must be below 400 nm in diameter to have any significant uptake for effective clinical and therapeutic effect [5]. The review by S.D.Steichen et al. also reported that 14 and 75 nm spherical nanoparticles were uptaken more readily by cells 3.75 to 5 times more than 74 by 14 nm rod-shaped particles [5].

Most studies so far have focused on how the various nanoparticle characteristics affect the cellular uptake of nanoparticles. Studies on how nanoparticles, in particular LbL NPs,

release drugs after entry into cells have been extremely scarce. Most studies have only been conducted in simulated extra-cellular medium.

For instance, R.Luo et al. investigated the release profiles of nanoparticles fabricated with different polyelectrolytes. They found that nanoparticle drug release profiles (in PBS) were regulated by the number of polyelectrolyte layers, the nature of polyelectrolyte, as well as by the chemical modification of polyelectrolyte [6]. In another study, S.Nimesh et al. compared the release profiles of nanoparticles in different pH conditions of the medium. They found that the release rates of encapsulant from nanoparticles were slower in both pH conditions higher and lower than 7.4, with fastest release rate at pH 7.4. They claimed that was because the NPs swell in aqueous dispersion with the swelling reaching a maximal at physiological pH [7]. So far, to our knowledge, there are little or no study done to show how NPs release drug within cells.

Generally for non-viral vectors, such as positively charged NPs, the major mechanism for cellular uptake is by endocytosis [8, 9]. For cationic polyelectrolyte coated NPs which are already highly protonated before entry into cells (no proton sponge effect possible), such as the particles designed in this work, interaction with phospholipid membranes can form pores large enough for the NPs to squeeze through into the cytosol [4, 10, 11] from within lysosomes after cell entry. Most particles entering cells escape from lysosomes “intact” with their cargo into the cytosol.

In this chapter, the siRNA release profile of the designed LbL NPs will be explored over time in simulated physiological conditions. The profile will be compared with particles of similar configurations which were however, unable to ensure prolonged gene silencing effects in cells. In addition, the degradation profile of the particles will be investigated over time following uptake by MCF cells. The degradation profile will provide information related to the siRNA behaviour of the particles and shed some light in explaining how the particles were able to deliver prolonged gene silencing effects both *in vitro* and *in vivo*.

6.2 Release Profile of LbL NPs

After finding out that the designed LbL NPs were able to induce prolonged gene silencing *in vitro* and *in vivo*, it was important to investigate the release behaviour of the fabricated particles.

An *in vitro* release study was conducted to find out the release profile of the designed double siRNA layered particles over time, as compared to single siRNA layered particles which were not able to deliver prolonged gene silencing. Three-layered LbL particles (HA-ARG-6FAM siRNA-ARG) and five-layered LbL particles (HA-ARG-6FAM siRNA-ARG-6FAM siRNA-ARG) fabricated from 1 mg HA respectively were dispersed in 600 µl of PBS and constantly shaken at 37˚C over 14 days. At the stipulated time points, the particle samples were centrifuged down and the supernatant collected and measured with the Tecan plate reader to affirm release amount compared against 6FAM siRNA standard curve. Fresh PBS was added for subsequent time point measurements. The results are as below:

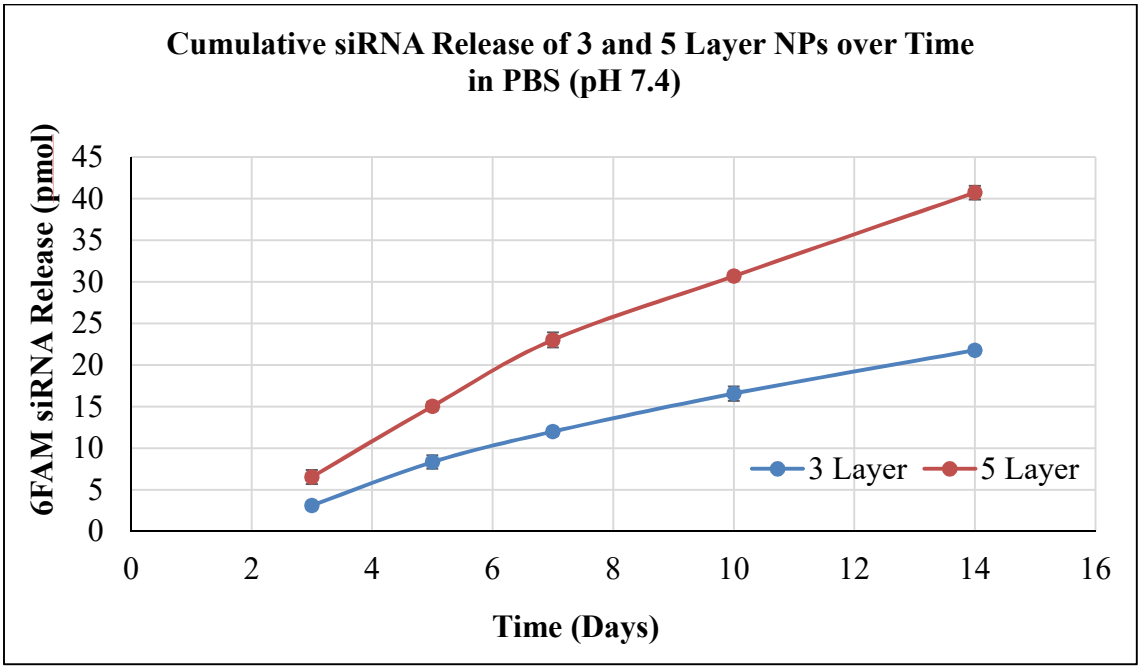

Figure 6.1 Graph of cumulative siRNA release from 3 and 5 layered LbL NPs over 14 days. Three-layered LbL particles (HA-ARG-6FAM siRNA-ARG) and five-layered LbL particles (HA-ARG-6FAM siRNA-ARG-6FAM siRNA-ARG) fabricated from 1 mg HA respectively were dispersed in

600 µl of PBS and constantly shaken at 37˚C over 14 days. At the stipulated time points, the particle samples were centrifuged down and the supernatant collected and measured with the Tecan plate reader to affirm release amount compared against 6FAM siRNA standard curve. Fresh PBS was added for subsequent time point measurements. All samples and measurements were conducted in triplicates.

From the graph, the accumulated siRNA released from single layered siRNA LbL NPs (3 layered NPs) amounted to 21.8 pmol at day 14. The accumulated siRNA released from double layered siRNA LbL NPs (5 layered NPs) amounted to 40.7 pmol at day 14. 5 layered NPs released about 87 % more siRNA than 3 layered NPs over 14 days. Also, based on the gradients of the 2 release curves, it can be seen that 5 layered NPs released siRNA faster than 3 layered NPs over 14 days.

From the activity studies both *in vitro* and *in vivo* shown earlier, the designed 5 layered NPs proved to be able to silence *SPARC* and Collagen genes over 14 days, meaning that the amount of siRNA that was released over the 14 days was enough to ensure prolonged silencing. The 3 layered NPs were however unable to deliver gene silencing over 14 days probably because they do not have an additional siRNA like the 5 layered NPs, and therefore no supplementary siRNA to sustain knockdown effect after exhausting the siRNA they trafficked into the cells.

6.3 Fate of the NPs after uptake into cells

It was shown earlier that the designed LbL NPs were able to be taken up by MCF cells. As described in the literature review (Chapter 6.1), the MCF cells were widely believed to be internalising the NPs via endocytosis. However, it was undetermined if the NPs would end up in the lysosomes within the cells. Thus, NPs with TRITC tagged HA were fabricated and added to MCF cells. Three days after treatment, the cells were then treated with CellLight GFP lysosomal stains overnight. The following day, the samples were prepared for CLSM imaging. The CLSM images are as below:

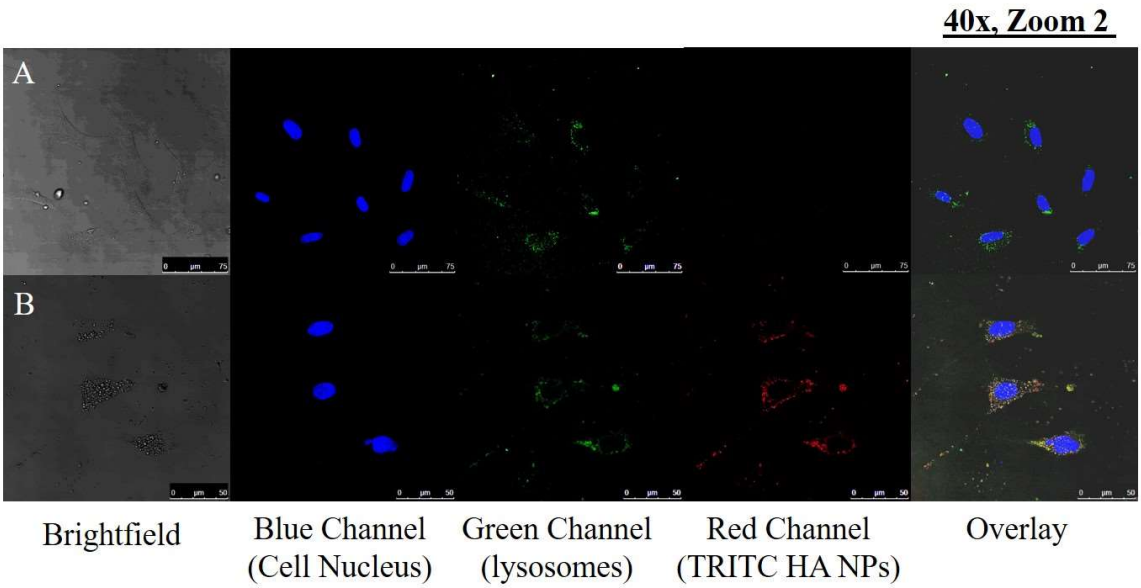

Figure 6.2 CLSM images from left, bright field, blue channel, green channel, red channel and overlay. Sample images (B), which were treated with TRITC HA core NP and CellLight (staining lysosomes green) were compared with control cells (A) not treated with particles but treated with CellLight (staining lysosomes green). Control cells showed no red signals but only green signals. Images were taken at 40X magnification, 2X zoom. CLSM images taken 3 days after treatment.

From the CLSM images of the MCF cells treated with TRITC HA core NPs, it was evident that there were some co-localisation observed of the NPs and the lysosomes (green) within the cells as represented by the yellow spots. Thus, it can be concluded that after entry into the cells, some of the NPs end up within lysosomes. As the successful *in vitro* and *in vivo* gene knock down studies done previously affirm significant siRNA activity within the cytosol, the NPs must have then escaped from the lysosomes, entering the cell cytoplasm. Furthermore, some of the particles could have also escaped from early endosomes into the cytoplasm. As described in the literature review (6.1), it was unlikely that the already highly protonated poly-l-arginine coated NPs had undergone the proton sponge effect, and burst out of the lysosomes. The highly positively charged NPs could most probably have caused extensive pore formation on the lysosomal membranes, escaping into the cytoplasm.

6.4 Defoliation and release study using FRET

After investigating the release profiles of the 3 and 5 layered nanoparticles in a simulated physiological environment and finding that the 5 layered LbL NPs actually had a more desirable release profile for prolonged effect on gene silencing, investigation on the degradation and siRNA release behaviours were attempted within the MCF cells.

To observe how long it will take for the two layers of siRNA to detach from the NPs once the particles were uptaken into cells, FRET pair fluorophores (FITC and TRITC) were tagged to the siRNA and adjacent Ploy-L-Arginine layers respectively. 0.108 mg of particles were treated to 30000 MCF cells. At stipulated time points, the cells were trypsinized and suspended in 0.4% trypan blue, centrifuged and then suspended in 200 uL of PBS for testing with Guava flow cytometer. The cell samples were subjected to blue laser excitation (488nm) and only the FITC tagged onto siRNA would be excited. If the adjacent TRITC tagged Poly-L-Arginine was still in close proximity, the TRITC would be able to receive the emission from FITC and get excited to release red signals. The FRET effect was measured and compared with controls over a period of time. The TRITC and FITC signals were normalised with TRITC and FITC signals of control samples consisting of cell samples treated with similar particles but only with either TRITC or FITC fluorescein. The normalised signals (signals involved in FRET) were then analysed over time. The FRET results of the tagged outer siRNA and Poly-L-Arginine layers were as presented below:

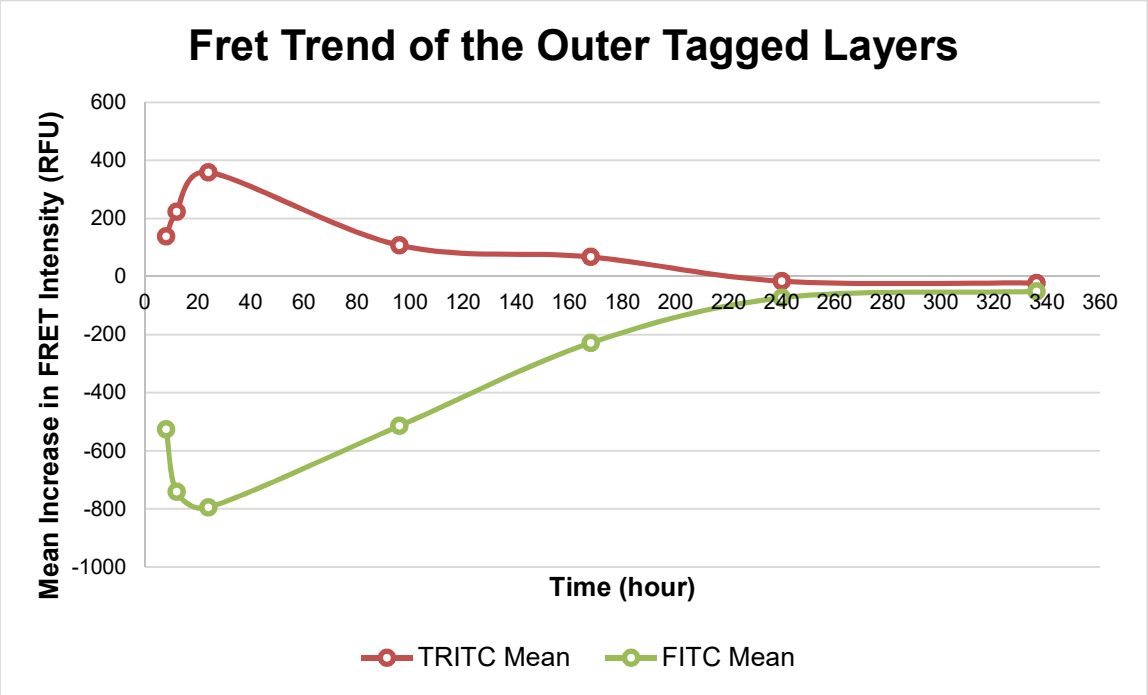

Figure 6.3 Graph of FRET degradation trend over 14 days. Outer siRNA was tagged with FITC and the adjacent inner Poly-L-Arginine layer was tagged with TRITC (HA-ARG-siRNA-TRITC ARG-FITC siRNA-ARG). 0.108 mg of particles were treated to 30000 MCF cells. At stipulated time points, the cells were trypsinized and suspended in 0.4% trypan blue, centrifuged and then suspended in 200 uL of PBS for testing with Guava flow cytometer. The cell samples were subjected to blue laser excitation (488nm) and only the FITC tagged onto siRNA would be excited. If the adjacent TRITC tagged Poly-L-Arginine was still in close proximity, the TRITC would be able to receive the emission from FITC and get excited to release red signals. The FRET effect was measured and compared with controls over a period of time. TRITC signals were compared with TRITC signals of control cell samples treated in the same way but with particles with only TRITC tagged Poly-L-Arginine. Similarly, FITC signals were compared with FITC signals of control cell samples treated in the same way but with particles with only FITC tagged siRNA. That was done so as to only consider signals involved in FRET for the analysis.

From Figure 6.3, it can be observed that red TRITC signals decreased and ultimately disappeared at day 9 within the MCF cells. As the samples were only exposed to blue laser during measurement, only FITC within the samples (tagged onto outer siRNA layer) could fluorescent. If the TRITC tagged outer Poly-L-Arginine layer was still within close enough proximity with the outer siRNA layer, TRITC would then be able to receive emission from

FITC and emit red signals. Thus it was evident from the results that by day 9, most of the outer Poly-L-Arginine layer has dislocated from the outer siRNA layer. The same experiment was repeated with the inner siRNA and Poly-L-Arginine layer with the results as displayed below:

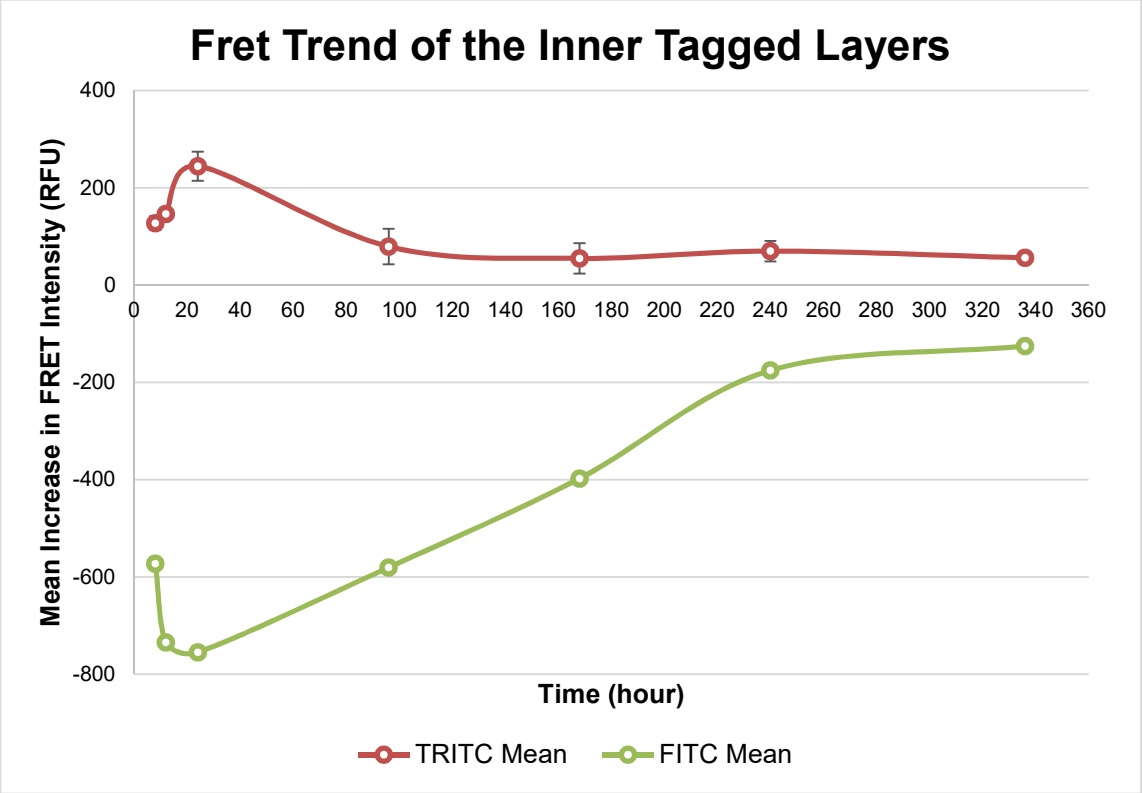

Figure 6.4 Graph of FRET degradation trend over 14 days. Inner siRNA was tagged with FITC and the adjacent inner Poly-L-Arginine layer was tagged with TRITC (HA-TRITC ARG- FITC siRNA- ARG- siRNA-ARG). 0.108 mg of particles were treated to 30000 MCF cells. At stipulated time points, the cells were trypsinized and suspended in 0.4% trypan blue, centrifuged and then suspended in 200 uL of PBS for testing with Guava flow cytometer. The cell samples were subjected to blue laser excitation (488nm) and only the FITC tagged onto siRNA would be excited. If the adjacent TRITC tagged Poly-L-Arginine was still in close proximity, the TRITC would be able to receive the emission from FITC and get excited to release red signals. The FRET effect was measured and compared with controls over a period of time. TRITC signals were compared with TRITC signals of control cell samples treated in the same way but with particles with only TRITC tagged Poly-L-Arginine. Similarly, FITC signals were compared with FITC signals of control cell samples treated in the same way but with particles with only FITC tagged siRNA. That was done so as to only consider signals involved in FRET for the analysis.

From Figure 6.4, it can be observed that unlike the trend observed for the outer siRNA and Poly-L-Arginine layer, the inner siRNA and Poly-L-Arginine layer displayed FRET throughout the 14 days. From the results, it can be observed that the outer siRNA layer dislocate first (in about 9 days) followed by the inner siRNA layer. It could be inferred that separating the total siRNA in a LbL NP into 2 layers could achieve a delayed control release of siRNA within a cell. That could be the reason why it was observed previously that LbL NPs loaded with a single siRNA was only able to achieve gene silencing for a week while NPs loaded with 2 siRNA layers were able to achieve gene silencing for 2 weeks in MCF cells.

References

[1] L. Phuc, A. Taniguchi. *International Journal of Molecular Sciences*. **2017**, 18, 1301.

[2] A. Muñoz Javier, O. Kreft, A. Piera Alberola, C. Kirchner, B. Zebli, A. S. Susha, E. Horn, S. Kempter, A. G. Skirtach, A. L. Rogach, J. Rädler, G. B. Sukhorukov, M. Benoit, W. J. Parak. *Small*. **2006**, 2, 394-400.

[3] J. K. Vasir, V. Labhasetwar. *Biomaterials*. **2008**, 29, 4244-4252.

[4] Y. F. Tan, R. C. Mundargi, M. H. A. Chen, J. Lessig, B. Neu, S. S. Venkatraman, T. T. Wong. *Small*. **2014**, 10, 1790-1798.

[5] S. D. Steichen, M. Caldorera-Moore, N. A. Peppas. *European Journal of Pharmaceutical Sciences*. **2013**, 48, 416-427.

[6] R. Luo, B. Neu, S. S. Venkatraman. *Small*. **2012**, 8, 2585-2594.

[7] S. Nimesh, R. Manchanda, R. Kumar, A. Saxena, P. Chaudhary, V. Yadav, S. Mozumdar, R. Chandra. *International Journal of Pharmaceutics*. **2006**, 323, 146-152.

[8] I. A. Khalil, K. Kogure, H. Akita, H. Harashima. *Pharmacological Reviews*. **2006**, 58, 32-45.

[9] M. Benfer, T. Kissel. *European Journal of Pharmaceutics and Biopharmaceutics*. **2012**, 80, 247-256.

[10] H. W. Huang, F.-Y. Chen, M.-T. Lee. *Physical Review Letters*. **2004**, 92, 198304.

[11] H. D. Herce, A. E. Garcia, J. Litt, R. S. Kane, P. Martin, N. Enrique, A. Rebolledo, V. Milesi. *Biophysical Journal*. **2009**, 97, 1917-1925.

Chapter 7

Discussion, Conclusions and Future Work

This chapter covers the discussion of the research findings gathered, giving conclusions of this work. By generating biocompatible, multi-layered hydroxyapatite-based LbL nanoparticles containing two alternating layers of siRNA, an siRNA delivery carrier that is non-toxic and is rapidly taken up and retained by cells for at least 14 days has been developed. The capability of these nanoparticles to enhance and prolong endogenous gene silencing effects for at least two weeks in vitro and in vivo in the mouse model of conjunctival scarring via a single dose direct injection into the target site was demonstrated. Lastly, possible future works based on the various findings of this work will be explored. Overall, the system designed have several potential applications. This chapter will focus on a possible application to utilize the system for type I diabetes mellitus management which can potentially be better than the current treatment especially in patient compliances.

7.1 Discussion and conclusions

LbL nanotechnology is, by design, a flexible platform that can be modified to suit therapeutic needs particularly for prolonged therapeutic applications. LbL nanoparticles containing two sandwiched layers of siRNA were not excessively altered in size as compared to the particles carrying a single layer of siRNA [1] and were rapidly taken up by cells. The multi-layering of the LbL particles conferred upon these carriers the capacity to elicit enhanced and protracted target gene silencing via its siRNA load without inducing a foreign body response or causing tissue toxicity. Hence, multi-layering of LbL nanoparticles is an effective strategy for not only achieving *in vivo* gene regulation, but also potentially a safe method for long-term therapeutic applications.

Over the years, several novel delivery systems for sustained release of antisense oligonucleotides or siRNA to achieve long-lasting gene silencing effects have been described. Such siRNA delivery vehicles have been constructed based on a variety of biomaterials, including cationic polymers [2], nanofibrous peptides [3], thermosensitive cationic hydrogels [4] and hybrid lipid-polymers [5]. Multi-layered particles similar to those described here but designed around other core materials such as gold have also been described [6]. These nanoparticles have been reported to deliver gene silencing effects from 5 days [2] to more than 3 weeks [5, 6]. However, there is no clear evidence from these studies that the sustained gene silencing was achieved *in vivo* for an endogenous target gene via a clinically relevant route of administration. Instead, these reports detailed gene silencing in experimental backdrops far from the clinical setting, including knockdown of a non-mammalian gene [6], experimentation only on cultured cells [2, 3], or investigation of xenografted tumors where tumor cells were pre-treated with the delivery vehicles carrying siRNAs before transplantation into recipient mice [4-6]. An exception to the latter was a study where the effectiveness of an elegant liposomal core/LbL carrier to deliver gene silencing to xenografted tumors was determined by intravenous injection [7]. In this study, the nanoparticles demonstrated long blood circulation half-lives and accumulated in tumor tissue by virtue of the enhanced permeation and retention (EPR) effect. Gene silencing over a period of 15 days however, required repeated injections, suggesting that a

single dose application of these nanoparticles may not suffice for sustained efficacy [7]. Hence, truly prolonged silencing of an endogenous gene in a target tissue by a single direct *in vivo* application has not been indubitably established for these nano-carriers. This study has gone beyond previous works to prove that clinically relevant endogenous gene silencing can be achieved on a protracted basis using a single dose application of siRNAs incorporated in LbL nanoparticles.

In the modular system described in this work, only clinically relevant materials such as HA and ARG for high siRNA loading, high transfection efficiency, biostability, and low cytotoxicity for potential clinical translation have been selected. HA was chosen as the core material due to its slow dissolution, biocompatibility and low cytotoxicity [3]. ARG is a promising candidate for *in vivo* applications due to its high siRNA loading capacity, high transfection efficiency [8, 9] and low cytotoxicity [10]. ARG may promote cellular uptake through electrostatic interactions with cell surface proteoglycans [11]. Moreover, as the outermost layer of the nanoparticles, ARG forms a shielding layer that may protect the siRNA from intracellular degradation via endosomal escape, and facilitates cell penetration through a hypothetical membrane disruptive mechanism [12, 13] As ARG is biodegradable, siRNA may be released from the polyplex as it biodegrades, thereby providing steady access of siRNA to its cellular target. Indeed, it has been reported that protease-degradable polycation is associated with controlled release of siRNA and prolonged gene silencing [6]. This study confirmed that the HA-ARG system can be adapted to enhance and sustain siRNA activity *in vitro* and *in vivo*.

The mouse model of conjunctival scarring may be used as a simplified model for filtration surgery performed on glaucoma patients [2, 14] where post-operative scarring is implicated as the main cause of surgical failure [15]. Hence, the success of the LbL nanoparticles as carriers for siRNA in the mouse model suggests that this may be a promising method for anti-fibrotic intervention in glaucoma filtration surgery. The direct injection of these nanoparticles into the conjunctiva is a method that can be easily administered in the clinical setting. Moreover, these nano-carriers can be readily monitored since the target area is localized, accessible and visualisable. By injecting the LbL nanoparticles directly into the

target conjunctival tissue after experimental surgery, it has been shown that these carriers can facilitate knockdown of endogenous *SPARC* gene expression, a clear demonstration of therapeutic effectiveness and efficiency. Furthermore, the nanoparticles did not induce an adverse foreign body reaction which is a normal physiological response/ mechanism involving inflammation and known to result in loss of functionality of nanoparticles. Most importantly, the long-term silencing effects facilitated by the nano-carriers suggested that re-injections are potentially not required and surgical success can be further improved along with a reduced surgical morbidity.

While the tendency of the HA LbL nanoparticles to coalesce may be particularly suitable for delivering a localised sustained effect in the conjunctiva, the value of these particles for systemic applications is unclear. A localised gene silencing effect in an accessible area of the eye delivered by the siRNA-loaded nanoparticles is arguably easier to achieve than attaining knockdown of target genes in systemic fibrotic disorders. The effectiveness of these LbL nanoparticles in systemic applications remains to be determined. Furthermore, I propose that the mouse model of conjunctival scarring is a compelling system for obtaining first indications of the *in vivo* efficacy and effectiveness of novel nanoparticles as potential therapeutic anti-fibrotic siRNA carriers.

In summary, it has been shown in this proof-of-principle study that safe, prolonged and significant endogenous target gene silencing in the conjunctiva is achievable with a single-dose administration using a progressively-layered system of siRNA and polycation (ARG) around a HA core. This property may be attributed to a delivery vehicle that enables high siRNA loading, rapid cellular uptake, and high intracellular stability, while at the same time, being non-toxic to cells or tissue, and non-provocative of an overt foreign body response. By simply constructing the desired number of siRNA/polycation layers appropriate for the target gene and cells/tissue concerned, this scalable modular system [16, 17] can potentially advance oligonucleotide therapeutics as effective and long-term therapies for not only conjunctival fibrosis, but also a wide range of fibrotic disorders where fibrosis contributes to disease pathology or hinders the therapeutic success.

In conclusion, by generating biocompatible, multi-layered hydroxyapatite-based LbL nanoparticles containing two alternating layers of siRNA, an siRNA delivery carrier that is non-toxic and is rapidly taken up and retained by cells for at least 14 days has been developed. I have demonstrated the capability of these nanoparticles to enhance and prolong endogenous gene silencing effects for at least two weeks *in vitro* and *in vivo* in the mouse model of conjunctival scarring via a single dose direct injection into the target site.

In summary, the results presented here not only provide a potential strategy to treat conjunctival fibrosis, which is the cause of failure in glaucoma filtration surgeries, but also a method for achieving prolonged gene therapy for other fibrotic diseases requiring sustained intervention. I also believe that localised administration (as opposed to systemic) of such systems will greatly enhance stability and efficacy with minimal off-target effects.

7.2 Future work

Using the designed multilayered LbL NP system to deliver therapeutic agents, such as siRNA, to curb diseases provides flexibility to cater for specific applications. For the application described in this paper, the NPs were modified for continual release of the same siRNA over a span of 2 weeks to curb a disease model. To tackle multiple undesirable proteins at the same time, multiple types of siRNA could be coated within a single layer within the NPs. To manage undesirable proteins which may be produced in sequence over different time frames, different siRNA could be coated within the NPs in different layers. Thus, the applications for this particle system is limitless. In the following part of this chapter, the particle system will be modified for application in type I diabetes mellitus management to illustrate the potential of this particle system.

7.2.1 Diabetes mellitus

Diabetes mellitus is a massive concern affecting public health globally currently. Epidemiological researchers have reported that 285 million people worldwide has been

diagnosed with diabetes in the year 2010, and this figure is expected to increase to 439 million people by 2030 [18]. This condition is characterized by a group of metabolic diseases that cause hyperglycemia when the body is unable to produce insulin, leading to abnormally high glucose levels in the bloodstream. As the disease progresses unchecked, chronic hyperglycemia sets in, resulting in failure and damage of various organs (such as the eyes, kidney and heart) [19]. Type 1 (T1D) and Type 2 (T2D) diabetes are the two main types of Diabetes mellitus. T1D makes up 5-10% of the disease and it occurs due to an autoimmune response where the body's immune system attacks the β-cells of the pancreas, leading to total loss of insulin secretion. Therefore, daily dose of insulin injection is needed for T1D patients to control glucose levels in the body [20]. T1D is typically treated with Neutral Protamine Hagedorn insulin and Detemir via subcutaneous injection [21, 22] or with a pump.

7.2.2 Current technologies developed to treat diabetes mellitus

Currently, a few technologies have been developed for diabetes management. Typical technologies developed include the multiple daily injections (MDI) and the continuous subcutaneous insulin infusion (CSII) therapies. MDI is currently the gold-standard of care for most patients with T1D. The therapy involves injecting insulin analogues, which are long acting insulin, once or twice daily as basal (background) dose and having additional injections of fast acting insulin at each meal time. On the other hand, CSII uses a device to pump insulin (fast acting) rapidly into the body through a catheter to keep blood glucose within the basal rate. The pump can be programmed to infuse insulin automatically or in response to the wearer's instructions [23].

7.2.3 Advantages and limitations of current treatments

With the various technologies developed to treat diabetes, there are both benefits and limitations intrinsic to the different treatment strategies. For instance, MDI is a less expensive option and involves minimal time needed in preparation of the injections. On top of that, patients have the flexibility to self-regulate insulin dosages before carrying out

certain physical activities or taking meals. However, the downside of MDI is that repetitive insulin injections at the same location can result in accumulation of fat and scar tissue at the area, a symptom known as lipohypertrophy [24].

CSII is a more convenient choice for glucose management. The cannulas are put into the skin every few days as compared to daily multiples injects of MDI. The patient can program his insulin infusions according to his daily needs by just pressing a few buttons. However, the drawbacks of CSII are that apart from being more costly than MDI, substantial technical support with extra time might be needed for training of pump operation, breakdown of the alarm and occlusion of needle or catheter [25].

7.2.4 New therapies for diabetes

The recurrent symptoms of hypoglycaemia in some patients with T1D leads to transplantation of the endocrine part of the whole pancreas. After the first successful pancreas transplant in the year 1966 onwards, pancreas transplant has served as a way to halt the progressive complications of diabetes. However, pancreas transplantation is typically performed with kidney transplantation preferably from the same suitable donor to minimize rejection which is immensely hard to come by [26]. Whole pancreas transplantation comes with major complications such as the graft thrombosis, pancreatic fistulae, pancreatitis, pseudocyst formation, and even death [27]. Hence, transplantation of islets is currently the improved procedure to cure T1D. Islet β-cells transplantation involves a less invasive approach with minimal or even no complications, as it involves the infusion of islets through a catheter having access to the percutaneous portal vein [28]. Although islet β-cells transplantation has shown successful outcome for some T1D patients, patients on this therapy need to be on lifelong immunosuppression to prevent rejection of transplanted cells [28]. In order to eliminate the need for immunosuppression, an encapsulation device has been developed to serve as a physical barrier between the transplanted β-cells and the patients. The encapsulating device acts as an environment that supports the secretion of insulin in response to vacillating levels of blood glucose, and also maintain the viability of cells by avoiding the attack from immune system, with efficacious

nutrient and waste exchange [29]. Unfortunately, due to incompatibility of the capsules with the biological system, extensive fibrosis usually occur post-transplantation, resulting in as much as 40% loss of transplanted islet mass [30]. It was speculated that the irregular shape of the capsules could have caused fibrosis and islet cells death due to protrusion of the islet cells in the biological system, initiating immune response [31].

7.2.5 Proposed resolution using modified devised LbL NP

To develop an alternative therapy aimed at managing insulin dependent diabetes mellitus, Type 1 diabetes (T1D), the major objective is to sustain the survival of the encapsulated islet cells by overcoming fibrosis which occurs post-transplantation. The approach used is to encapsulate islet cells in an immune-isolated alginate hydrogel film, incorporating the siRNA releasing polyelectrolyte LbL NPs into the scaffold to prevent failure by fibrosis. LbL siRNA-incorporated HA NPs would be coated on the alginate film after modification to suit requirements for the application. This application requires the anti-fibrosis effect to be sustained as long as possible. Thus, the particles should be modified to load more siRNA within the siRNA layers or to add additional siRNA layers to achieve more prolonged anti-fibrotic effects with one application.

7.2.6 Increasing siRNA/poly-electrolyte loading of the LbL NPs

To load more siRNA within each siRNA layer of the designed LbL NPs, more siRNA was used during the coating of a layer of siRNA during fabrication. Two different NPs were fabricated (one using 1.2 nmol, the other 2.4 nmol siRNA, for siRNA layer coating) and the zeta potential of each layer was measured after every coating. The particle configurations were: HA|ARG|siRNA(1.2 nmol)|ARG and HA|ARG|siRNA(2.4 nmol)|ARG. The zeta potential of each layer of the respective NPs are as below:

Table 7.1 Table showing zeta potential of every layer of 3 layered LbL NP. Samples were taken after every layer of coating. A: HA|ARG|siRNA (1.2 nmol)|ARG and B: HA|ARG|siRNA (2.4 nmol)|ARG. All readings were measured in triplicates.

A HA/ARG/siRNA (1.2 nmol)/ARG			B HA/ARG/siRNA (2.4 nmol)/ARG		
NPs configuration	**Average Zeta Potential (mV)**	**STDEV**	**NPs configuration**	**Average Zeta Potential (mV)**	**STDEV**
HA	-5.62	1.21	HA	-5.62	1.21
HA-ARG	34.03	0.93	HA-ARG	34.03	0.93
HA-ARG-siRNA(1.2 nmol)	-17.53	1.33	HA-ARG-siRNA(2.4 nmol)	-20.00	0.69
HA-ARG-siRNA(1.2 nmol)-ARG	32.07	0.97	HA-ARG-siRNA(2.4 nmol)-ARG	27.23	1.01

From Table 7.1, it can be observed that doubling the amount of siRNA coating concentration to synthesize the siRNA layer did not cause significant change in the siRNA layer zeta potential. That intrinsically meant that the 1.2 nmol siRNA coating concentration was probably close to the optimized coating concentration for maximum amount of siRNA to be coated on the NPs. To reaffirm that, 1 mg of each of the two particles (triplicates conducted) were dispersed in trypsin and shaken overnight at 37 ˚C to disassemble the particles to release all their siRNA contents and compared to verify that their contents were similar in siRNA amounts (measured with Nanodrop). The particle fabricated with 1.2 nmol siRNA coating solution had an average of 8351.96 ng of siRNA while that fabricated with 2.4 nmol siRNA coating solution had average of 9775.22 ng of siRNA. Doubling the siRNA coating solution only increased the siRNA loading by about 17%. Most of the siRNA that was not coated was wasted.

Since using a more concentrated siRNA coating solution failed to increase the siRNA content of each siRNA layer significantly, different poly-electrolyte coating concentrations were then used to try to manipulate the poly-electrolyte thickness which can then, in turn, potentially increase siRNA coating. Three different NPs were fabricated and the zeta potential of each layer was measured after every coating. The particle configurations were: HA/ARG(0.5 mg)/siRNA/ARG(0.5 mg), HA/ARG(2 mg)/siRNA/ARG(0.5 mg) and

HA/ARG(0.5 mg)/siRNA/ARG(2 mg). The zeta potential of each layer of the respective NPs are as below:

Table 7.2 Table showing zeta potential of every layer of 3 layered LbL NPs. Samples were taken after every layer of coating. A: HA/ARG(0.5 mg)/siRNA/ARG(0.5 mg), B: HA/ARG(2 mg)/siRNA/ARG(0.5 mg) and C: HA/ARG(0.5 mg)/siRNA/ARG(2 mg). All readings were measured in triplicates.

A HA/ARG(0.5 mg)/siRNA/ARG(0.5 mg)			B HA/ARG(2 mg)/siRNA/ARG(0.5 mg)			C HA/ARG(0.5 mg)/siRNA/ARG(2 mg)		
NPs configuration	**Average Zeta Potential (mV)**	**STDEV**	**NPs configuration**	**Average Zeta Potential (mV)**	**STDEV**	**NPs configuration**	**Average Zeta Potential (mV)**	**STDEV**
HA	-3.74	0.92	HA	-3.74	0.92	HA	-3.74	0.92
HA-ARG(0.5 mg)	32.90	0.53	HA-ARG(2 mg)	33.03	0.90	HA-ARG(0.5)	32.90	0.53
HA-ARG(0.5 mg)-siRNA	-17.33	1.06	HA-ARG(2 mg)-siRNA	-17.13	0.72	HA-ARG(0.5)-siRNA	-17.33	1.06
HA-ARG(0.5 mg)-siRNA-ARG(0.5 mg)	25.50	1.35	HA-ARG(2 mg)-siRNA-ARG(0.5 mg)	22.87	0.42	HA-ARG(0.5 mg)-siRNA-ARG(2 mg)	23.83	0.75

From Table 7.2, it can observed that changing the amount of poly-electrolyte coating concentrations to synthesize the polymeric layers did not cause significant change in the polymeric layer zeta potential. That intrinsically meant that the original 0.5 mg/1 mg HA poly-l-arginine coating concentration was probably close to the optimized coating concentration for maximum amount of poly-electrolyte to be coated on the NPs. To reaffirm that, 1 mg of each of the three particles (triplicates conducted) were dispersed in trypsin and shaken overnight at 37 ˚C to disassemble the particles to release all their siRNA contents and compared to verify that their contents were similar in siRNA amounts (measured with Nanodrop). A thicker poly-electrolyte layer was assumed to potentially be able to coat a thicker siRNA layer, loading more siRNA in the particle. Expectedly, all NPs had similar siRNA contents with A having 9773.5 ng, B having 9782.0 ng and C having 9822.6 ng of siRNA. Hence, it was concluded that using more siRNA or poly-electrolyte coating concentrations will not affect the layer thickness or loading. The other way to increase siRNA loading in the NPs was to increase an additional siRNA layer.

7.2.7 Additional siRNA layer for a more sustained anti-fibrotic effect

To achieve a more sustained anti-fibrotic effect to protect the islet cells in the scaffold with one application, an additional layer of siRNA was added to the designed NP configuration when the previous modifications to increase siRNA content in the NP proved unsuccessful. Two different NPs were fabricated and the zeta potential of each layer was measured after every coating. The particle configurations were, A: HA/ARG/6FAM siRNA/ARG/6FAM siRNA/ARG and B: HA/ARG/6FAM siRNA/ARG/6FAM siRNA/ARG/6FAM siRNA/ARG. To confirm that NP B has a higher siRNA content, 1 mg of each of the two particles (triplicates conducted) were dispersed in trypsin and shaken overnight at 37 ˚C to disassemble the particles to release all their siRNA contents and compared (measured with Tecan plate reader). From the results, NP A fabricated with 1 mg of HA contained 0.84 nmol of siRNA while NP B fabricated with 1 mg of HA contained 1.15 nmol of siRNA. NP B has 37% more siRNA than NP A. Besides, from the results discussed in chapter 6, it could be inferred that NP B which had 3 layers of siRNA could possibly sustain release siRNA longer than NP A which has 2 layers of siRNA. The zeta potential of each layer of the respective NPs are as below:

Table 7.3 Table showing zeta potential of every layer of LbL NPs. Samples were taken after every layer of coating. A: HA/ARG/6FAM siRNA/ARG/6FAM siRNA/ARG and B: HA/ARG/6FAM siRNA/ARG/6FAM siRNA/ARG/6FAM siRNA/ARG. All readings are measured in triplicates.

A HA/ARG/6FAM siRNA/ARG/6FAM siRNA/ARG

NPs configuration	Average Zeta Potential (mV)	STDEV
HA	-3.41	0.24
HA-ARG	32.1	0.98
HA-ARG-6FAM	-19.87	1.07
HA-ARG-6FAM siRNA-ARG	26.00	0.82
HA-ARG-6FAM siRNA-ARG-6FAM siRNA	-17.53	1.10
HA-ARG-6FAM siRNA-ARG-6FAM siRNA-ARG	24.33	1.00

B HA/ARG/6FAM siRNA/ARG/6FAM siRNA/ARG/6FAM siRNA/ARG

NPs configuration	Average Zeta Potential (mV)	STDEV
HA	-3.41	0.24
HA-ARG	32.1	0.98
HA-ARG-6FAM	-19.87	1.07
HA-ARG-6FAM siRNA-ARG	26.00	0.82
HA-ARG-6FAM siRNA-ARG-6FAM siRNA	-17.53	1.10
HA-ARG-6FAM siRNA-ARG-6FAM siRNA-ARG	24.33	1.00
HA-ARG-6FAM siRNA-ARG-6FAM siRNA-ARG-6FAM siRNA	-15.27	0.12
HA-ARG-6FAM siRNA-ARG-6FAM siRNA-ARG-6FAM siRNA-ARG	25.23	0.81

7.2.8 siRNA release profiles

NPs A and B fabricated as discussed in 7.2.7 were used for siRNA release study to investigate their release profiles. NPs fabricated from 1 mg HA of NP A and B (triplicates conducted) were dispersed in 600 µL of PBS and spun at 1500 rpm at 37 ˚C in the thermoshaker. At specific time intervals, samples were spun down with their supernatant collected and tested for siRNA content released using the Tecan plate reader at gain 60. The results are as below:

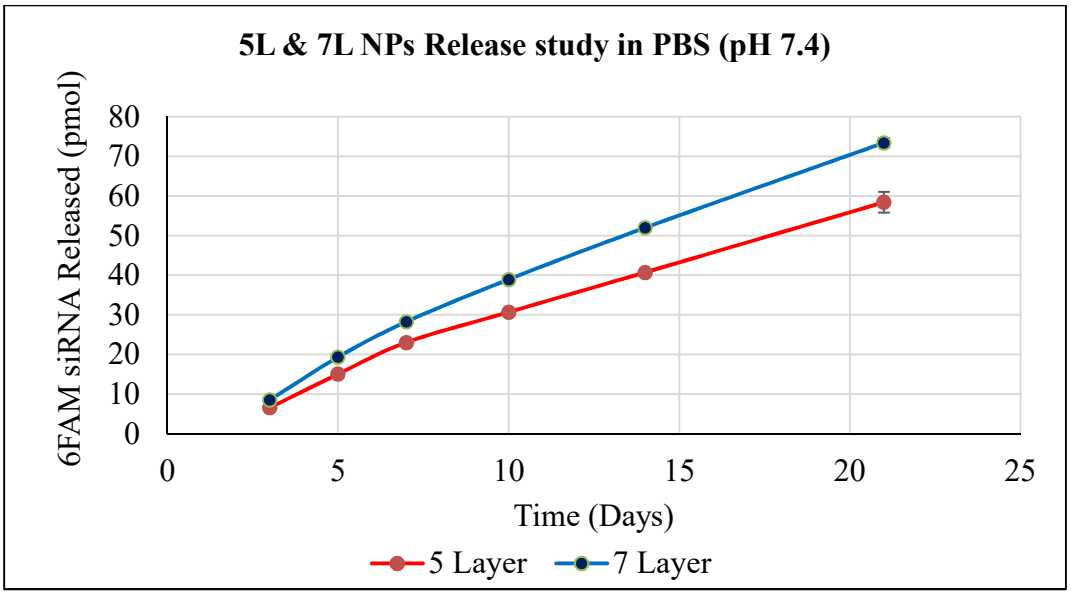

Figure 7.1 Graph of cumulative siRNA release from 5 (HA/ARG/6FAM siRNA/ARG/6FAM siRNA/ARG) and 7 layered (HA/ARG/6FAM siRNA/ARG/6FAM siRNA/ARG/6FAM siRNA/ARG) LbL NPs over 21 days. Each NP fabricated from 1 mg of HA were dispersed in 600 µl of PBS and constantly shaken at 37˚C over 21 days. At the stipulated time points, the particle samples were centrifuged down and the supernatant collected and measured with the Tecan plate reader to affirm release amount compared against FAM siRNA standard curve. Fresh PBS was added for subsequent time point measurements. All samples and measurements were conducted in triplicates.

From Figure 7.1, both NPs were gradually releasing siRNA over 21 days steadily. The 5 layered NP released an average of 58.4 pmol of siRNA while the 7 layered NP released an average of 73.4 pmol of siRNA by day 21. The 7 layered NP released 25% more siRNA as compared to the 5 layered NP. 7 layered NP, with the increased siRNA released over time could potentially be more effective in knocking down *SPARC* and collagen genes. Furthermore, from Figure 7.2 below, the 7 layered NP had only released an average of 6.4 percent of its total siRNA content by day 21, meaning that its anti-fibrotic ability could potentially be longer than 21 days.

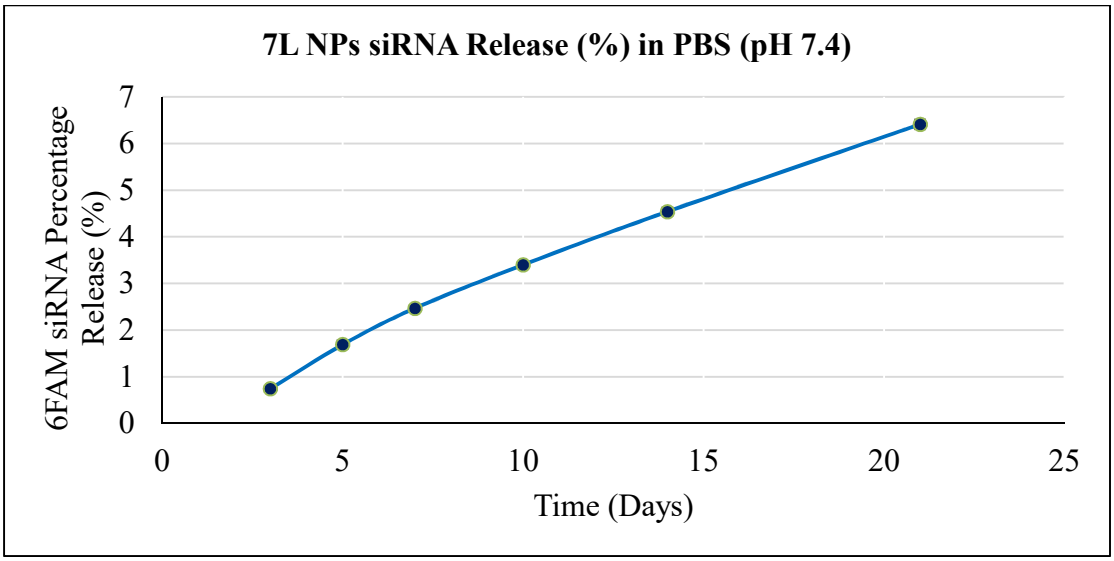

Figure 7.2 Graph of cumulative siRNA release percent from 7 layered (HA/ARG/6FAM siRNA/ARG/6FAM siRNA/ARG/6FAM siRNA/ARG) LbL NPs over 21 days. All samples and measurements were conducted in triplicates.

7.2.9 NP uptake in retroperitoneal human fibroblast cells

As the intended application site of the scaffold for islet cells was the peritoneum cavity, the particles were expected to be able to enter peritoneum human fibroblast cells to stop fibrosis. Hence, uptake study was conducted where FITC tagged HA NPs (FITC-HA/ARG/siRNA/ARG/siRNA/ARG/siRNA/ARG) were treated to human retroperitoneal fibroblast cells. One day after treatment, the samples were imaged with confocal microscopy and measured with GUAVA flow cytometry to track NP uptake in the cells. Both uptake studies showed NPs successfully getting uptaken by the cells one day after treatment. Flow cytometry showed an average of 53.4 % of the cells uptaking the NPs just one day after NPs treatment. Confocal microscopy images showed the green NPs within the human retroperitoneal fibroblast cells. Figure 7.3 below shows the confocal images.

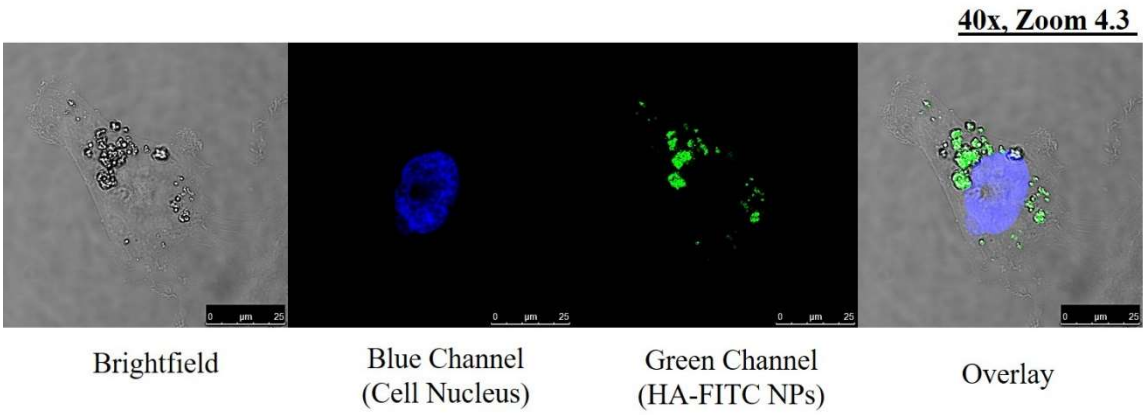

Figure 7.3 Confocal microscopy of human retroperitoneal fibroblast cells imaged one day after treatment of NP with FITC tagged HA core (FITC-HA/ARG/siRNA/ARG/siRNA/ARG/siRNA/ARG). Images were taken at 40X magnification and 4.3X zoom. Sample cells were compared with untreated control cells which showed no green FITC signals.

7.2.10 Conclusion

Further work should be done to affirm that the 7 layered LbL NPs modified from the original NP configuration for the diabetes therapy application could actually illicit *SPARC* and collagen gene knock down, exhibiting anti-fibrotic property to protect the islet cells. FRET studies should be conducted on 3-layered nanoparticles to prove that they exhaust siRNA before 9 days. Additional work should be done to incorporate the particle into or onto the hydrogel scaffold with the islet cells. Extensive release studies should be done to observe release behaviours of the particles from the hydrogel scaffold and to assure that the released particles could readily be uptaken by fibroblast cells to induce substantial gene silencing. However, the results and modifications above displayed the flexibility of the designed HA cored LbL NP system to cater to different applications for various disease models with just simple modifications. Most importantly, the designed LbL NP system could potentially deliver prolonged therapeutic effects with just a single application which could dramatically improve patient compliancy, effectively tackling various diseases today.

References

[1] Y. F. Tan, R. C. Mundargi, M. H. A. Chen, J. Lessig, B. Neu, S. S. Venkatraman, T. T. Wong. *Small*. **2014**, 10, 1790-1798.

[2] R. E. Vandenbroucke, B. G. De Geest, S. Bonné, M. Vinken, T. Van Haecke, H. Heimberg, E. Wagner, V. Rogiers, S. C. De Smedt, J. Demeester. *The journal of gene medicine*. **2008**, 10, 783-794.

[3] S. Bulut, T. S. Erkal, S. Toksoz, A. B. Tekinay, T. Tekinay, M. O. Guler. *Biomacromolecules*. **2011**, 12, 3007-3014.

[4] Y.-M. Kim, M.-R. Park, S.-C. Song. *ACS nano*. **2012**, 6, 5757-5766.

[5] J. Shi, Y. Xu, X. Xu, X. Zhu, E. Pridgen, J. Wu, A. R. Votruba, A. Swami, B. R. Zetter, O. C. Farokhzad. *Nanomedicine: Nanotechnology, Biology and Medicine*. **2014**, 10, e897-e900.

[6] S. K. Lee, C. H. Tung. *Advanced functional materials*. **2013**, 23, 3488-3493.

[7] Z. J. Deng, S. W. Morton, E. Ben-Akiva, E. C. Dreaden, K. E. Shopsowitz, P. T. Hammond. *ACS Nano*. **2013**, 7, 9571-9584.

[8] P. Opanasopit, J. Tragulpakseerojn, A. Apirakaramwong, T. Ngawhirunpat, T. Rojanarata, U. Ruktanonchai. *Int. J. Nanomedicine*. **2011**, 6, 2245-2252.

[9] E. Nemoto, H. Ueda, M. Akimoto, H. Natsume, Y. Morimoto. *Biological and Pharmaceutical Bulletin*. **2007**, 30, 1768-1772.

[10] M. Lozano, G. Lollo, M. Alonso-Nocelo, J. Brea, A. Vidal, D. Torres, M. Alonso. *Journal of nanoparticle research*. **2013**, 15, 1515.

[11] E. Gonçalves, E. Kitas, J. Seelig. *Biochemistry*. **2005**, 44, 2692-2702.

[12] B. R. Liu, Y.-w. Huang, J. G. Winiarz, H.-J. Chiang, H.-J. Lee. *Biomaterials*. **2011**, 32, 3520-3537.

[13] J. S. Appelbaum, J. R. LaRochelle, B. A. Smith, D. M. Balkin, J. M. Holub, A. Schepartz. *Chemistry & biology*. **2012**, 19, 819-830.

[14] L.-F. Seet, R. Su, V. Barathi, W. S. Lee, R. Poh, Y. M. Heng, E. Manser, E. N. Vithana, T. Aung, M. Weaver. *PloS one*. **2010**, 5, e9415.

[15] W. H. Morgan, D. Y. Yu. *Clinical & experimental ophthalmology*. **2012**, 40, 388-399.

[16] S. W. Morton, K. P. Herlihy, K. E. Shopsowitz, Z. J. Deng, K. S. Chu, C. J. Bowerman, J. M. DeSimone, P. T. Hammond. *Advanced Materials*. **2013**, 25, 4707-4713.

[17] J. J. Richardson, H. Ejima, S. L. Lörcher, K. Liang, P. Senn, J. Cui, F. Caruso. *Angewandte Chemie International Edition*. **2013**, 52, 6455-6458.

[18] J. E. Shaw, R. A. Sicree, P. Z. Zimmet. *Diabetes Research and Clinical Practice*. **2010**, 87, 4-14.

[19] *Diabetes Care*. **2014**, 37, S81-S90.

[20] D. Daneman. *The Lancet*. **2006**, 367, 847-858.

[21] R. Aathira, V. Jain. *World Journal of Diabetes*. **2014**, 5, 689-696.

[22] F. S. Malik, C. E. Taplin. *Pediatric Drugs*. **2014**, 16, 141-150.

[23] S. Schmidt. *Dan Med J*. **2013**, 60, B4746.

[24] P. Karagianni, C. Sampanis, C. Katsoulis, G. Miserlis, S. Polyzos, I. Zografou, S. Stergiopoulos, I. Douloumbakas, C. Zamboulis. *Hippokratia*. **2009**, 13, 93-96.

[25] P. Scuffham, L. Carr. *Diabetic Medicine*. **2003**, 20, 586-593.

[26] M. Qi. *Advances in medicine*. **2014**, 2014.

[27] T. Desai, L. D. Shea. *Nature Reviews Drug Discovery*. **2016**.

[28] R. C. Gaba, R. Garcia-Roca, J. Oberholzer. *Journal of Vascular and Interventional Radiology*. **2012**, 23, 583-594.

[29] P. de Vos, M. Spasojevic, M. M. Faas, in *Therapeutic Applications of Cell Microencapsulation*, Springer, 2010, 38-53.

[30] P. De Vos, J. Van Straaten, A. G. Nieuwenhuizen, M. de Groot, R. J. Ploeg, B. J. De Haan, R. Van Schilfgaarde. *Diabetes*. **1999**, 48, 1381-1388.

[31] H. A. Hobbs, W. F. Kendall, M. Darrabie, E. C. Opara. *Journal of Investigative Medicine*. **2001**, 49, 572-575.